January 2016

THE ROLE OF NADPH OXIDASE IN NEURITE OUTGROWTH AND ZEBRAFISH NEURODEVELOPMENT

Cory J. Weaver
Purdue University

Graduate School Form
30 Updated 12/26/2015

PURDUE UNIVERSITY
GRADUATE SCHOOL
Thesis/Dissertation Acceptance

This is to certify that the thesis/dissertation prepared

By Cory J. Weaver

Entitled
THE ROLE OF NADPH OXIDASES IN NEURITE OUTGROWTH AND ZEBRAFISH NEURODEVELOPMENT

For the degree of Doctor of Philosophy

Is approved by the final examining committee:

Daniel M. Suter
Chair

Yuk Fai Leung

Christopher J. Staiger

Joseph P. Ogas

To the best of my knowledge and as understood by the student in the Thesis/Dissertation Agreement, Publication Delay, and Certification Disclaimer (Graduate School Form 32), this thesis/dissertation adheres to the provisions of Purdue University's "Policy of Integrity in Research" and the use of copyright material.

Approved by Major Professor(s): Daniel M. Suter

Approved by: Daoguo Zhou 5/14/2016

Head of the Departmental Graduate Program Date

THE ROLE OF NADPH OXIDASES IN NEURITE OUTGROWTH AND ZEBRAFISH NEURODEVELOPMENT

A Dissertation

Submitted to the Faculty

of

Purdue University

by

Cory J. Weaver

In Partial Fulfillment of the

Requirements for the Degree

of

Doctor of Philosophy

August 2016

Purdue University

West Lafayette, Indiana

"For me, it is far better to grasp the Universe as it really is than to persist in delusion, however satisfying and reassuring."

- Carl Sagan, The Demon-Haunted World: Science as a Candle in the Dark

ACKNOWLEDGEMENTS

My project would not have been possible without tremendous support from many people. I first would like to acknowledge my graduate mentor, Dr. Daniel M. Suter. His support and guidance are irreplaceable. He pushed me to be a better scientist, mentor and communicator, and gave me the confidence to pursue a unique research path. I am very grateful and those lessons will remain with me throughout my life.

I have also benefited from an excellent advisory committee. Dr. Yuk Fai Leung, my committee chair, graciously provided space in the animal facility to conduct the zebrafish work. Dr. Chris Staiger, Dr. Joseph Ogas and Dr. Paul Collodi provided critical discussion and poignant criticism to advance the quality of my research. I appreciate that each committee member was dedicated to my professional advancement and this was evident in their continued push for excellence in experimental quality and scientific communication.

I would also like to thank all of the labs involved in the care and maintenance of the fish facility, but especially Deborah Biesemeier for her tireless effort to keep the facility in excellent condition. Without the dedication of all involved, my project and so many others would be impossible.

I have had the privilege of being a teaching assistant for several courses during my time at Purdue. My teaching experience deepened my scientific knowledge, improved

my communication and gave me the confidence to pursue a career in science. I would specifically like to thank Dr. Peter Hollenbeck, Dr. John Anderson, Dr. Susan Karcher, Dr. Laurie Iten, Dr. Clark Gedney and Deborah Anderson for giving me the opportunity to teach in their courses.

I would like to extend my gratitude to former lab members Dr. Vidhya Munnamalai and Dr. Yingpei He for their mentoring and support. I would also like to thank our current post-doc and graduate students Dr. Ahmad Athammneh, Yuan Ren, Haley Roeder and Aslihan Terzi. It has been a privilege to be a part of such an insightful and talented group.

Finally, none of this work would have been possible without the overwhelming support of my family. I especially want to extend my deepest gratitude to my wife. Her unwavering encouragement and confidence inspired me regardless of the circumstance. I admire you more than you know. It is a profound failure of language that all I can say is thank you. To my daughter, your intelligence and curiosity leave nothing out of your reach. I am proud of the person you are and excited to see the person you will become.

TABLE OF CONTENTS

Page

Page

Page

Page

LIST OF TABLES

LIST OF FIGURES

LIST OF ABBREVIATIONS

3V	Third ventricle
6-HD	6-hydroxydopamine
AA	Aortic arch
AD	Alzheimer's disease
ADF	Actin depolymerizing factor
AIR	Autoinhibitory region
ALS	Amyotrophic lateral sclerosis
ASK1	Apoptotic signal-regulating kinase 1
ASMC	Aortic smooth muscle cell
ASW	Artificial seawater
aud	Auditory capsule
bb	Basibranchials
bh	Basihyal
BMP	Bone morphogenetic protein
C	Central domain
CAM	Cell adhesion molecule
cb i-v	Ceratobranchials I-V
CGD	Chronic granulomatous disease
CGN	Cerebellar granule neuron
ch	Ceratohyal
CRISPR	Clustered regularly-interspaced short palindromic repeats
CRMP	Collapsin response mediator protein
CV	Cardinal vein
DA	Dorsal aorta

DAPI	Diamidino-2-phenylindole
DC	Diencephalon
DCF	2’,7’-dichlorofluorescin
DIC	Differential interference contrast
DIG	Digoxigenin
DUOX	Dual oxidase
dv	Dorsal vein
E	Eye
EGF	Epidermal growth factor
eth	Ethmoid plate
FA	Focal adhesion
FAK	Focal adhesion kinase
FGF	Fibroblast growth factor
GCL	Ganglion cell layer
gRNA	Guide RNA
H_2O_2	Hydrogen peroxide
HB	Hindbrain
HPF	Hours post-fertilization
hys	Hyosymplectic
ISeV	Intersegmental vessels
ISH	In situ hybridization
JNK	c-Jun N-terminal kinase
LPS	Lipopolysaccharide
MAG	Microangiography
MAP	Microtubule associated protein
MC	Mesencephalon
MCeV	Medial cerebral vein
Mical	Molecules interacting with CasL
Mk	Meckle’s cartilage
MOX1	Mitogenic oxidase 1

MyC	Myelencephalon
NADPH	nicotinamide adenine dinucleotide phosphate
NC	Notochord
NCSC	Neural crest stem cell
NGF	Nerve growth factor
NOS	Nitric oxide synthase
NOX	NADPH oxidase (protein; species unspecified)
Nox	NADPH oxidase (zebrafish protein)
nox	NADPH oxidase (zebrafish gene)
nv	Nasal vein
ON	Optic nerve
OT	Optic tectum
OV	Otic vesicle
P	Peripheral domain
PA	Pharyngeal arches
PAM	Protospacer adjacent motif
PDBu	Phorbol 12,13-dibutyrate
PDGF	Platelet-derived growth factor
pec	Pectoral fin
PF-6	Peroxyfluor-6 acetoxymethyl ester
pq	Palatoquadrate
Prdx	Peroxyredoxin
PTP	Protein tyrosine phosphatase
PTU	N-Phenylthiourea
pty	Pterygoid process of the quadrate
qPCR	Quantitative polymerase chain reaction
RBI	Restrained bead interaction assay
RGC	Retinal ganglion cell
ROS	Reactive oxygen species
RT	Room temperature

SC	Spinal cord
SH3	Src homology 3
Shh	Sonic hedgehog
SM	Somites
SSC	Saline sodium citrate
T	Transition zone
TBI	Traumatic brain injury
TC	Telencephalon
Tec	Tectum
TecV	Tectal ventricle
VEGF	Vascular endothelial growth factor
VSMC	Vascular smooth muscle cell
vv	Ventral vein
WAVE	WASP-family verprolin homologous protein
YSE	Yolk sac extension

ABSTRACT

Weaver, Cory J. Ph.D., Purdue University, August 2016. The Role of NADPH Oxidases in Neurite Outgrowth and Zebrafish Neurodevelopment. Major Professor: Daniel M. Suter.

Nicotinamide adenine dinucleotide phosphate oxidases (NOX) are a family of enzymes that produce reactive oxygen species (ROS). The first NOX enzyme was discovered in leukocytes and associated with host defense in the immune system. Subsequent findings of ROS production in non-immune cells led to the identification of six additional NOX isoforms, and opened new avenues for research into NOX-mediated cellular functions. Since then, NOX-derived ROS have been found to be involved in a tremendous number of cell signaling pathways. Of particular interest is the well-established function of NOX-derived ROS in signaling pathways that drive cytoskeletal rearrangements and motility in several cell types. Our lab is interested in the highly motile neuronal growth cone that guides axonal growth during neurodevelopment and regeneration. Others have reported that inhibition of NOX enzymes during development causes a decrease in the size of some brain areas, and NOX deficiencies in humans are correlated with diminished cognitive function. Despite the fact that NOX activity is necessary for some cell motility in non-neuronal cells and a loss of NOX function during development has impacts on brain structure, it is still unclear what role NOX plays in

axonal growth and guidance or the establishment of connections in the central nervous system.

In this series of studies, I investigated the function of NOX enzymes in neurite outgrowth and neurodevelopment using both *in vitro* and *in vivo* approaches. I report that NOX activity is necessary for the extension of neurites in culture. Inhibition NOX activity leads to a disorganization of the actin cytoskeleton, a decrease in retrograde flow and a loss of neurite outgrowth. Using embryonic zebrafish, I showed that four separate *nox* genes are expressed broadly throughout the central nervous system during the first two days of development. Functional studies in zebrafish revealed that NOX inhibition leads to expansion of the ganglion cell layer in the retina and decrease in the size of the optic nerve. Subsequent studies using a site-specific, RNA-guided mutagenesis approach (CRISPR/Cas9) showed that optic nerve thinning resulted from developmental delays while ganglion cell expansion was a permanent defect caused by the mutation of a specific NOX isoform, NOX2/CYBB. The targeting of optic nerve axons to the optic tectum of the midbrain was also disrupted in NOX2/CYBB mutants. These results show that NOX activity is critical for neurite outgrowth in cultured cells in addition to retinal development and axon targeting *in vivo*.

CHAPTER 1. INTRODUCTION

1.1 Reactive oxygen species as cellular signals

Reactive oxygen species (ROS) are a class of small, oxygen-containing compounds that readily react with many classes of biomolecules (Finkel, 2001). Typically, ROS are associated with the oxidation of free thiol groups in cysteine or methionine residues (Fomenko et al., 2007; Jones and Go, 2011). Oxidized residues can readily form inter- or intramolecular disulfide bridges that effect protein structure and function (Dalle-Donne et al., 2002; Comito et al., 2011). Being promiscuous, ROS do not discern among targets in the same way as a prototypical ligand. Therefore, oxidation by ROS must be controlled by other means. One mechanism for controlling oxidation sites is the creation of reactive cysteines. Under normal physiological conditions, free cysteine thiols have a pKa ≥ 8 (Finkel, 2011). This means that they will not readily oxidize. In some cases, protein folding can create a microenvironment wherein the pKa of a cysteine thiol can reach as low as 4 making it primed for oxidation by ROS (Finkel, 2011).

ROS do not diffuse over great distances within the cell (Finkel, 2011; Lim et al., 2016). Therefore, another mechanism to control oxidative specificity is to maintain redox-sensitive targets in close approximation to sources of ROS. One example of this is protein tyrosine phosphatase (PTP) 1B. Epidermal growth factor (EGF) signaling

propagates via kinase cascades and PTP-1B acts as a negative regulator of this pathway by removing phosphate groups from downstream target proteins (Flint et al., 1997). PTP-1B is also redox sensitive, and becomes inactive when oxidized (Salmeen et al., 2003). In addition to the initiation of kinase cascades, EGF binding leads to the production of ROS at the membrane. Since PTP-1B localizes to the membrane, it becomes oxidized and inactivated upon EGF binding (Lee et al., 1998; Finkel, 2011). Redox inactivation of PTP-1B allows EGF signaling to propagate locally to the site of activated EGF receptor while PTP-1B outside of the local ROS gradient remains active.

A large part of the reason that ROS do not diffuse in cells is the presence of antioxidants. Cells maintain a battery of antioxidants that serve to regulate the redox balance including peroxiredoxin, glutathione peroxidase, catalase, thioredoxin, superoxide dismutase and others (Cerutti et al., 1994; Sarsour et al., 2009). Antioxidants have been shown to be active components of signaling pathways. In the PTP signaling pathway detailed above, the local activity of peroxiredoxins would quickly clear ROS, leading to PTP activation and a loss of kinase-mediated signaling. To counter this, peroxiredoxin I is inactivated by phosphorylation downstream of the activated EGF receptor which allows a sustained, local increase in ROS that maintains PTP-1B inactivation (Woo et al., 2010). Alternatively, antioxidants can act more directly in signaling pathways. Thioredoxin has been shown to bind and inhibit apoptotic signal-regulating kinase 1 (ASK1) (Saitoh et al., 1998). Binding is blocked when thioredoxin is oxidized by ROS which allows ASK1-mediated apoptotic signaling to proceed. Similar inhibitory antioxidant binding has been shown to contribute to cardiac hypertrophy via the regulation of histone deacetylases (Yamamoto et al., 2003; Ago et al., 2008).

Collectively, these studies show that ROS can act as cellular signals despite their biochemical promiscuity.

1.2 Sources of ROS and downstream effectors

Having established that ROS act as cellular signals, we should next consider the sources of ROS and targets of ROS-mediated oxidation. ROS are produced from several enzymes, but the most significant contributors are a class of enzymes called nicotinamide dinucleotide phosphate (NADPH) oxidases (NOX) and mitochondria (Wilson and Gonzalez-Billault, 2015). Functions of mitochondrial ROS in cell signaling have been extensively reviewed elsewhere (Finkel, 2012; Shadel and Horvath, 2015). NOX-derived ROS are excellent candidates for cellular signals because NOX enzymes can be localized to specific sites. Unlike mitochondria, the activity of many NOX enzymes can be regulated to restrict the production of ROS. These enzymes have been implicated in various signaling pathways, many of which will be discussed in this and later chapters.

Our lab is interested in the growth and guidance of neuronal growth cones. Growth cones are actin-rich structures located at the tips of developing axons and neurites that guide these processes toward their final targets (Levitan and Kaczmarek, 2002). Growth cones can be divided into three domains: the peripheral domain (P), the transition zone (T) and the central domain (C, Figure 1.1) The peripheral domain is comprised largely of actin and contains filopodia, long bundles of actin filaments, and lamellipodia, a meshwork of actin (Figure 1.1). Both filopodia and lamellipodia are dynamic, adding new actin monomers at the leading edge and depolymerizing actin

structures at the transition zone. This, along with action of myosins, leads to a constant retrograde flow of actin from the periphery to the transition zone (Levitan and Kaczmarek, 2002). Growth cone turning is accomplished by asymmetric changes in actin dynamics that lead to biased protrusion on one side versus the other. Full turning responses are accompanied by the extension of the microtubule-rich central domain into the actin-based protrusions. Growth cone guidance is the fundamental process that underlies axon outgrowth during neurodevelopment and regeneration. Since growth cone motility is dependent on the cytoskeleton, it shares basic, cell biological mechanisms with other cellular functions in motile cells. Therefore, we are most interested in NOX enzymes as they relate to cell motility, cytoskeletal remodeling, neurodevelopment and nervous system function.

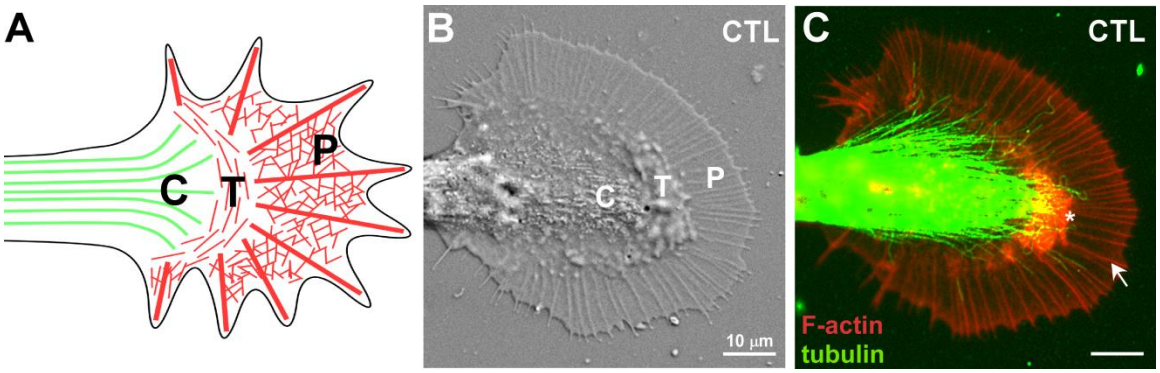

Figure 1.1: Neuronal growth cones (A) Schematic of cytoskeletal organization in the growth cone. Microtubules (green) and actin (red) are highly organized in the three domains: peripheral (P), transition zone (T) and central (C). (B) *Aplysia* growth cone imaged using DIC optic with the domains labeled. (C) The same growth cone shown in B labeled for actin and microtubules.

Axon guidance and the subsequent establishment of neuronal connections are dependent on interpretation of external cues by the neuronal growth cone that cause turning. These cues include secreted ligands, growth factors, extracellular matrix proteins,

cell-surface proteins and proteoglycans (O'Donnell et al., 2009; Kolodkin and Tessier-Lavigne, 2011; Masu, 2015). NOX enzymes have been implicated in signaling downstream from many of these molecules. Specific examples will be discussed in Chapters 6 and 7 with respect to the results obtained in my experiments. However, the net result of all the aforementioned signaling pathways is cytoskeletal modification that drives axon guidance. Given the central importance of the cytoskeleton in axon outgrowth and neurodevelopment, it is important to understand how redox regulation impacts the organization and dynamics of actin and microtubules.

1.2.1 Redox regulation of actin

Treatment of monomeric actin with 5-20mM hydrogen peroxide (H_2O_2) decreases assembly rates (DalleDonne et al., 1995). The same study found that oxidized actin took longer to reach equilibrium *in vitro* and the resulting actin filaments were more fragile than those derived from non-oxidized monomers. From additional data, the same group concluded that fragment instability was caused by weaker interactions with actin binding proteins such as alpha actinin (DalleDonne et al., 1995; Milzani et al., 1997). They then found that specific methionine residues along with cysteine 374 were the targets of oxidation, and they identified increased actin oxidation in human patients suffering from neurodegeneration (Dalle-Donne et al., 2001; Dalle-Donne et al., 2002). In a separate study, the authors showed that reversible S-glutathionylation of cysteine 374 decreases actin polymerization rate by subtly altering the conformation of the actin monomer (Dalle-Donne et al., 2003). Additional studies showed that cysteine 272 was oxidized

specifically by the addition of hydrogen H_2O_2, and this oxidation caused a weaker interaction with cofilin leading to filament instability (Lassing et al., 2007).

In addition to actin, myosin has also been shown to be redox sensitive. Treatment of skeletal muscle with high doses of H_2O_2 (5 and 50mM) caused structural changes in myosin, and decreased actomyosin contractility (Prochniewicz et al., 2008). However, it should be noted that 50mM H_2O_2 may not be physiologically relevant, and the authors did not account for the impact of actin oxidation on contractile responses.

Most published work shows that oxidation via H_2O_2 reduces actin polymerization. All of these studies used concentrations of H_2O_2 in excess of 5mM. Application of 1-5mM H_2O_2 to p388DI cell lysates *in vitro* caused as much as a 50% increase in polymerized actin (Omann et al., 1994). The authors went on to show that this increase was not due to a greater number of nucleation events. Another study used endothelial monolayer wounding assays to show that increased ROS production at the wound margin correlated with increased actin assembly and faster cell migration (Moldovan et al., 2000). The authors also used ROS scavengers to demonstrate the necessity of ROS production to actin assembly in these cells. In endothelial cells, ROS stimulation enhances actin retrograde flow leading to protrusion and the leading edge of the membrane (Taulet et al., 2012). Our lab has show that reductions in exogenous ROS lead to decreased actin flow rates and slower neurite outgrowth in neuronal growth cones (Munnamalai and Suter, 2009). Integrin-based cell adhesions are accompanied by ROS production. One study showed that ROS in this pathway leads to actin glutathionylation which caused persistent stress fibers and a lack of cell spreading (Fiaschi et al., 2006). The authors found that this was due to the stability of the actomyosin complex when actin was oxidized.

1.2.2 Redox regulation of microtubules

Like many other proteins, monomeric tubulin can be reversibly modified to regulate microtubule dynamics (Janke, 2014). Unlike actin, much of the literature on redox regulation of tubulin focuses on reactive nitrogen in lieu of ROS (Landino et al., 2007; Wilson and Gonzalez-Billault, 2015). Tubulin monomers can undergo S-glutathionylation after oxidation by reactive nitrogen, and the sites of these modifications have been identified via crystallography (Lowe et al., 2001; Nogales and Zhang, 2016). Studying the direct oxidation of tubulin *in vitro* is difficult given the short lifetime of reactive nitrogen in the conditions necessary for microtubule polymerization. The challenges and necessary compromises are detailed in other literature (Sparaco et al., 2006; Wilson and Gonzalez-Billault, 2015), but the central message is how tubulin oxidation affects microtubule dynamics is still not fully understood.

Oxidation has been shown to impact microtubule dynamics by modifying microtubule associated proteins (MAPs). H_2O_2-induced oxidation of cysteines in tau and MAP2 caused a decrease in microtubule assembly and stability *in vitro* (Landino et al., 2004). This effect of this oxidation was reversible suggesting a possible role for redox regulation of microtubules via MAPs. It has also been shown that MAPs impact the transport of cargo along microtubules by interacting with specific motor proteins (Dixit et al., 2008). One study showed that nitrosylation of MAP1B caused neurite retraction by decreasing microtubule stabilization (Stroissnigg et al., 2007). Neurite retraction was dependent on dynein suggesting an interaction between MAPs, cytoskeletal motors and microtubule stability.

1.3 Linking extracellular signaling to redox control of the cytoskeleton

Many of the studies on redox regulation of the cytoskeleton have used cell-free, *in vitro* polymerization assays to determine the impact of oxidation or reduction. Some have used migrating cells to correlate ROS production with actin dynamics and migration. However, none of the studies discussed to this point described a signaling pathway that begins with an extracellular ligand and leads to ROS-mediated changes in the cytoskeleton that affect motility. In the last decade, studies focused on a protein called molecules interacting with CasL (Mical) elucidated this type of redox-mediated pathway that directs the growth of axons in *Drosophila*.

The structure of Mical was resolved by two different groups around the same time (Nadella et al., 2005; Siebold et al., 2005). Mical was then shown to be critical for transduction of semaphorin-plexin-mediated collapse responses in *Drosophila* neurons during central nervous system development (Ayoob et al., 2006). Collapsin response mediator proteins (CRMPs) are necessary for axon turning in response to repulsive semaphorin cues. Association with CRMP, induced by semaphorin, activated Mical, and this activity was necessary for axon guidance *in vivo* (Schmidt et al., 2008). Although Mical was now firmly established as a mediator of semaphorin-induced axonal guidance, the link to ROS was still unknown.

In 2010, a study reported that Mical was capable of producing ROS via a flavoprotein domain (Hung et al., 2010). More importantly, it was found that ROS production was necessary for semaphorin-induced growth cone collapse, and that Mical associates directly with f-actin. Additional studies showed that Mical-derived oxidation

of actin at methionine 44 mediates cytoskeletal collapse and growth cone turning (Hung et al., 2011). In order to be a useful signaling mechanism, actin oxidation must be reversible. In 2013, it was found that a reductase enzyme called SelR reduces methionine 44 and restores normal actin polymerization (Hung et al., 2013). In addition to actin, Mical-derived ROS was also found to activate CRMP via direct oxidation (Morinaka et al., 2011). Collectively, these studies resolved a complete circuit of redox-mediated signaling that drives axon guidance.

Most of this work focused on Mical in the *Drosophila* nervous system, but a recent study implicated semaphorin-Mical signaling in human melanoma cells. The authors reported that depletion of Sema6A or Mical1 decreased stress fiber formation and chemotaxis (Loria et al., 2015). Over expression of either protein caused cells to be more invasive and have higher growth rates. Beyond cell motility, Mical has also been implicated in vesicle trafficking via association with Rab proteins (Fukuda et al., 2008). Mical knockouts lead to disruptions in endoplasmic reticulum to Golgi trafficking and endocytosis (Fischer et al., 2005; Van Battum et al., 2014). It has been proposed that Mical-actin interactions are important for trafficking, but it should be noted that these studies did not address Mical-derived ROS directly. Therefore, it remains unclear whether or not ROS production is necessary for trafficking.

While there is still more to discover about Mical proteins, the research into Mical's role in growth cone guidance is as complete a picture of ROS-mediated axon guidance as is currently available. Other sources of ROS in cells, like NOX, likely contribute to the propagation of guidance signals, but this remains to be studied.

1.4 Introduction of the NOX isoforms

Research into NOX enzymes and redox biology extends as far back as 1908 when a respiratory burst was observed during the fertilization of sea urchin eggs (Warburg, 1908). From these initial experiments, there emerged a field of study aimed at characterizing the respiratory burst and identifying the cellular machinery responsible. In the intervening century, not only was a specific isoform of NOX implicated in the respiratory burst, but six additional NOX isoforms, each with unique functions, were characterized. NOX dysfunction was also shown to be the cause of a potentially fatal immune disease, and knowledge derived from the study of patients was critical for identifying the genes encoding NOX subunits. In the sections that follow, each NOX isoform is introduced in the order in which they were discovered. Included is a description of the enzyme complexes, a brief overview of activation mechanisms and a review of the known functions with respect to the nervous system.

1.4.1 NOX2

In 1933, a respiratory burst similar to that in sea urchin eggs was observed in phagocytes (Baldridge and Gerard, 1933). This burst proved clinically significant in 1957 with the discovery of a rare immunological disease. Patients, typically males, developed severe infections and excessive inflammation often in the form of persistent granulomas (Berendes et al., 1957). Ten years later, the disease now called chronic granulomatous disease (CGD) was attributed to a lack of oxidant production at infection

sites. The decreased ROS production was linked leukocytes, a type of phagocyte (Baehner and Nathan, 1967; Holmes et al., 1967; Quie et al., 1967). In the mean time, studies had identified that the respiratory burst in leukocytes produced H_2O_2, and that NADPH, not NADP, served as an electron donor for the reaction (Iyer et al., 1961; Rossi and Zatti, 1964).

Nearly thirty years after the initial identification of CGD, one of the primary genes responsible was identified and cloned (Royer-Pokora et al., 1986; Teahan et al., 1987). The gene was located on the X chromosome explaining the predominantly male, X-linked recessive pattern of CGD inheritance. The gene product was initially called $gp91^{phox}$, but is now commonly referred to as NOX2 or CYBB. It quickly became clear that NOX2 was part of a larger enzyme complex when it was discovered that deficiency of another gene encoding a protein called $p22^{phox}$, CYBA, also led to CGD (Dinauer et al., 1987; Segal, 1987). The gene for $p22^{phox}$ is located on chromosome 16 explaining the autosomal recessive pattern of inheritance of $p22^{phox}$-based CGD.

The advent of cell-free systems led to the identification of additional cytosolic subunits called $p47^{phox}$, NCF1, and $p67^{phox}$, NCF2 (Bromberg and Pick, 1985; Nunoi et al., 1988; Volpp et al., 1988). By 1994, it was established that the small GTPases Rac1/2 were also members of the NOX2 complex (Abo et al., 1991; Knaus et al., 1991; Abo et al., 1994). Seven years after the initial cloning of the gene encoding NOX2, the final subunit of the NOX2 complex was identified as $p40^{phox}$, NCF4 (Wientjes et al., 1993).

NOX2 and $p22^{phox}$ are both transmembrane proteins, and they are tightly associated within the cell to form the enzymatic core called the flavocytochrome (Nauseef, 2004). With the exception of NOX5 and DUOX, all NOX isoforms require

$p22^{phox}$. Additionally, all NOX isoforms have six transmembrane alpha helices forming a pseudochannel that shuttles electrons from NADPH in the cytosol to the oxygen acceptor on the opposite face of the membrane (Kawahara and Lambeth, 2007). Alpha helices III and IV each contain two histidine residues that are responsible for the binding of heme cofactors involved in shuttling electrons (Brandes et al., 2014). The composition of the NOX2 complex and other NOX complexes are shown in Figure 1.1.

Returning specifically to NOX2, ROS production is initiated when the enzyme complex assembles on a membrane. The complex can be activated in several ways, but the most commonly described involves the phosphorylation of the scaffolding protein, $p47^{phox}$, and the activation of Rac. In the absence of phosphorylation, the autoinhibitory region (AIR) of $p47^{phox}$ interacts with the phosphoinositide-binding domain, PX, to bury many of the functional domains (Groemping et al., 2003). This closed conformation prevents $p47^{phox}$ from acting as a scaffold to bring other proteins to the flavocytochrome. Upon phosphorylation and release of autoinhibition, $p47^{phox}$ adopts an open conformation that allows the PX domain to act as a membrane anchor and protein scaffold. (Ago et al., 2003). Dual Src homology 3 (SH3) domains in $p47^{phox}$ directly bind to the flavocytochrome via proline-rich regions of $p22^{phox}$ (Nakanishi et al., 1992). $p47^{phox}$ also interacts with $p67^{phox}$ to bring the latter into close proximity of the NOX2 active site (el Benna et al., 1994b). $p67^{phox}$ contains an activation domain that significantly increases the rate of NOX2 electron transfer when aligned to the active site (Han et al., 1998). Activated Rac translocates to the membrane independently of $p47^{phox}$, but shows a strong association with $p67^{phox}$ (Diekmann et al., 1994). In fact, strong activation of Rac is sufficient to drive $p67^{phox}$ to the membrane (Gorzalczany et al., 2000).

Owning to its discovery in CGD patient cells, NOX2 is most commonly associated with functions in phagocytic cells of the immune system. However, NOX2 is expressed in neurons, microglia, vascular smooth muscle cells, skeletal muscle, cardiomyocytes, hepatocytes, endothelial cells, hematopoietic stem cells and fibroblasts (Pagano et al., 1997; Bedard and Krause, 2007; Brown and Griendling, 2009; Nayernia et al., 2014). NOX2 has been shown to be involved in growth factor signaling, angiogenesis, cell death and blood pressure regulation (Bedard and Krause, 2007; Brown and Griendling, 2009). However, it is noteworthy that NOX2 is found in cells of the nervous system. Accordingly NOX2 has been implicated in nervous system function and maintenance in a number of ways.

CGD patients were critical in identifying and characterizing NOX2, and researchers are again turning to patients to understand the full of range of NOX2 functions in the nervous system. CGD patients suffer from mild cognitive deficiencies including below average IQ scores (Pao et al., 2004; Cole et al., 2013). However, it should be noted that severe infections in CGD patients often lead to prolonged hospitalization and social isolation (Chiriaco et al., 2015). The authors of both studies cited above caution that lack of social and educational exposure may contribute to cognitive declines. However, NOX2 is expressed in neurons and several neuronal functions are known so there remains a possibility that the enzyme plays a direct role in brain development.

In adult mouse brains, there is direct evidence that hippocampal neurons express NOX2, and that the enzyme plays a significant functional role. One of the first studies on this topic showed that mice overexpressing superoxide dismutase, a potent antioxidant

enzyme, do not undergo long-term potentiation (Thiels et al., 2000). In cultured hippocampal neurons, NOX2 subunits were identified in cell bodies and dendrites via immunohistochemistry (Tejada-Simon et al., 2005). Further, direct activation of NOX led to the colocalization of NOX2 regulatory subunits at presynaptic sites. A separate study found that inhibition of NOX2 leads to polarization defects and decreased neurite extension in mouse hippocampal neurons (Wilson et al., 2015). The authors confirmed that NOX2 subunits were localized throughout the cell, and found that several NOX2-specific inhibitors caused alterations in the actin cytoskeleton that presumably led to neurite outgrowth defects. Studies performed on mice lacking either NOX2 or $p47^{phox}$, rodent models of CGD, identified impairments in spatial and context dependent-fear memory formation (Kishida et al., 2006). Both of these behaviors are mediated by the hippocampus. Additionally, these *in vivo* experiments showed that NOX2 deficient mice do not undergo long-term potentiation in hippocampal neurons. All of these studies, taken together, clearly show the importance of NOX2 in learning and memory processes mediated by the hippocampus. See Figure 1.1 for a summary of the known roles for NOX2 in the nervous system.

Neural stem cell potency is dependent on the maintenance of high ROS levels in progenitors (Le Belle et al., 2011; Wang et al., 2015). Adult hippocampal stem cells rely on high ROS levels to maintain self-renewal and normal progenitor function. It is perhaps unsurprising that NOX2 has been identified as a major source of ROS in adult hippocampal stem cells (Dickinson et al., 2011). Inhibition of NOX2 leads to depletion of neural progenitors and defective neurogenesis. This may suggest that NOX2 function is critical for hippocampal development and maintenance in addition to memory and

learning. It is tempting to speculate that cognitive declines in CGD patients may stem from NOX2 dysfunction in the hippocampus that impacts memory, learning and/or neurogenesis. This speculation remains untested, but is worthy of further investigation.

Moving out of the hippocampus, NOX2 has also been found in cerebellar granule neurons (CGN). CGNs are small, tightly packed neurons that allow for complex coding of input information. In 2009, a group found that staurosporine-induced apoptotic death in CGNs was mediated by NOX2 activity (Guemez-Gamboa and Moran, 2009). CGNs derived from NOX2 knockout mice were less sensitive to staurosporine than wild type controls. Apoptosis in CGNs can be triggered in multiple ways, and researchers found that NOX2 was specifically activated by staurosporine and not other apoptotic signals. This finding indicates that NOX2 is not a general apoptotic signal, but acts in a specific pathway.

While the previous study implicates NOX2 in cell death, NOX2 has also been shown to promote the maturation of CGNs (Olguin-Albuerne and Moran, 2015). Using CGN cultures, authors showed that NOX inhibitors and general antioxidants caused a decrease in neuronal maturity after three days *in vitro*. Maturity was measured by morphology as well as the presence of mature neuronal markers, Tau and MAP2. NOX2 was identified in the growth cones and filopodia of developing CGN neurites, and colocalized to the sites of H_2O_2 production. Additionally, the authors described an increase in ROS at one day *in vitro* that was critical for CGN survival. CGNs derived from NOX2 knockout mice displayed short neurites which is consistent with what was observed in response to NOX inhibitors (Olguin-Albuerne and Moran, 2015).

NOX2 is also implicated in tissue damage following brain injury. Inflammation driven by NOX2-derived ROS has been shown to promote tissue damage following ischemic stroke (Carbone et al., 2014). NOX inhibitors have been shown to ameliorate the inflammation and tissue damage in laboratory studies. Unfortunately, NOX2 activity might also directly increase the probability of stroke occurrence by contributing to the formation of arterial plaques (Sierra et al., 2011). A separate study showed that the application of a NOX inhibitor, apocynin, attenuated nearly all markers of neural damage following traumatic brain injury (TBI) in mice (Lu et al., 2014). Apocynin-treated mice showed a decrease in neuronal apoptosis, blood-brain barrier disruption and cognitive deficiency. The authors focused on cortical injuries, and found that NOX2 expression sharply increased immediately following TBI. This may indicate that NOX2 is a marker of inflammation and damage in cortical cells.

Amyotrophic lateral sclerosis (ALS) is a disease characterized by the progressive atrophy of motor neurons that eventually leads to a loss of muscle control. As there is no cure, current treatments focus on slowing disease progression. Rac1, a critical regulator of NOX function, is known to be involved in cytoskeletal organization in mature neurons. Through the misregualtion of Rac1, NOX has been implicated in ALS disease progression (D'Ambrosi et al., 2014). NOX2 has been identified as a key source of damaging ROS in ALS models (Boillee and Cleveland, 2008). A recent study of human ALS patients confirmed the experimental results from rodent models. This study showed that lower levels of endogenous NOX2 activity lead to modest increases in patient survival (Marrali et al., 2014). This makes NOX2 a promising therapeutic target for future studies.

Alzheimer's disease (AD) is a neurodegenerative condition causing dementia and memory loss. In the United States, approximately 5 million individuals over the age of 65 have AD (Association, 2014). The disease is characterized by the progressive loss of neurons due to the formation of extracellular amyloid plaques and intracellular neurofibrillary tangles (Association, 2014). Compared to non-diseased, age-matched controls, human cortical sections from AD patients exhibited higher expression of genes encoding $p47^{phox}$, $p67^{phox}$ and $p40^{phox}$, but not NOX2 itself (Ansari and Scheff, 2011). Further, NOX2 activity correlated well with symptom severity suggesting that ROS production is a predictor of disease progression. As with the TBI study mentioned earlier, these experiments focused on cortical tissues from AD patients. In both cases, it is unclear whether NOX2 contributes to normal cellular function in the cortex or is expressed only in the diseased state. The answer to this question may shed light on what role, if any, NOX2 plays in disease onset as opposed to progression. AD patients also have lesions in the hippocampus leading to memory loss (Association, 2014). Given the well-established function of NOX2 in the hippocampus, it is possible, although untested, that NOX2 misregulation contributes to the onset of AD pathology in this brain region.

Although NOX2 activity correlates well with AD severity, mouse models of AD treated with the NOX inhibitor apocynin were not significantly protected (Dumont et al., 2011). Inhibitor-treated mice showed no change in the extent of brain lesions or cognitive declines. Conversely, a previous study showed that genetic NOX2 deficiency in the same AD mouse model improved cognitive and histopathological symptoms (Park et al., 2008). Drug administration is less potent than genetic knockouts, and this may explain the discordant results. However, it should be noted that NOX2 deficient mice also develop

CGD. This poses serious ethical questions regarding the viability of NOX2 as a target for gene therapy or other genetic manipulations. Nonetheless, these studies present a paradox concerning the viability of NOX2 as a target for AD therapies that is worthy of continued study.

1.4.2 NOX1

Researchers were surprised to find that fibroblasts and neutrophils from CGD patients were capable of producing a respiratory burst (Emmendorffer et al., 1993). This clearly showed that ROS production in these cells was not mediated by NOX2. As the final components of the NOX2 complex were identified in 1993, the search was on for additional enzymes capable of generating bursts of ROS. In 1999, a homolog of NOX2 called mitogenic oxidase 1 (MOX1, now NOX1) was identified and cloned (Suh et al., 1999). Cytosolic subunits for the NOX1 complex, NOXO1 and NOXA1, were found four years later (Banfi et al., 2003; Geiszt et al., 2003).

Similar to $p47^{phox}$, NOXO1 functions as a scaffold to bring the activation domain of NOXA1 near to the active site of NOX1. NOXO1 contains similar PX, SH3 and PRR domains that mediate protein-protein interactions involved in scaffolding. One critical difference between $p47^{phox}$ and NOXO1 is the absence of the AIR in NOXO1 (Cheng and Lambeth, 2004). This means that NOXO1 activity is not phosphorylation dependent. However, NOX1 activity is still dependent on Rac giving the complex some degree of regulation despite the constitutive activity of NOXO1 (Park et al., 2004; Miyano et al., 2006; Ueyama et al., 2006). Like $p67^{phox}$, NOXA1 interacts directly with Rac in addition

to NOXO1, and contains an activation domain necessary for optimal NOX1 function (Brandes et al., 2014).

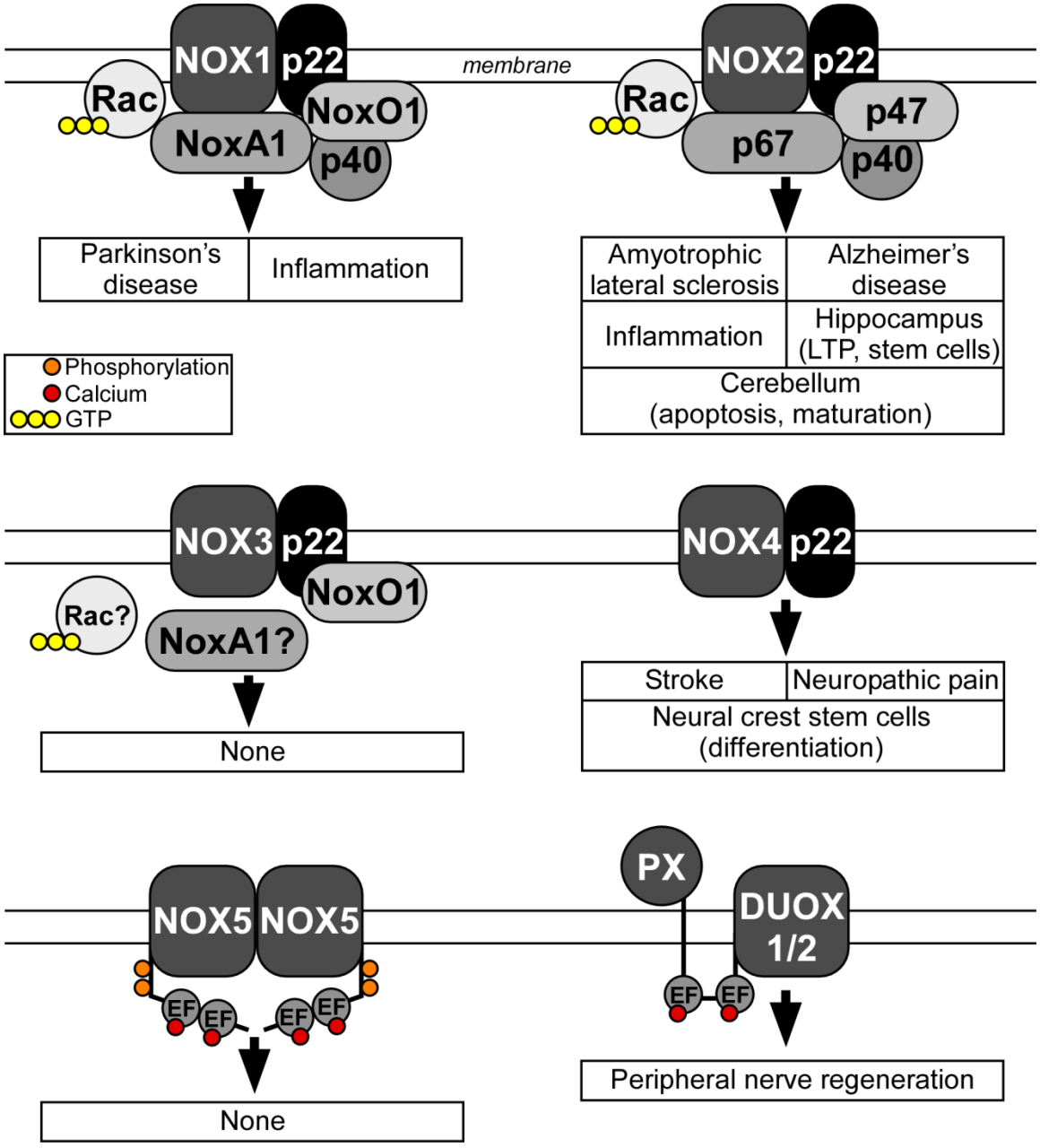

Figure 1.2: Composition of the NOX complexes The active form of each NOX enzyme complex is shown. The enzyme complexes assemble on the plasma membrane or vesicular membranes. It is unknown whether NOXA1 and Rac are necessary for NOX3. Misregulation leads to the conditions and/or diseases listed below each complex, discussed and cited in the text. There have been no functions associated with NOX3/5 in the nervous system. PX indicates the peroxidase-like domain of DUOX1/2.

NOX1 is most closely associated with expression in the colon epithelia, but expression has also been shown in endothelial cells, vascular smooth muscle cells, retinal pericytes, uterus, placenta and prostate (Cui et al., 2006; Rokutan et al., 2008; Brown and Griendling, 2009; Sorce and Krause, 2009). NOX1 has been implicated in canonical Wnt-beta catenin signaling, and hypoxic injury (Kajla et al., 2012; Spencer et al., 2013). NOX1 is also important for the migration of vascular smooth muscle cells and colon adenocarcinoma cells suggesting a possible role in cancer metastasis (Schroder et al., 2007; Sadok et al., 2008; Zimmerman et al., 2011). The enzyme has also been identified in the nervous system, but the functions of NOX1 are less extensively studied compared with NOX2.

Parkinson's disease is a neurodegenerative condition characterized by the loss of dopaminergic neurons in the substantia nigra which leads to progressively worsening movement disorders (Jimenez-Shahed, 2016). Current therapies aim to slow progression of the symptoms, but there is still no cure. Cell culture models revealed that a selective dopaminergic neuronal toxin, 6-hydroxydopamine (6-HD), causes increased expression of NOX1 mRNA (Choi et al., 2012). Another study using the same culture model showed that protein kinase C delta and NOX1 mediate cell death in dopaminergic neurons under oxidative stress conditions (Cristovao et al., 2013). Knockdown of protein kinase C delta led to a subsequent decrease in NOX1 activity and increased neuronal survival. In live rats, injection of 6-HD into the brain also increased NOX1 expression in the substantia nigra, but the protein was surprisingly localized to the nucleus (Choi et al., 2012). Accordingly, 6-HD treated rats exhibited oxidative DNA damage and death of

dopaminergic neurons. Knockdown of NOX1 ameliorated both conditions. Collectively, these findings portray NOX1 as a potential therapeutic target for Parkinson's disease.

Inflammation is a common hallmark of many neuropathologies including trauma to the central nervous system (Ansari and Scheff, 2011; Lu et al., 2014; Marrali et al., 2014; Zhao et al., 2016). Microglia are responsible for inflammation in the central nervous system, and are thus often targeted in therapies for brain and spinal cord injury. Using purified microglia from mice, researchers found that activation via lipopolysaccharide (LPS) elicits an increase in NOX1 activity which leads to nitric oxide synthase (NOS) activation and neurotoxicity (Cheret et al., 2008). Both NOX1 and NOX2 contribute to this process, but NOX1 was necessary for maximum ROS production. NOX1 knockout mice were protected from LPS-induced neurodegeneration, and showed decreased NOS activity. As inflammation is a symptom of many neuropathologies, the discovery of NOX1 in this signaling pathway may be the most promising therapeutic target yet presented.

1.4.3 NOX3

NOX3 was first identified in 2000 by several independent groups (Kikuchi et al., 2000; Cheng et al., 2001; Banfi et al., 2004a). $p22^{phox}$ is necessary for activity, but the additional regulatory subunits of the NOX3 complex are still a matter of some debate. It is clear that NOXO1 is needed for optimal ROS production, but it may not be essential for basal NOX3 activity (Bedard and Krause, 2007). NOX3 is highly expressed in the inner ear, an organ involved in balance control. NOXO1 deficient mice exhibit

locomotion and balance defects that indicate inner ear dysfunction (Kiss et al., 2006). The same study went on to link NOXO1 in the inner ear with NOX3 activity. This provides evidence that NOXO1 is needed for NOX3 activity *in vivo*. Whether NOXA1 or Rac are necessary for NOX3 function is currently unclear (Bedard and Krause, 2007).

As stated, NOX3 expression is closely associated with the inner ear, but additional expression has been identified in a range of human fetal tissues including kidney and spleen (Cheng et al., 2001). Additionally, NOX3 expression has been found in human colon epithelial cells (Kikuchi et al., 2000). There is currently no data on NOX3 expression in the nervous system, and no NOX3-associated functions. However, it is possible that hearing and balance defects in NOX3 knockouts are caused disruptions in the connections between the inner ear and nervous system. Additional studies into the specific mechanisms of NOX3-mediated signaling are needed to address this possibility.

1.4.4 NOX4

The gene encoding NOX4 was originally identified in kidney tissue in the year 2000 (Geiszt et al., 2000; Shiose et al., 2001). NOX4 is unique from other isoforms in that function is not dependent on any cytosolic subunits (Bedard and Krause, 2007). NOX4 does interact with $p22^{phox}$, however, and this interaction is necessary for activity. The absence of cytosolic subunits led many to speculate that NOX4 is constitutively active, and this is confirmed in cell free systems (Bedard et al., 2012). However, NOX4 is comparatively sensitive to cellular conditions such as the presence of free oxygen, and this may act as a mechanism modulate NOX4 activity (Nisimoto et al., 2014). Activation

may also be controlled at the level of transcription. Many NOX4-dependent signaling pathways have been shown to control the expression of NOX4 mRNA (Brandes et al., 2014).

While details regarding the mechanisms of regulation are still being investigated, NOX4 has been identified in many cell and tissue types. As mentioned, NOX4 was first discovered in kidney tissue. Since then NOX4 has been found in neurons, osteoclasts, vascular smooth muscle cells, hematopoietic stem cells, fibroblasts, keratinocytes, melanomas and neural crest cells (Bedard and Krause, 2007; Lee et al., 2014). NOX4 activity is involved in vascular smooth muscle cell function, and NOX4 deficient mice are predisposed for obesity (Lyle et al., 2009; Li et al., 2012a). Adding to the range of NOX4 functions, the enzyme is also necessary for influenza A replication in lung epithelia (Amatore et al., 2015).

Damage to peripheral neurons, either by injury or disease, can result in prolonged pain. This condition is clinically known as neuropathic pain, and approximately 20 million people in the United States have been diagnosed with some form of this condition (Yawn et al., 2009). A widespread cause of neuropathic pain is peripheral neuropathy, commonly caused by diabetes or chemotherapy treatment. Additional routine causes of neuropathic pain include injury, surgical complications or other unknown sources (Yawn et al., 2009). One group found NOX4 expression in peripheral nerves and dorsal root ganglia in the mouse. They went on to show that mice lacking NOX4 exhibit a decrease in peripheral nerve demyelination following nerve injury (Kallenborn-Gerhardt et al., 2012). The NOX4-deficient mice also display a decrease in behaviors indicative of neuropathic pain. The study provides evidence that NOX4 may contribute both to the

extent of nerve injury and to the perception of neuropathic pain in mouse models. Given the prevalence of neuropathic pain in humans, this is an important discovery that may lead to improved therapeutic strategies.

The role of NOX2 in cell death following ischemic stroke was presented earlier, but a separate study found that NOX4 is more important in post-stroke neuroprotection. The research showed that NOX4 expression is increased in both humans and mice following ischemia (Kleinschnitz et al., 2010). NOX4 deficient mice, but not those deficient in NOX1/2, were protected from neuronal apoptosis, and this was specifically due to the reduction of oxidative stress. The extent of neuroprotection was unaffected by age. Mice treated with a NOX inhibitor, VAS2870, hours after the onset of ischemic stroke showed decreased neuronal apoptosis and improved long-term cognitive function compared to sham-treated controls. This has major clinical significance since viable therapies for use in humans must be effective even when applied long after the onset of a stroke (Zhang et al., 2016).

NOX4 contributes to the survival and fate determination of neural crest stem cells (NCSCs) during development. Cultured NCSCs treated with bone morphogenetic protein 2 (BMP2) differentiate into neurons, and this process is dependent on the production of ROS (Lee et al., 2014). One group found that NOX4 was expressed in NCSCs, neuronal differentiation was blocked in NOX4 knockouts (Lee et al., 2014). This effect was reproduced in cells treated with NOX inhibitors. Strangely, NOX4 deficient mice do not display any defects in NCSC-derived tissues. The authors note that homozygous NOX4 knockout pups are not born at the expected rate, suggesting NOX4 knockout may be lethal, and they speculate that molecular compensation might mask the phenotype.

1.4.5 NOX5

NOX5 was first identified in the testis, spleen and lymph node in 2001 (Banfi et al., 2001). In lieu of cytosolic subunits, NOX5 relies on direct phosphorylation and calcium binding for activation (Banfi et al., 2004b). NOX5 contains two EF hand motifs that cooperatively bind calcium ions to elicit protein function (Bedard et al., 2012). NOX5 has been shown to interact directly with calmodulin, and calmodulin modulates the calcium sensitivity of NOX5 (Tirone and Cox, 2007). Additionally, NOX5 can be phosphorylated at two sites to induce ROS production (Brandes et al., 2014). NOX5 forms a homodimer in order to function, and activity does not require the presence $p22^{phox}$ like all of the previously described NOX isoforms (Brandes et al., 2014).

In addition to the tissues mentioned above, NOX5 is also expressed in endothelial cells, vascular smooth muscle cells, pancreas, placenta, ovary, uterus, stomach and multiple fetal tissue (Bedard and Krause, 2007). NOX5 has been shown to be involved in thrombin-mediated proliferation in human endothelial cells, and platelet derived growth factor-mediated proliferation in smooth muscle cells (BelAiba et al., 2007; Jay et al., 2008). There is currently no known function for NOX5 in the nervous system.

1.4.6 DUOX1/2

Originally called thyroid oxidases, dual oxidases (DUOX1 and DUOX2) were the last NOX-related isoforms to be identified (Dupuy et al., 1999; De Deken et al., 2000). Like NOX5, DUOX1/2 are activated by calcium binding to EF hand motifs. The proteins

are called ‘dual’ oxidases because they contain a large N-terminal peroxidase-like domain in addition to the flavocytochrome (Lambeth et al., 2007). There is significant debate regarding the importance of the extracellular peroxidase-like domain, but patients with mutations in this domain exhibit hypothyroidism (Bedard and Krause, 2007), suggesting some nominal function. DUOX1/2 are claimed to directly produce H_2O_2, but this seems unlikely given the biochemical restraints of the monoelectron reactions of NOX family members. Rather, some have postulated that superoxide is direct product, but DUOX1/2 facilitate rapid dismutation into H_2O_2 (Bedard and Krause, 2007).

DUOX1/2 are expressed, as the original name implies, in the thyroid. Additionally, they are expressed in the epithelia of the airway and gastrointestinal tract, testis, uterus, gall bladder, pancreas and cerebellum (Harper et al., 2006; Lambeth et al., 2007). As mentioned, DUOX2 mutations have been shown to cause hypothyroidism thus demonstrating function in the thyroid. Additionally, DUOX has been show to be involved in cytokine-mediated neutrophil recruitment in zebrafish (de Oliveira et al., 2015). There are no studies of DUOX expression or function in nervous system cells. However, DUOX activity has tangentially been shown to guide and promote the regeneration of damaged peripheral nerves in the zebrafish tail (Rieger and Sagasti, 2011). In this study, peripheral nerves were damaged either by tail clipping or laser nerve ablation. Normally, new axons completely reinnervate the regenerated tail, and this is accompanied by tissue-scale ROS production. The authors found that DUOX knockdown decreased overall axon outgrowth and caused less extensive reinnervation. Further investigation showed that the ROS gradient stemmed from DUOX expressed in damaged keratocytes, not from the neurons themselves. The DUOX-derived ROS created a tissue-scale gradient that acted as

a cue to guide the newly growing axons. While this study did not provide any evidence that DUOX has a cell-autonomous role in neurons, it is noteworthy that damaged axons followed an increasing gradient of ROS in this system. In contrast, most models of axon regeneration posit that ROS inhibit axon outgrowth. From what is known, overproduction of ROS by the glial scar acts as an inhibitory signal for axon regrowth, but antioxidant therapies for brain and spinal cord injuries have been largely unsuccessful (Hall, 2011). It is possible that low concentrations of ROS might act as positive growth signals while higher concentrations are inhibitory. This idea is supported by earlier work from our lab (Munnamalai and Suter, 2009), and extended by my work (Chapter 3).

1.5 Additional roles for NOX in the nervous system

General ROS production was shown to affect neuronal fate determination in cortical cultures from embryonic rats (Tsatmali et al., 2006). Consistent with what is known about neuronal precursors in mouse hippocampus (Dickinson et al., 2011), cortical neurons from embryonic day 15 rats displayed a high level of ROS production (Tsatmali et al., 2006). ROS levels were found to be reliable predictors of neuronal subtype, and antioxidant treatments shifted this distribution without affecting cell survival. Further, the authors reported that ROS production was limited to cortical progenitors by postnatal day 20. While the study did not specify a source of ROS, the findings are similar to the pattern of NOX2-derived ROS in the hippocampus described earlier. Regardless of the source, the current study shows that ROS contributes to fate determination in cortical neurons.

Staying with neuronal differentiation, PC12 cells treated with nerve growth factor (NGF) display neurite outgrowth and the expression of neuron-specific genes such as AP-1. NGF stimulation of PC12 cells is accompanied by ROS production and inhibiting this ROS blocks the adoption of a neural fate (Suzukawa et al., 2000). This study did not directly prove the involvement of NOX in this process, but the authors did show that a dominant negative Rac1 also blocks ROS production and neuronal differentiation. Therefore, it is possible that a Rac1-dependent NOX isoform is involved in the induction of PC12 cells to a neuronal fate.

NOX activity has also been linked to brain development. The prenatal administration of apocynin led to gross morphological changes in the rat cerebellum. ROS production was reduced in the cerebellum of inhibitor-treated rats, and cerebellar folia were underdeveloped as a result (Coyoy et al., 2013). Accordingly, rats treated with apocynin showed decreased motor coordination indicative of cerebellar dysfunction. Recall that NOX2 promotes CGN maturation (Olguin-Albuerne and Moran, 2015). It is then reasonable to speculate that NOX inhibitor application may lead to the underdevelopment of the cerebellum by blocking NOX2-mediated CGN maturation.

1.6 Overview of experimental work

Our lab investigates cellular signaling involved in the growth and guidance of neuronal growth cones. Growth cones are specialized, highly motile structures that direct axons to their targets by receiving and interpreting extracellular signals. Therefore, axon guidance and the neuronal connectivity are dependent on the function of growth cones.

There is very little known about the role of NOX or even ROS in axonal growth and guidance. However, axon outgrowth and turning are driven by actin and microtubule-based cellular machinery and both of these proteins are redox sensitive. Furthermore, Mical, another ROS-generating enzyme, mediates axon guidance by direct oxidation of actin. Finally, signaling pathways that induce cell migration and cytoskeletal rearrangements in non-neuronal cells require NOX-derived ROS. The basic cellular machinery that drives motility in these cells is often conserved in growth cones. Our lab has previously shown that growth cones from cultured *Aplysia* (*Aplysia californica*) neurons are sensitive to changes in ROS. Specifically, we found that application of antioxidants led to decreased neurite outgrowth, disorganization of the actin cytoskeleton and slowed actin retrograde flow (Munnamalai and Suter, 2009). The first part of my study was to determine whether NOX-derived ROS are important for the outgrowth and overall viability of cultured *Aplysia* neurons (Chapter 3). In this set of experiments, we identified a NOX2-like protein in *Aplysia* neurons and showed that NOX activity is necessary for proper neurite outgrowth. Additionally, we showed that elements of the NOX2 complex colocalize with actin and depend on actin for transport.

In vivo, the proper function of growth cones leads to the formation of axon tracts and the establishment of neuronal connections. In addition to axon guidance, many events including, but not limited to cell migration, proliferation, stem cell maintenance and differentiation contribute to the larger process of neurodevelopment. Most of these cellular functions have been linked to ROS or NOX in non-neuronal cells. With this knowledge and having shown that NOX is important for neurite outgrowth, I investigated the impact of NOX on neurodevelopment.

Zebrafish (*Danio rerio*) are ideal for studying vertebrate neurodevelopment due to their transparent bodies and external fertilization that make them highly compatible with *in vivo* imaging. However, many NOX studies use mice and rats since they are mammalian systems that often translate well to humans. Despite the fact that rodents do not carry NOX5, the availability of NOX1-4 and DUOX2 knockout mice has contributed to their popularity (Altenhofer et al., 2012; Bedard et al., 2012). Additionally, it has been comparatively difficult to generate targeted mutations in zebrafish so the production of gene knockouts has been rare. However, the advent of site-specific mutagenesis strategies designed especially for zebrafish has made an already powerful developmental model even more so (Jao et al., 2013). It is now possible to precisely edit the zebrafish genome and generate mutant lines using a process that is comparatively simple when measured against generating genetic mutants in mammals. Therefore, I used zebrafish embryos to study the role of NOX in neurodevelopment.

I first characterized *nox* gene expression in the zebrafish nervous system during the first two days development, a period that coincides with a great deal of neurodevelopment. Using quantitative PCR and extensive in situ hybridization, I discovered broad but dynamic expression of *nox1*, *nox2/cybb*, *nox5* and *duox* (Chapter 4). The expression domains were overlapping indicating the simultaneous presence of multiple *nox* genes in many tissues. While the results of this study did not provide information on cell-type specific *nox* expression, they do show that *nox* genes are expressed in the nervous system which may suggest a function.

I then investigated the function of NOX in neurodevelopment (Chapter 5). I found that optic nerve development was affected by the application of NOX inhibitors. Using

site-specific mutagenesis (CRISPR/Cas9) I determined that NOX2 (CYBB in zebrafish) mutants had similar defects in the optic nerve indicating that NOX2/CYBB was important for development. Finally, I found that NOX2/CYBB homozygous mutants displayed an expansion of retinal ganglion cells in the eye and mistargeting of axons to the midbrain.

In summary, the aim of this study was to investigate the role of NOX in axon outgrowth and neurodevelopmental. I first showed that NOX is expressed in *Aplysia* neurons and is important for neurite outgrowth. I then transitioned to *in vivo* work to show that *nox* genes are expressed in the zebrafish nervous system during development. Finally, I performed functional studies in zebrafish to show that NOX activity is necessary for retinal development and axon targeting.

CHAPTER 2. METHODS

2.1 General methods

2.1.1 Zebrafish housing and breeding

All animal work and experimental protocols were approved by the Purdue Animal Care and Use Committee. Zebrafish (*Danio rerio*) of the AB or *Tg(ath5:GFP)* line were maintained according to standard procedures (Westerfield, 2000; Hensley and Leung, 2010). NOX mutant lines were generated as described in section 2.4.7. To generate embryos, parental fish were placed into breeding tanks and separated by a clear divider overnight. The following morning, adults were moved to a new breeding tank with fresh water, the divider was removed and the breeding basket was tilted to force the parents into close proximity. Embryos were collected at 15-minute intervals to obtain cohorts of the same stage. Embryos were maintained in E3 medium at 28°C and staged as described prior to harvest (Kimmel et al., 1995). Medium was changed daily and dead embryos were removed to discourage bacterial and fungal growth. Between 12 and 23 hours post-fertilization (hpf) embryos used for live imaging, *in situ* hybridization, immunolabeling and microangiography were treated with 0.003% N-Phenylthiourea (PTU) (Sigma, St. Louis, MO) in E3 medium to inhibit melanization (Li et al., 2012b).

2.1.2 Mounting embryos in 1% low melting point agarose

Agarose for mounting was dissolved in E3 media or 1x PBS depending on the experiment. For 20 mL, 0.2 g of analytical grade low melting point agarose (Promega, Madison, WI, Cat. V2111) was added to 20 mL of solvent in an 18 x 150 mm glass culture tube. The tube was capped with foil to prevent evaporation and placed into a preheated water bath. The tube was vortexed every 5 minutes until the agarose completely dissolved. 10 mL aliquots were stored in 15 mL conical tubes at 4°C. Prior to mounting, an aliquot was microwaved briefly, no more than 10 seconds at a time, and vortexed until all the agarose had liquefied. It is important not to overheat or open the tube during heating to prevent molten agarose from escaping. The aliquot was then equilibrated in a 40°C water bath for 30 minutes prior to use.

For mounting, a yellow pipette tip was cut to create an opening large enough to accommodate a single embryo. Live embryos were anesthetized in 0.016% Tricaine methanesulfonate while fixed, immunolabeled samples were not anesthetized, and were transected posterior to the hindbrain to facilitate mounting. In either case, a single embryo was collected into the pipette tip. The embryo was carefully deposited into the tube containing molten agarose, and quickly recollected into the tip along with 20-30 µL of agarose. The embryo was then placed onto the dish or coverslip in a drop of agarose and positioned using a pin. Agarose solidifies within 1-2 minutes so embryos were positioned quickly. Once all samples were solidified, E3 media was added to prevent the samples from drying.

2.1.3 Preparation of 7.5% N-Phenylthiourea stock

This recipe is taken from the ZFIN Wiki (https://wiki.zfin.org/display/prot/PTU-2). PTU is very toxic so eye shields, gloves and face shields were worn during handling. 0.75 g of PTU powder (Sigma) was dissolved in 10mL of anhydrous DMSO (Sigma). This stock formulation was chosen because PTU dissolves quickly in DMSO without the need to heat or stir. PTU stock was then split into 1mL aliquots and stored at 4°C. 40 µL of 7.5% stock was used per 100 mL of E3 media to obtain a final concentration of 0.003%.

2.1.4 Determination of zebrafish Nox domains

Amino acid sequences for human NOX1 (Q9Y5S8), NOX2 (P04839), NOX5 (Q9Y5S8) and DUOX1 (Q9NRD9) were downloaded and manually annotated using domain and binding site information from UniProt (http://www.uniprot.org). Transmembrane helices, calcium binding domains, peroxidase-like domains and substrate binding domains were mapped to the human amino acid sequences using Vector NTI version 8.0 (InforMax, Inc. now Thermo Fisher). Corresponding zebrafish protein sequences were downloaded from GenBank (Nox1, NP_001095857.1; Nox2/Cybb, NP_956708; Nox5, XP_009296060.1; Duox, BAF33370.1). The sequences for each domain of the human protein were individually aligned to the full sequence of the zebrafish protein in Vector NTI. In all cases, the zebrafish sequences retained ≥80% similarity within domains. Outside of these domains, the sequences varied. Importantly,

transmembrane helices III and IV retained the critical heme-binding histidine residues confirming that these sites mapped to the human sequence. Mutant proteins sequences were predicted by translating the mRNA sequences, determined for each line, using the Vector NTI. The resulting amino acid sequences were aligned to the wild type sequence to determine which functional domains were lost. Figure 7.2 shows all of the predicted domains that remain in the NOX mutant lines generated thus far.

2.2 Methods for Chapter 3

2.2.1 Aplysia bag cell neuronal culture

Aplysia bag cell neurons were plated on coverslips coated with 20µg/ml poly-L-lysine (70-150 kDa) as previously described (Lee et al., 2008; Suter, 2011). Cells were kept in L15 medium (Invitrogen, Carlsbad, CA) supplemented with artificial seawater (L15-ASW: L15 plus 400 mM NaCl, 10 mM $CaCl_2$, 27 mM $MgSO_4$, 28 mM $MgCl_2$, 4 mM L-glutamine, 50 µg/ml gentamicin, 5 mM HEPES, pH 7.9) overnight at 14^{o} C. All reagents were from Sigma (St. Louis, MO) unless otherwise specified.

2.2.2 Live cell imaging and neurite outgrowth analysis

For live-cell imaging, a chamber containing *Aplysia* bag cell neurons cultured for 1 day was prepared as recently described (Lee et al., 2008; Suter, 2011). 0.1% DMSO

(vehicle control), 5 µM VAS2870 (Enzo Life Sciences, Farmingdale, NY) or 5µM celastrol (Cayman Chemical, Ann Arbor, MI) dissolved in L15-ASW medium were sequentially applied to live neurons, while cells were observed with a 60x 1.4 NA oil objective (plus 1.5x magnification) using a Nikon TE2000 Eclipse microscope (Nikon, Melville, NY; (Munnamalai and Suter, 2009). An OG590 long-pass red filter (Chroma Technology Corp., Bellows Falls, VT) was used to eliminate shorter wavelengths harmful in live cell imaging. Each drug was pre-incubated for 5 min before differential interference contrast (DIC) time-lapse imaging at 10 second intervals was performed. VAS2870 and celastrol were applied for a total of 20 min. The drug was then washed out with fresh L15-ASW. For retrograde flow analysis, three kymographs of DIC time-lapse sequences were constructed from each growth cone using line scans across the peripheral (P) domain using MetaMorph 7 software (Molecular Devices, Downingtown, PA). Retrograde flow rates of individual growth cones were determined by averaging 5 velocity measurements from each kymograph.

Neurite outgrowth experiments were carried out as described previously (Munnamalai and Suter, 2009). Neurons were imaged in L15-ASW medium 4 hours after plating using a 10x phase objective. The medium was then replaced with L15-ASW medium containing 0.05% DMSO or 2.5µM VAS2870 or 1µM celastrol. Cells were then incubated at 14°C for 24 hours prior to a second round of imaging. Drugs were then washed out extensively with fresh L15-ASW and cells were incubated at 14°C for an additional 24 hours prior to the collection of a final set of images. Total neurite length was calculated by summing the lengths of all neurites per cell. Only cells with total neurite length of $\geq$ 50µm were included in the analysis.

2.2.3 Immunolabeling and fluorescent imaging

After 1d in culture, bag cell neurons were fixed with 3.7% formaldehyde/400mM sucrose/ASW, pH 7.6 for 20 min at room temperature (RT). Following fixation, cells were permeabilized with 0.1% saponin in fixation solution for 15 min. After three washes with PBS/0.01% saponin, cells were incubated with 2 units/ml (1:100) Alexa 488-phalloidin (Invitrogen) in PBS/0.01% saponin for 20 min. Following three washes, cells were blocked with 5% BSA in PBS/0.01% saponin for 30 min. For detection of NOX2, the rabbit anti-gp91^{phox} antibody R2085 was incubated at 1:500 in blocking solution for 1h. This antibody was raised against a peptide corresponding to AA 548-560 in human gp91^{phox} (Quinn et al., 1989). For peptide blocking experiments we used the human NOX2 548-560 peptide KQSISNSESGPRG or the corresponding *Aplysia* NOX2 peptide KHCNRFSSSESK (XP_005090645). The NOX2 antibody was diluted at 1:500 in blocking solution together with the same dilution of either the human or *Aplysia* peptide (10 mg/ml stock; Genscript, Piscataway, NJ) over night at 4° C before the antibody was applied to fixed neurons. A mouse anti-p40^{phox} was used at a 1:200 dilution in blocking solution for 1 h at RT. This antibody was raised against full length human p40^{phox} (Gauss et al., 2002). apCAM was detected with the monoclonal antibody 4E8 diluted to 10 µg/ml in blocking solution (Suter et al., 1998). Following three washes, primary antibodies were detected by applying either 4 µg/ml Alexa 568 or Alexa 647 labeled goat-anti-rabbit or mouse secondary antibodies (Invitrogen) in the same blocking solution for 30 min at RT.

Fluorescent images were acquired in 20 mM n-propyl-gallate in PBS/80% glycerol pH 8.5 on a Nikon TE2000 Eclipse microscope equipped with a 60X 1.4 NA oil

(plus 1.5x magnification) objective, an X-cite 120 metal halide lamp (EXFO, Mississauga, Ontario, Canada), appropriate fluorescence filter sets (Chroma, Bellows Falls, VT), Cascade II cooled CCD camera (Photometrics, Tucson, AZ) and MetaMorph 7 software (Molecular Devices, Downingtown, PA). Neuronal cell bodies were imaged by acquiring z-stacks with 10µm intervals on a Zeiss LSM 710 confocal microscope equipped with 488, 568 and 610 nm lasers and appropriate filters.

2.2.4 ROS imaging

For quantitative ROS imaging, we used a hydrogen peroxide (H_2O_2)-specific fluorescent dye Peroxyfluor-6 acetoxymethyl ester (PF-6) kindly provided to us by Dr. Christopher Chang, University of California, Berkeley CA (Dickinson et al., 2011). After one day in culture, growth cones were incubated for 20 min in the dark with artificial seawater (ASW) containing 5µM PF-6 (for H_2O_2 detection) together with 250nM Calcein Red-Orange AM (Invitrogen), a cell permeable fluorescent dye used as volume marker for ratiometric imaging (Li et al., 2009). Three washes with ASW were performed to remove free dye. Pre-treatment images (time 0) were captured using a Nikon TE2000 Eclipse microscope using a 480 nm excitation and 535 nm emission filter for PF-6 and a 575nm excitation and 610nm emission filter for Calcein Red-Orange. The growth cones were then treated with ASW containing 0.1% DMSO, 0.1 µM phorbol 12,13-dibutyrate (PDBu; a protein kinase C activator), 5 µM VAS2870 or a combination of PDBu and VAS for up to 15 min before a second set of images were taken of the same growth cones.

Average fluorescent intensities of both PF-6 and Calcein Red-Orange signals were measured in three regions in the growth cone periphery and then background-subtracted using MetaMorph software. Each PF-6 and Calcein Red-Orange growth cone measurement was then normalized by the average DMSO control value at the same time point to correct for experimental variability. The DMSO-normalized signals were then volume-corrected by dividing PF-6 values by the corresponding Calcein Red-Orange values. Volume-corrected PF-6 signals were calculated as percent changes of H_2O_2 levels at specific time points by dividing each value by the time 0 value.

2.2.5 Image Processing, Fluorescence Intensity and Colocalization Analysis

Photoshop CS3 extended (Adobe, San Jose, CA) was used for image processing and making videos. Canvas X **(**ACD Systems of America, Inc, Miami, FL) was used for final figure assembly. For quantification of NOX2 and $p40^{phox}$ signals, the average NOX2 and $p40^{phox}$ fluorescence intensities per unit area was determined in the growth cone P domain using MetaMorph 7.0. For quantification of $p40^{phox}$ colocalization with NOX2 or F-actin, each signal was thresholded at the level of the average intensity plus 10% for a given area. After thresholding, the colocalization analysis function in MetaMorph was used to determine the % area overlap of $p40^{phox}$ with either NOX2 or F-actin or the % area overlap of NOX2 with either $p40^{phox}$ or F-actin.

2.2.6 Statistical Analysis

Quantified data are presented as mean values ± SEM. STATISTICA 10 Academic software (StatSoft, Inc., Tulsa, OK) was used for statistical data analysis. Significant differences between two conditions were determined with Student's t-tests if data showed normal distribution. Comparison of multiple conditions was performed with a one-way ANOVA followed by Dunnett's T3 post-hoc test. Significance levels were labeled as follows: *P<0.05; **P<0.01; ***P<0.001; ****P<0.0001.

2.3 Methods for Chapter 4

2.3.1 Quantitative PCR

Total RNA was isolated from 12, 24, 36 and 48 hpf embryos with TRIzol reagent (Life Technologies, Carlsbad, CA). 36 and 48 hpf embryos were anesthetized with 0.016% Tricaine methanesulfonate (Sigma) prior to RNA isolation. First-strand cDNA was prepared using the polyA primers supplied in the SuperScript®III First-Strand Synthesis System (Life Technologies). Primer sets against *nox1*, *nox2/cybb*, *nox5,* and *duox*, *β-actin* and *ribosomal protein L13a* were designed to target exons using ProbeFinder software (version 2.50, Roche Diagnostics, Indianapolis, IN). See Table 2.1 for a summary of primer sequences. For each gene and each stage, samples were analyzed in three independent wells in a single 96-well plate. The experiment was repeated with two

biological replicates of total RNA isolated from independent cohorts of embryos. Samples were run in a LightCycler96 (Roche Diagnostics, USA) for 35 cycles, and the relative expression levels were analyzed with the accompanying software (version 1.0.0.1240; RRID: rid_000088). Relative expression levels were calculated using the cumulative ratio of the cycle threshold of the target gene to the cycle threshold of two reference genes (*rpl13a* and *beta-actin*). These two genes were chosen as they show the most consistent expression pattern of commonly used reference genes (Tang et al., 2007). These calculated values were then normalized against the relative expression value for *nox2/cybb* at 12 hpf. *nox2/cybb* was chosen for normalization because of the stability of expression throughout the testing period. One-way ANOVA and direct comparisons via Dunnett's post-hoc analyses were carried out using GraphPad Prism software version 6.05 (RRID: rid_000081).

Table 2.1: Quantitative PCR primers

Gene	Gene ID	Primer	5' to 3'
nox1	NM_001102387.1	Forward	GCTCCAAGACTCCAGTGAATTA
		Reverse	GACCCGCAATACTGGTGAATA
nox2/cybb	NM_200414.1	Forward	CTTTCGTTATGAAGCGGTGATG
		Reverse	GGTTCTCCTGGACGTGTTTAT
nox5	XM_009297785.1	Forward	TCATGTGCCGCTATCGTATG
		Reverse	CCACCTTCCTCAGCTTCATT
duox	XM_001919359.5	Forward	CCTGGGAGGACTTTCACTTTC
		Reverse	CTTGTGCTGTCTGCCTAGTT
Rpl13a	NM_212784.1	Forward	TCCTCCGCAAGAGAATGAAC
		Reverse	TGTGTGGAAGCATACCTCTTAC
β-actin	NM_007393.3	Forward	CCTTCCAGCAGATGTGGATTAG
		Reverse	TGAAGTGGTAACAGTCCGTTTAG

Gene IDs are taken from GenBank.

2.3.2 *in situ* hybridization

Probe sequences were amplified from 3 day-old zebrafish cDNA, prepared as described above, and cloned into the pGEM-T Easy vector (Promega, Madison, WI). Primers used for amplification are indicated in Table 2.2. Probe sequences were selected by aligning the zebrafish *nox* genes, and identifying isoform-specific regions. Each prospective sequence was then used as the query for a BLAST search against the zebrafish RefSeq RNA database. The selected probes did not align to any other gene besides the target. The sizes of the riboprobes are as follows: *nox1*- 207 nucleotides (NM_001102387.1 position 645-851), *nox2/cybb*- 207 nucleotides (NM_200414.1 position 719-925), *nox5*- 202 nucleotides (XM_009297785.1 position 512-713) and *duox*- 1000 nucleotides (XM_001919359.5 position 1013-2012). Probe-containing vectors were then linearized, and riboprobes synthesized using the DIG RNA Labeling Kit (Roche Diagnostics) and purified with 4M LiCl (Sigma) precipitation.

The *in situ* hybridization protocol was adapted from previous reports (Thisse and Thisse, 2008; Hensley et al., 2011). Whole-embryos were anesthetized in 0.016% Tricaine methanesulfonate (Sigma) at 24, 36 and 48 hpf before fixation in 4% paraformaldehyde in PBS (Sigma). Samples from the same time-point were processed together. The samples were then dehydrated stepwise in methanol (30%, 50% 70%, 100%), digested with 10 µg/mL Proteinase K (Worthington Biochemical Corp., Lakewood, NJ) for 5 min (24 hpf), 12 min (36 hpf) or 20 min (48 hpf), and pre-hybridized in hybridization buffer (50% formamide, 5x saline sodium citrate (SSC), 0.1% Tween 20, 5 mg/mL torula RNA, 50 µg/mL heparin) overnight at 65°C. Embryos were

then incubated overnight with 100 ng of riboprobe in 0.5 mL of hybridization buffer at 65°C. Excess and imperfectly bound probes were then removed by washing twice with 50% formamide/2x SSCT (SSC, 0.1% Tween 20) at 65°C, once in 2x SSCT and twice in 0.2x SSCT. Finally, embryos were washed twice with PBST (1x PBS, 0.1% Tween 20). Anti-digoxigenin (DIG) antibodies (Roche Diagnostics) were pre-adsorbed by diluting 1:1000 in blocking solution (2 mg/mL bovine serum albumin, 2% normal sheep serum, 1x PBST) containing ≥ 50 embryos of various stages overnight at 4°C on a shaker. RNA-hybridized embryos were incubated in blocking solution for 2 h at room temperature. DIG-containing riboprobes were labeled overnight at 4°C on a rocker with pre-adsorbed anti-DIG antibody diluted 1:3 in blocking solution. Excess antibody was removed with five washes in PBST and three washes in staining buffer (100 mM Tris pH 9.5, 50 mM $MgCl_2$, 100 mM NaCl, 0.1% Tween 20, 1 mM levamisol). The colorimetric reaction was carried out by incubation in nitro blue tetrazolium/5-bromo-4-chloro-3-indolyl-phosphate (Sigma) diluted in water at room temperature until slight color was visible in the sense control samples. The incubation times were kept consistent among time points for each gene (*nox1* for 3 h, *cybb* for 3 h, *nox5* for 4 h and *duox* for 2.5 h). Non-specific signals were washed out with a series of methanol washes (30%, 50% 70%, 100%) and a two-min incubation in benzyl alcohol/benzyl benzoate solution (2:1). Finally, the destained embryos were rehydrated with a series of methanol washes (100%, 70% 50%, 30%) and three washes in PBST.

Labeled embryos were stored in 4% paraformaldehyde in PBS at 4°C and imaged as whole-mounts on a microscope slide in 3% methylcellulose using an Olympus SZX16 stereo microscope (Olympus Corp., Center Valley, PA) with an SDF PLAPO 1xPF

objective prior to being embedded in blocks of Tissue Freezing Media (Triangle Biosciences, Cincinnati, OH). A series of 10 µm transverse sections was collected from the most anterior region of the embryo through the spinal cord using a Leica CM 1510S cryostat (Leica Biosystems, Buffalo Grove, IL). Sections were mounted on microscope slides in VectaMount permanent mounting medium (Vector Laboratories, Burlingame, CA). Cryosections were imaged on an Olympus BX51 upright microscope at with UPlanFL 10x/0.3 and UPlanS Apo 20x/0.75 objectives, respectively (Olympus Corp.). Images from both microscopes were captured using a SPOT RT3 2.0Mp Slider CCD camera (SPOT Imaging Solutions, Sterling Heights, MI). At minimum, five individual samples were processed for each gene and time-point combination.

Table 2.2: PCR primers used to amplify *in situ* probes

Gene	Gene ID	Primer	5' to 3'
nox1	NM_001102387.1	Forward	TGCTGGTTTAGTTTTCCACG
		Reverse	AGCAGCCGTTCACAAATGTA
nox2/cybb	NM_200414.1	Forward	CATTGGATTGGTGCTTCATG
		Reverse	CTCTCACAGACATACAGGAACATG
nox5	XM_009297785.1	Forward	ACAACAGTGGCTCCATCACA
		Reverse	CCGTACAGGCAAAGGAAGAAG
duox	XM_001919359.5	Forward	ATATAAAAGGAACAGGACGTGTCA
		Reverse	GAAGGTCTGGAAAACTTTCTTCTC

Gene IDs are taken from GenBank.

2.4 Methods for Chapter 5

2.4.1 Inhibitor treatment of live embryos

Chorions were removed from embryos at approximately 24 hpf (prim-5 stage) using sharp forceps. Embryos were then maintained at 28°C until they reached 32 hpf (prim-16 stage). E3 media was then replaced with media containing 2.5µM celastrol (Cayman Chemical, Ann Arbor, MI) dissolved in DMSO. Control embryos received media containing 0.1% DMSO alone. Embryos were then returned to the incubator for 4 hours after which they were washed extensively with fresh E3 media. Following drug treatment, embryos were returned to the incubator and maintained in E3 media containing 0.003% PTU.

2.4.2 Immunolabeling

At the indicated stages, samples were anesthetized in 0.016% tricaine and fixed overnight in 4% PFA/1x PBS at 4°C. All steps were carried out in 1.5mL microcentrifuge tubes unless specified otherwise. Embryos were then washed twice with 0.5mL PBT (1x PBS, 0.5% TritonX-100) at RT for ten minutes per wash. Next, samples were incubated in pre-chilled acetone for 30 (48 hpf), 40 (72 hpf), 50 (96 hpf) or 60 minutes (120 hpf) at -20°C. Samples were then washed four times with 0.5mL PBT for five minutes per wash. Samples were then incubated with 10µg/mL Proteinase K (dissolved in PBT) at RT (Worthington Biochemical Corp.). Proteinase K digestion times were 10 (48 hpf), 15 (72

hpf), 20 (96 hpf) or 30 minutes (120 hpf). Embryos were then post-fixed in 4% PFA/1x PBS for 30 minutes, and washed four times with 0.5mL PBT for 30 minutes per wash. Samples were then incubated with blocking solution (10% goat serum in PBT; Sigma) for 2 hours at RT. Mouse monoclonal antibody against zebrafish alcama, zn-8 (Zebrafish International Resource Center [ZIRC], Eugene, OR), was diluted 1:500 in blocking solution and spun at max speed for 30 minutes at RT. Samples were then incubated in primary antibody solution overnight at 4°C. The following day, samples were washed four times with 0.5mL PBT for one hour per wash. Secondary antibody, goat anti-mouse Alexa Fluor 488 (Thermo Fisher, Rockford, IL), was diluted 1:500 in blocking solution. The nuclear counterstain diamidino-2-phenylindole (DAPI) was added to the secondary solution at a 1:500 ratio (Thermo Fisher). Samples were incubated overnight in secondary antibody solution at 4°C. The following day, samples were washed four times with 0.5mL PBT for one hour per wash and stored at 4°C in the dark.

Immunolabeled samples were positioned on coverslips in 1% low melting point agarose dissolved in 1x PBS as described in section 2.1.2. A microscope slide was prepared by filling a grease ring with 70% glycerol/1x PBS. The coverslip containing samples was then inverted onto the microscope slide, and pressed down to seal onto the grease ring. Excess 70% glycerol/1x PBS was aspirated and the slide was cleaned with glass cleaner. Z-stacks were collected at 1µm intervals using a Zeiss LSM 710 inverted scanning confocal microscope equipped with a 40x LD C-Apochromat 1.1 NA W Korr M27 objective (Zeiss USA, Thornwood, NY). Panels showing zn-8 labeling are maximum intensity projections while DAPI panels show a single optical section. Maximum intensity projections were created using ImageJ software (Schneider et al.,

2012) and additional image processing was performed with Photoshop CS3 extended (Adobe, San Jose, CA).

2.4.3 Live-imaging of transgenic lines

We used *Tg(ath5:GFP)* embryos to visualize RGCs and RGC axons in live embryos (Poggi et al., 2005). Samples were anesthetized in 0.016% tricaine methanesulfonate (Sigma) and mounted in 1% low melting point agarose on 35mm glass-bottom dishes. Dishes were then filled with E3 media containing 1x tricaine. Images were acquired from the anterior perspective showing the eyes and optic chiasm on a Nikon TE2000 Eclipse microscope equipped with a 10x Plan Fluor 0.3 NA oil objective, an X-cite 120 metal halide lamp (EXFO), appropriate fluorescence filter sets (Chroma), Cascade II cooled EM-CCD camera (Photometrics) and MetaMorph 7.8 software (Molecular Devices). Dorsal images showing the optic tecta were collected on a Zeiss LSM 710 laser scanning confocal microscope using a 20x Plan-Apochromat 0.8 NA M2 objective (Zeiss USA). For multi-day imaging, embryos were removed from agarose with a scalpel and forceps and maintained in 24-well plates at 28°C. The embryos were then remounted as described each subsequent day.

2.4.4 Hydrogen peroxide rescue

In celastrol-treated embryos, 2mM H_2O_2 was applied immediately following drug washout (section 2.4.1). Samples were maintained in H_2O_2-containing media until harvest.

We chose not to co-incubate celastrol and H_2O_2 due to possible complications arising from the direct oxidation of celastrol which may interfere with activity. gRNA-injected embryos were maintained in media containing 2mM H_2O_2 from injection to harvest. We tested the effects of prolonged exposure to H_2O_2 concentrations ranging from 1-5mM H_2O_2. Using *Tg(ath5:GFP)* embryos, we found that concentrations less then 2.5mM did not affect embryonic survival, morphology or optic nerve outgrowth (see Figure 5.2). We did find that H_2O_2-treated embryos showed more melanization compared to non- H_2O_2 exposed groups even when treated with 0.003% PTU. At later stages, this increased pigment caused dark spots in fluorescent images. This can be observed in Fig. 5.3H".

2.4.5 gRNA design and synthesis

gRNAs were designed with software from Massachusetts Institute of Technology (http://crispr.mit.edu/) that generates a list of scored candidate gRNAs as well as a list of scored potential off-target regions. Scores range from 0-100 with 100 being the top score. The algorithm used to calculate scores is not available, but it is clear that gRNAs with few, poorly matched off-targets have the best scores. Off-target scoring is determined by the number and position of mismatches. The higher the off-target score, the higher probability that the gRNA will bind. Coding sequences from the each of the zebrafish *nox* genes were input into the software to generate a list of candidate gRNAs. Each was then evaluated for their location in the target gene and the probability of off-target binding. We identified two gRNAs per isoform targeting early regions of the coding sequence and with a score ≥ 95 (Table 2.3 and shown in Fig. 5.3A & 7.2). In order for a gRNA to be

chosen, it's predicted off-target sites met the following criteria: score ≤ 0.5, ≥ 2 mismatches in the 11 nucleotides adjacent to the protospacer adjacent motif (PAM), ≥ 4 mismatches overall and ≤ 2 predicted exonic off-targets. These strict parameters were chosen to minimize the probability of off-target mutagenesis. A summary of the predicted off-target sites for each gRNA is given in Table 2.4.

Table 2.3: gRNAs targeting zebrafish *nox* genes

gRNA	Sequence (5'-3')	PAM	Score	Gene ID	Chr.
nox1 I	GGGAAAGGGATTAAGGTAAG	TGG	96	555604	14
nox1 II	GGTTTAGTTTTCCACGGCGC	AGG	98		
nox2/cybb I	GGAAACTTTGCTGCAAATGA	AGG	97	393386	11
nox2/cybb II	GGATTGGTGCTTCATGGAAT	CGG	97		
nox5 I	GGTGACCCATTCCAGCCAGC	GGG	99	100149800	25
nox5 II	GGGAGATCGCACTCTCTCGC	AGG	96		
duox I	GGTGCTGATCCTCCGAGGGT	TGG	95	565097	25
duox II	GGCAGACTGGGACACGAGCA	CGG	99		

gRNA sequences are listed along with the protospacer adjacent motif (PAM). Ideal PAM sites should are 'NGG'. Scores were assigned by the design software. Gene IDs refer to GenBank accession numbers.

We then used a set of zebrafish codon optimized plasmid constructs to transcribe the gRNAs and Cas9 mRNA (Jao et al., 2013). The full protocol for plasmid construction is given at http://www.addgene.org/crispr/Chen. Forward and reverse oligos matching the gRNA sequences shown in Table 2.3 were ordered from Integrated DNA Technologies (Coralville, IA). $TAGGN_{18}$ was added to the forward strand and $AAACN_{18}$ was added to the reverse strand to facilitate cloning. 2µL of 100mM stock from the forward and reverse oligos was combined with 2µL NEBuffer 1 (New England Biolabs, Ipswitch, MA) and 14µL ultrapure water. The tube was then heated in a thermal cycler to 95°C for 5 minutes, ramped down to 50°C for 10 minutes and held at 4°C.

Annealed oligos were cloned into the pT7-gRNA vector (Cat. 46759; Addgene, Cambridge, MA) by combining the following: 1 µl annealed oligos, 400ng pT7-gRNA vector, 1µl 10x NEBuffer 3, 1µl 10x T4 ligase Buffer, 0.5µl BsmBI, 0.3µl BglII, 0.3µl SalI, 0.5µl of T4 DNA ligase, and water to a total of 10µl. All buffers and enzymes were from NEB. The single-step digestion and ligation was carried out in a thermal cycler with three cycles of 20 minutes at 37°C and 15 minutes at 16°C. Samples were then incubated for 10 minutes at 37°C, 15 minutes at 55°C, and 15 minutes at 80°C.

The product was transformed into lab-made, chemically competent E. coli (DH5-alpha strain) according to the following protocol. 50µL of cells were thawed for < 5 minutes on ice. 2µL of the ligated gRNA vector was added to the cells and then incubated for 30 minutes on ice. Cells were then heat shocked in a water bath at 42°C for 30 seconds and returned to ice for 5 minutes. Cells were diluted in 300µL of pre-warmed SOC media and incubated at 37°C on a shaker for 1 hour. 50-100µL of the cell suspension was plated onto LB plates containing 50µg/mL carbenicillin (Sigma) and incubated at 37°C overnight. The following day, single colonies were picked and growth in 3mL liquid cultures overnight. DNA was isolated using the Wizard SV plus miniprep system (Promega), and analyzed via restriction digest and Sanger sequencing. pCS2-nls-zCas9-nls plasmid (Addgene Cat. 47929) was also transformed into bacteria and isolated via miniprep.

Plasmids were then linearized with BamHI (gRNA vector) or NotI (Cas9 vector) and purified using the Wizard SV PCR cleanup system (Promega). Cas9 mRNA was transcribed using the mMessage mMachine SP6 kit (Thermo Fisher), and gRNAs were

synthesized using the MEGAshortscript T7 kit (Thermo Fisher). DNA was then quantified using a NanoDrop Lite (Thermo Fisher).

Table 2.4: Potential off-target sites for gRNAs

gRNA	Sequence (5'-3')	PAM	Score	Gene ID	Chr.
nox1 I	***A*** GGAAAG***AT*** ATTAAGGT***G*** AG	GAG	0.2	567212	15
nox1 II	GGTTT***T*** GTTTTCC***CA*** GGC***T*** C	CAG	0	567798	2
nox2/cybb I	G***C*** A***G*** ACTTT***C*** CT***C*** CAAATGA	AGG	0.5	387260	8
nox2/cybb II	GGATTGG***G*** GCTTC***G*** TGGA***GG***	AGG	0	393852	7
nox5 I	GGT***CT*** CCCA***C*** TCC***T*** GCCAGC	AAG	0.2	568565	20
nox5 II	G***T*** GAGATCGCA***G*** TC***C*** CTCG***A***	AAG	0.1	368662	2
duox I	G***A*** TGCTG***T*** TCCTCCGA***T*** GG***A***	CAG	0.3	563429	5
duox II	GG***GG*** GACTG***C*** GA***A*** ACGAGCA	GAG	0.5	368415	12

Sequences for the predicted off-target sites along with the accompanying PAM. Bold characters represent mismatches. Scores were assigned by the design software. Gene IDs refer to GenBank accession numbers, and the chromosome on which each sequence appears is given.

2.4.6 gRNA injection

Microneedles were prepared by pulling 1mm borosilicate capillaries (World Precision Instruments, Sarasota, FL, Cat. 1B100F-4) with a single pull at 68°C on a vertical puller (Narishige Intl. Inc., East Meadow, NY, Model PP-830). The tips of the needles were broken with fine forceps under a stereomicroscope (AmScope, Irvine, CA, Cat. ST-6TP) to a width of 5-10µm. The injection mix was prepared by diluting the gRNA to 90-120ng/µL and Cas9 mRNA to 150ng/µL in a solution containing phenol red (1:10, Sigma) as a tracer. The injection needle was filled with 1-2µL of injection mix using a narrow pipette tip and secured into the micromanipulator (World Precision Instruments).

Embryos were collected as described in section 2.1.1, and transferred to injection molds consisting of 1.5% agarose in E3. One nanoliter of a mix containing 90-120ng/µL gRNA and 150ng/µL Cas9 mRNA was injected into single-cell embryos. After injection, the embryos were collected in petri dishes and maintained at 28°C. Dead embryos were removed the following day and media was changed daily.

2.4.7 Genotyping

Genomic DNA was isolated from 72 hpf tail biopsies (Wilkinson et al., 2013) or whole embryos (Meeker et al., 2007). Tail biopsies were performed by first anesthetizing embryos in 0.016% Tricaine. Embryos were then placed onto the lid of a petri dish, and a small region of the tail was cut with a clean scalpel. The embryo was then placed into one well of a 24-well plate filled with fresh E3 for recovery. The tail biopsy was transferred into a 0.5mL tube containing 13.5µL of 50mM NaOH with a clean 10µL pipette. Fish can be maintained in the 24-well plate up to 5 days post-fertilization. Whole embryos were anesthetized and directly dissolved in 50mM NaOH. In either case, samples in 50mM NaOH were incubated for 10 minutes at 95°C. One-tenth volume of 1M Tris HCl pH 8.0 was added to neutralize, and the samples were stored at -20°C. DNA was then quantified using a NanoDrop Lite (Thermo Scientific, Wilmington, DE). 5-10ng of DNA was used for PCR amplification using GoTaq Flexi polymerase (Promega).

Table 2.5: PCR primers for genotyping

gRNA	PCR primer sequence (5'-3')	Product length (bp)
nox1 I	ACA GTT TAG AGG GTG AAG AC	143
	CTC TGA CAG GAC TGG TTT A	
nox1 II	GTA CAC GCA TCA CCT CTT C	139
	TTG GAC GAA AGC GTC TG	
nox2/cybb I	CCC GAT AGC TTA CGA TAA CAA A	105
	CTC TCG ATC TCA TCT CCT GAT	
nox2/cybb II	GAA TAG AAG CAA ACC CTC ACC	109
	GTC ATC CGA AGG TCC TAC TT	
nox5 I	AATTTCACCCCTCACCATCC	903
	GACATGTTTCTTCTGACACAAC	
nox5 II	AAT GTG ATG GAG CCA CTG	142
	CTA TAG ACC CAG ATG AGT TGC	
duox I	TCT CTG GTC CGT CTG TAT C	143
	ACG CTT CTG TTC TTG TGG	
duox II	GTC TCC AAC TCT TCA CAG C	105
	GTA TAC ACG CAC CTG TGT C	

Genotyping was done using a gel based method that was previously published (Zhu et al., 2014). Briefly, gRNA target regions were amplified via PCR using the primers listed in Table 3. Following PCR amplification, samples were heated to 95°C and allowed to cool for 10 minutes at RT. Samples were then loaded onto a 15% acrylamide gel (29:1 acrylamide:bis ratio, Bio-Rad Laboratories, Hercules, CA) without SDS and run for 2.5 hours at 150V. Gels were stained with 50µg/mL ethidium bromide (Sigma) for 10 minutes to visualize DNA bands. Heteroduplexes indicative of heterozygous mutants or chimeras exhibited slower electrophoretic mobility as described previously (Zhu et al., 2014). In addition, we were able to reliably distinguish wild type and homozygous mutants due to the electrophoretic shift as a result of DNA deletions (data not shown; see Fig. 4A for a mutant sequences). For each set of PCR primers, the gel-based method described here was initially verified with Sanger sequencing to ensure reliability.

2.4.8 Generation of stable mutant lines

NOX2/CYBB gRNAs and Cas9 mRNA was injected into embryos from a cross of AB strain, wild type fish. The injected embryos were genotyped via tail biopsy, and mutants were raised to adulthood. Adult injectants were outcrossed with an unrelated AB line, and the resultant embryos were again genotyped via tail biopsy at 72 hpf. DNA from heterozygotes showing the formation of heteroduplexes on acrylamide gels was re-amplified and purified with the Wizard SV Gel and PCR Clean-Up System (Promega). Purified DNA was then cloned into the pGEM-T Easy vector (Promega) for sequencing. Mutant sequences were confirmed with at least three technical replicates showing the same mutation from an individual larva. We then used Vector NTI (Thermo Fisher) to determine the resulting amino acid sequences, and these were aligned to the wild type protein sequences. Heterozygous larva carrying mutations leading to truncated NOX2/CYBB proteins were used to found lines by outcrossing with AB strains to achieve a stable population of *nox2/cybb*$^{+/-}$ adults. *nox2/cybb*$^{-/-}$ embryos were produced by crossing these heterozygous lines. Homozygous, *nox2/cybb*$^{-/-}$, embryos used for analysis were identified via gel-based genotyping and/or Sanger sequencing.

2.4.9 Quantification of retinal and tectal anatomy

Length and area measurements were performed on raw images using MetaMorph 7 software (Molecular Devices). Optic nerve thickness was measured 5-10µm medial to the ganglion cell layer (Figure 5.1A). Two measurements were taken per embryo and

these were averaged to produce single value per sample. Area of the GCL was measured from single images (*Tg(ath5:GFP)*) or max intensity projections from 10, 1µm optical sections centered on the optic nerve (zn-8 labels). Retinal areas were measured from phase images (*Tg(ath5:GFP)*) or a single 1µm optical section from the DAPI channel centered in the optic nerve (zn-8 labels). GFP- or zn-8-positive area measurements were divided by the corresponding total retinal area to obtain the values reported. Again, two values were averaged per embryo. Tectal area was measured from maximum intensity projections compiled from 25-30, 1µm optical sections. An example of the measured area of one tectum is shown in Figure 5.1I. Areas from the left and right tecta were averaged to produce a single value for each embryo. Line scans of zn-8 fluorescent intensity in the optic tectum were performed with MetaMorph 7 software using raw, maximum intensity projections from 30-35, 1µm optical sections through the midbrain. Lines were drawn from ~10µm outside of the sample to a depth of ~250µm (72 hpf) or 300µm (120 hpf) into the midbrain. Average intensity was collected from 25 pixels on either side of the line. Examples of the position of the line scans is shown in Figure 5A & D. Graphs of average intensity along the length of each line scan were produced using GraphPad Prism software version 6.05. Integrated intensity values were calculated from the area under the curve for each condition.

2.4.10 Statistical analysis

Data sets were analyzed using GraphPad Prism software version 6.05 (GraphPad Software, Inc, La Jolla, CA). All raw data was assessed for normality using the

D'Agostino-Pearson omnibus test included in GraphPad. All data displayed a normal distribution ($p \geq 0.05$), and no transformations were necessary. Outliers were automatically identified and removed using the ROUT algorithm with a Q-value of 1%. In all cases, ≤ 2 outliers were identified per group. Since all data sets contained three or more groups, one-way ANOVA was used to identify differences among means, and p-values less than 0.05 were considered significant. Corresponding F statistics and p-values are reported in the Results section. If a significant difference was detected with the ANOVA, the Tukey HSD method was used for multiple comparisons among groups or the Dunnett's test was used for specific comparisons to a control. The test used is specified in the figure legend. Tukey or Dunnett's adjusted p-values are displayed in the figures and the Results section. Graphs in Chapter 5 show mean ± standard deviation for each group.

2.5 Methods for Chapter 6

2.5.1 SiR-actin and SiR-tubulin labeling

NIH/3T3 fibroblasts were seeded at 3000 cells per cm^2 on uncoated 35mm glass bottom dishes. Media was DMEM (Thermo Fisher) supplemented with 10% calf serum, Pen/strep, 20mM HEPES and 20mM L-glutamine (all from Sigma). The cells were allowed to adhere for 6-10 hours at 37°C in a humidified incubator with 5% CO_2. Once the cells start to become adherent, media was replaced with 2-3mL of media containing

SiR-actin or SiR-tubulin probes at 100-200nM. The dishes were then maintained in the incubator for ~12 hours and imaged using a Nikon TE2000 Eclipse microscope equipped with a 60X 1.4 NA oil (plus 1.5x magnification) objective, an X-cite 120 metal halide lamp (EXFO), appropriate fluorescence filter sets (Chroma), Cascade II cooled CCD camera (Photometrics) and MetaMorph 7 software (Molecular Devices).

2.5.2 Dissociated neuronal culture

Protocol was modified from Chen et al. 2013. At 33-34 hpf embryos from the transgenic *Tg(ath5:GFP)* line were sterilized with 70% ethanol and then transferred to a new dish containing sterile E2 media (15mM NaCl, 0.5mM KCl, 1mM $MgSO_4$, 0.15mM KH_2PO_4, 0.05mM Na_2HPO_4,1.0mM $CaCl_2$, 0.7mM $NaHCO_3$). Chorions were removed with sharp forceps and embryos were sacrificed by decapitation. Whole eyes were extracted, triturated 20-30 times in L15 media (Invitrogen, Carlsbad, CA) supplemented with 2% FBS, 0.4% pen/strep, and 12.5% saline solution (10 mM D-glucose, 5 mM Na-pyruvate, 1.26 mM $CaCl_2$, and 32 mM HEPES, all from Sigma) Individual cells were then plated on coverslips pre-coated with 0.5 mg/ml poly-D-lysine (70-150 kDa) (Sigma) and 20 µg/ml laminin (Sigma). Cells were maintained in supplemented L15 medium overnight at room temperature.

2.5.3 Measurements of neurite outgrowth in cultured neurons

For live-cell imaging, coverslips containing overnight retinal cultures were transferred from culture dishes to a custom-made open imaging chamber described previously (Suter, 2011). Prior to imaging, media was replaced with serum-free L15. Imaging was performed with the Nikon TE2000 Eclipse microscope and Cascade II cooled CCD camera described above. A 60x 1.4 NA oil objective (Nikon) and an OG590 long-pass red filter (Chroma Technology Corp.) were also used for this set of experiments. Media was replaced with 1-2mL of serum-media containing nerve growth factor (NGF, 20ng/mL), netrin-1 (Netrin, 250ng/mL) and semaphorin 3E (Sema3E, 5µg/mL). Controls received fresh serum-free media. After a 15 minute pre-incubation, initial DIC images were acquired (time 0 minutes). Additional images were acquired at 20, 40 and 60 minutes. Using MetaMorph 7.8 software, neurite lengths were measured from the base of the cell body to the tip of the growth cone lamellipodia on cells having processes $\geq 15\mu m$. Neurite growth rates of individual cells were determined by subtracting the length at time 0 from the length at time 60 and dividing the difference by the elapsed time.

2.6 Methods for Chapter 7

2.6.1 Microangiography

Methods are adapted from published protocols (Hoffman et al., 2012). A detailed protocol can be found at: http://zfish.nichd.nih.gov/Intro%20Page/angiography.html. Embryos were collected as described in section 2.1.1. Microneedles were prepared by pulling 1mm borosilicate capillaries (World Precision Instruments) with a single pull at 68°C on a Narishige puller (Model PP-830). The tips of the needles were then broken with fine forceps under a stereomicroscope to a width of 5-10µm. Holding pipets were prepared by flame polishing 1mm capillaries in a Bunsen burner to a width of 0.2-0.5mm depending on the age of the embryos being injected. The injection mixture was prepared by dissolving 3kDa dextran-Texas Red (10% w/w; Thermo Fisher) in nanopure water containing 1% BSA. The solution was spun at maximum speed for 20 minutes, and the supernatant was distributed into 5µL aliquots and frozen at -20°C.

On the day of the injection, embryos were removed from chorions using sharp forceps and anesthetized in 0.016% Tricaine diluted in E3 media. The injection apparatus was assembled as shown in Figure 2.1. The holding pipet was secured into a micromanipulator (World Precision Instruments) on the left, and attached to a 1mL syringe. The injection needle was filled with 1-2µL of injection mix and secured in the micromanipulator on the right. The injection volume was calibrated to < 1nL in mineral oil by delivering short pulses with a pneumatic PicoPump with a foot pedal attachment (World Precision Instruments). An embryo was positioned with the lateral side of the

yolk touching the opening of the holding pipette. A small amount of suction was applied with the 1mL syringe to immobilize the embryo such that the ventral side is up. It is critical not to apply too much suction as this will destroy the embryo. Once secured, the needle was inserted into the sinus venosus and 1-2 small boluses are injected. The dye should be observed entering the heart, not the pericardium, and the injections may cause temporary cardiac arrest. If the heartbeat has not resumed within a few seconds, the embryo was discarded. Once the cardiac rhythm was established, dye was quickly injected 15-20 more times while ensuring that the heart continues to beat and the dye is moving through the bloodstream. The embryo was then released from the holding pipette by application of negative pressure and transferred to a dish containing fresh E3 for recovery. The injection was then repeated for the remaining embryos.

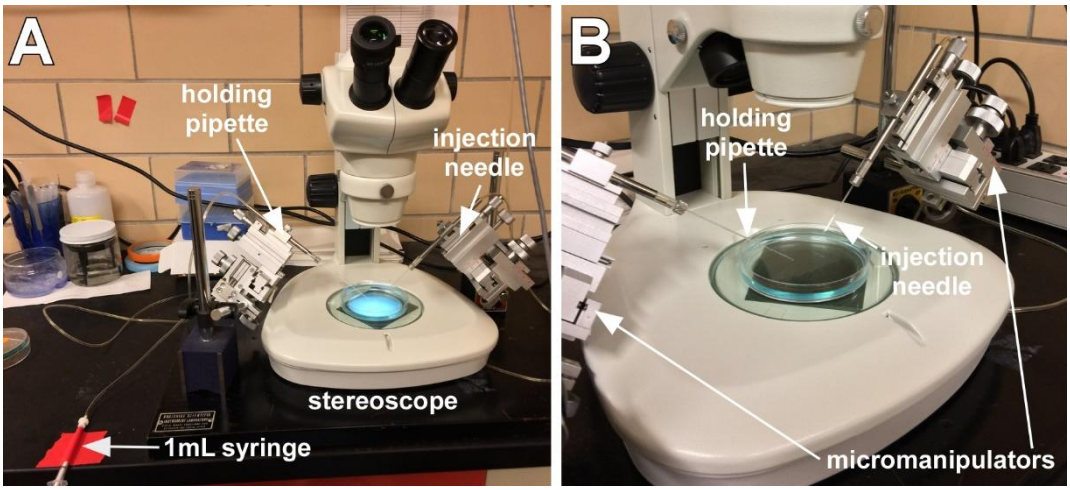

Figure 2.1: Microangiography setup (A) Photo showing the entire injection setup for microangiography. Injection needle is connected to a pneumatic PicoPump (not shown). Holding pipette connects to the 1mL syringe to apply pressure to immobilize embryos. (B) Higher magnification view of the injection dish showing the positions of the holding pipette and injection needle.

Once all the injection are complete (no more then 20-30 minutes), the embryos are again anesthetized in 0.016% Tricaine methanesulfonate and mounted in 1% low

melting point agarose on 35mm glass-bottom dishes. Dishes were then filled with E3 media containing 0.016% Tricaine methanesulfonate. Z-stacks were collected at 1µm intervals using a Zeiss LSM 710 inverted scanning confocal microscope equipped with a 20x Plan-Apochromat 0.8 NA M2 objective or a 40x LD C-Apochromat 1.1 NA W Korr M27 objective (Zeiss USA).Maximum intensity projections were created using ImageJ software (Schneider et al., 2012) and additional image processing was performed with Photoshop CS3 extended (Adobe).

2.6.2 Alcian blue staining

Methods were adapted from a protocol published in 2007 (Walker and Kimmel, 2007) An updated, detailed protocol is available here: https://wiki.zfin.org/pages/viewpage.action?pageId=13107315. 2% Alcian blue stock was prepared by dissolving 0.2g of Alican blue powder (Sigma) in 11.2mL of 50% ethanol. The solution was warmed and stirred gently for 30-60 minutes to allow the powder to dissolve completely. Once all of the powder dissolved, the solution was brought to 100mL with 95% ethanol. 10mL aliquots of the 2% stock were stored in parafilm-sealed 15mL conical tubes at room temperature. The parafilm is necessary to prevent evaporation.

5 day old embryos were anesthetized in 0.016% Tricaine methanesulfonate then fixed in 2% paraformaldehyde/1x PBS for 1 hour at room temperature. All steps were performed in 1.5mL centrifuge tubes. Embryos were washed twice for 10 minutes each in a solution containing 100mM Tris pH 7.5 and 10mM $MgCl_2$. The staining solution (0.04% Alcian blue, 10mM $MgCl_2$) was prepared by combining 10mL of 2% Alcian blue stock

with 5mL 1M Tris pH 7.5, 0.5mL 1M MgCl2, 32.6mL 95% ethanol and 1.9mL water. Wash solutions were replaced with 1mL staining solution, and the tubes were incubated overnight with gentle agitation at room temperature. The next day, embryos were washed for 5 minutes with 100mM Tris pH 7.5/10mM $MgCl_2$/80% ethanol. This was followed by one 5 minute wash in 50% ETOH/100mM Tris pH 7.5 and a final wash in 25% ETOH/100mM Tris pH 7.5.

After washing, 1mL of bleaching solution (3% H_20_2/0.5% KOH) was added to the tubes and incubated for 10 minutes without agitation. Tube lids were left open during this incubation. After bleaching, the samples were washed extensively with 25% glycerol/0.1% KOH until bubbles are no longer visible. Samples were then washed twice with 50% glycerol/0.1%KOH for 10 minutes each and stored at 4°C in the final wash solution.

Samples were imaged on a depression slide using an Olympus SZX16 stereo microscope (Olympus Corp.) with an SDF PLAN APO 1x objective at 3.2x magnification. Image processing was performed using Photoshop CS3 extended software. Pharyngeal arch labels in Figure 7.4 are derived from published literature (Schilling et al., 1996).

CHAPTER 3. LOCALIZATION AND FUNCTION OF NOX IN NEURONAL GROWTH CONES

This work described in this chapter was previously published. The text presented here is adapted, with permission, from the original publication to highlight my individual contributions (Munnamalai et al., 2014).

3.1 Introduction

As introduced in Chapter 1, this study is focused on the role of NOX enzymes in the growth and development of axons. One critical component of axon outgrowth is regulation of the cytoskeleton to drive leading edge protrusion. There is little known about the ways in which NOX-derived ROS contribute to axon outgrowth and neurite extension. A recent study found that NOX2 inhibition led to alteration in mouse hippocampal neuronal maturation, and neurite extension (Wilson et al., 2015). This certainly suggests that NOX2 plays a positive role in the regulation and promotion of neurite outgrowth in these cells. What that study lacks is a detailed description of the subcellular localization of NOX2 subunits. This is important since as I introduced in the previous chapter, one way to regulate ROS-mediated signaling is to maintain ROS production and downstream effectors in close approximation within the cell. Studies of

NOX subcellular localization may yield insights into downstream ROS effectors and signaling.

With the dearth of localization and functional studies focused on NOX enzymes in neurons, it is necessary to turn instead to non-neuronal cells. NOX subunits have previously been identified at sites relevant to adhesion and cell migration including focal adhesions and leading edge protrusions in non-neuronal cells (Ushio-Fukai, 2006). NOX-derived ROS have been implicated in fibroblast cell adhesion and (Chiarugi et al., 2003) migration in endothelial cells (Moldovan et al., 2000; Ushio-Fukai et al., 2002; Ikeda et al., 2005), HeLa cells (Nimnual et al., 2003; Kim et al., 2009), smooth muscle cells (Schroder et al., 2007; Lee et al., 2009) and keratinocytes (Kim et al., 2011a). Despite the many similarities between cell migration and neurite outgrowth, the role of NOX in the latter process is largely unexplored.

As introduced in Chapter 1, NADPH oxidase family members NOX1, NOX2, NOX3, and NOX4 are expressed in different portions of the nervous system, particularly in neurons and microglia (Sorce and Krause, 2009; Hernandes and Britto, 2012). Also reviewed in Chapter 1, NADPH oxidase-derived ROS have been implicated in hippocampal synaptic plasticity and memory formation (Kishida et al., 2006), NMDA receptor activation (Brennan et al., 2009), nerve growth factor induced neuronal differentiation and neurite outgrowth of PC-12 cells (Suzukawa et al., 2000; Ibi et al., 2006), and neuronal apoptosis (Tammariello et al., 2000; Guemez-Gamboa and Moran, 2009). On the other hand, microglial cells and proinflammatory cytokine-treated neurons release NADPH oxidase-derived superoxide leading to neuronal toxicity (Barth et al., 2012), as described in Alzheimer's and Parkinson's disease (Sorce and Krause, 2009; Gao

et al., 2012). We have recently reported that ROS derived from NOX regulate F-actin organization, dynamics, and neurite outgrowth (Munnamalai and Suter, 2009); however, the exact subcellular localization and interactions of NOX with the actin cytoskeleton in neuronal growth cones have not been investigated.

Here, we report on the first localization of a NOX2-type NADPH oxidase in neuronal growth cones. NOX inhibition with VAS2870 or celastrol resulted in reduced retrograde F-actin flow and neurite outgrowth, confirming our earlier results. NADPH oxidase activation with a PKC activator resulted in increased ROS levels in the growth cone periphery. We found that the regulatory cytosolic subunit $p40^{phox}$ exhibited F-actin-association in unstimulated growth cones and little co-localization with plasma membrane-bound NOX2. Additional works presented here shows that upon growth cone stimulation with the cell adhesion protein apCAM, $p40^{phox}$ and NOX2 accumulated and co-localized at adhesion sites. In summary, these findings point towards an interesting bidirectional relationship between NADPH oxidase and the actin cytoskeleton in neuronal growth cones.

3.2 Results

3.2.1 NADPH oxidase inhibition impacts the actin cytoskeleton and neurite outgrowth

We previously reported that lowering cytosolic ROS levels in Aplysia neuronal growth cones by either a general radical scavenger, α-N-tert-butyl-phenylnitrone, or by

NOX inhibition via phenylarsine oxide and apocynin resulted in reduced actin content, impaired actin dynamics, and decreased neurite outgrowth (Munnamalai and Suter, 2009). Phenylarsine oxide is a highly potent inhibitor, but being a vicinal dithiol-binding reagent it is not exclusively specific to NOX (Le Cabec and Maridonneau-Parini, 1995; Jaquet et al., 2009). Apocynin is still widely used as NADPH oxidase inhibitor; however, there is now evidence that it may act as antioxidant and require the presence of myeloperoxidase to function as a NADPH oxidase inhibitor (Heumuller et al., 2008; Jaquet et al., 2009; Wind et al., 2010). To confirm that our previous results were indeed caused by reduced NADPH oxidase activity, we repeated oxidase inhibition experiments with one of the most specific chemical pan-NADPH oxidase inhibitors currently available, VAS2870 (ten Freyhaus et al., 2006; Wind et al., 2010; Altenhofer et al., 2012).

Treatment of *Aplysia* growth cones with 5 µM VAS2870 for 20 min reduced transition (T) zone ruffling, flattened the peripheral (P) domain, caused extension of the central (C) domain and filopodial lengthening when compared to DMSO control pre-treatment (Fig. 3.1 A-C). These effects were partially reversible 60 min following drug washout (Fig. 3.1D). NOX inhibition significantly decreased the F-actin content in T zone ruffles, as well as in filopodial actin bundles and lamellipodial actin networks in the P domain (Fig. 3.1 E-H). Treatment with 5µM VAS2870 reduced retrograde actin flow rates by 35% compared to DMSO pre-treatment (Fig. 3.1I; mean flow rates ± SEM were 4.6±0.1 µm/min in DMSO vs. 3.0±0.1µm/min in VAS2870). Flow rates nearly recovered to control values following drug washout. Total neurite length per neuron was strongly reduced in neurons treated with 2.5µM VAS2870 for a 24 h when compared to medium

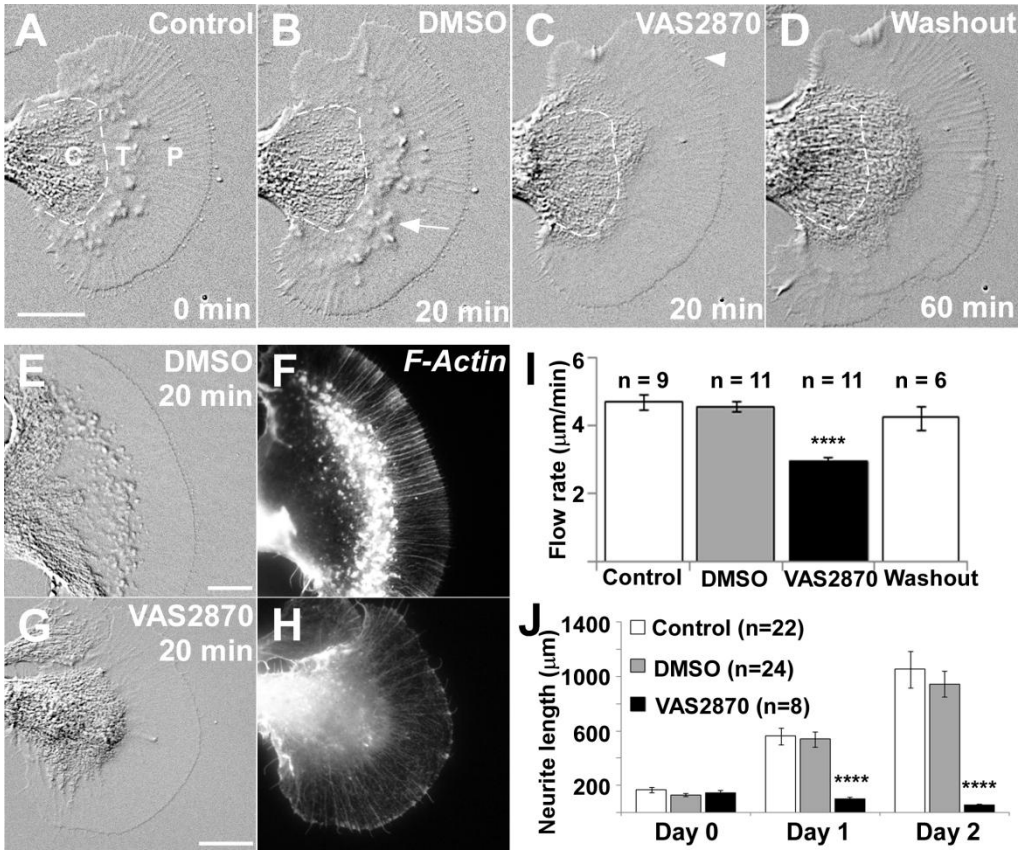

Figure 3.1: NADPH oxidase inhibition reduces F-actin content in growth cones as well as neurite outgrowth (A) DIC image of *Aplysia* bag cell neuronal growth cone cultured for 1d. C domain, T zone, and P domain, as well as C domain boundary (dashed line) are indicated. (B) Treatment with 0.1% DMSO for 20 min did not noticeably affect growth cone morphology or motility. Arrow points towards T zone ruffle. (C) Treatment with 5μM VAS2870 for 20 min caused flattening of the T zone and P domain as well as some extension of the C domain and filopodia (arrowhead). (D) Drug washout for 60 min partially reversed these effects, resulting in further growth cone protrusion. (E-H) 5μM VAS2870 for 20 min reduced F-actin content in the T zone and P domain, including in ruffles, filopodial bundles, and intervening lamellipodial networks. (I) NADPH oxidase inhibition by 5μM VAS2870 resulted in reduced retrograde flow rates (Mean flow rates ± SEM; n=11 growth cones; one-way ANOVA followed by Dunnett's T3 post-hoc test; ****P<0.0001). (J) NADPH oxidase inhibition by 2μM VAS2870 between day 0 and 1 reduced neurite outgrowth irreversibly when compared with medium or DMSO-containing medium. The drug was washed out between day 1 and day 2. Mean values of total neurite length per cell ± SEM are given for different times in culture: before drug application (day 0); 24h after drug treatment (day 1); and 24h after drug washout (day 2). n=number of neurons; one-way ANOVA followed by Dunnett's T3 post-hoc test; ****P<0.0001. Scale bars: 10 μm.

only or DMSO control conditions (Fig. 3.1J; 81% reduction compared to DMSO). Extensive drug washout over the following 24 h period did not reverse total neurite length values. This is likely due to the significantly longer drug incubation time when compared to the results of the 20 min VAS2870 treatments. Using a different NOX

inhibitor, celastrol (Jaquet et al., 2011), we observed similar effects on growth cone morphology, actin flow, and neurite outgrowth (Fig. 3.2A-D). In summary, we found that treatment of cultured *Aplysia* neurons with VAS2870 or celastrol resulted in similar effects as our previous approaches of NOX inhibition (Munnamalai and Suter, 2009), confirming our findings that NOX activity is critical for controlling actin organization and dynamics in growth cones as well as neurite growth.

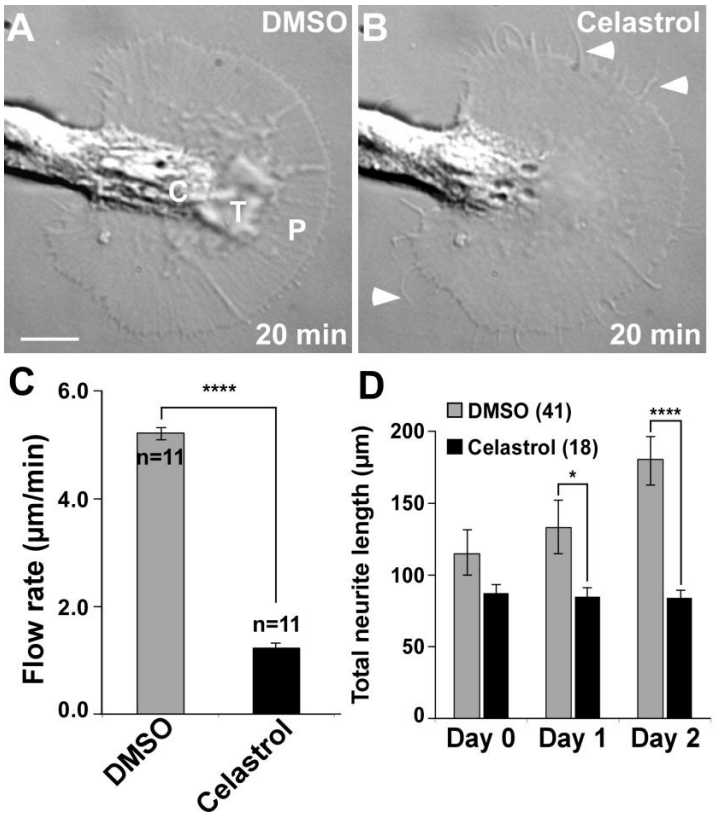

Figure 3.2: NADPH oxidase inhibition via celastrol reduces retrograde flow and neurite outgrowth
(A) DIC image of an *Aplysia* bag cell neuronal growth cone following a treatment with 0.1% DMSO for 20 min. C domain, T zone, and P domain are indicated. (B) Treatment with 5µM celastrol for 20 min caused flattening of the T zone and P domain as well as some extension of filopodia (arrowheads). (C) NADPH oxidase inhibition by 5µM celastrol resulted in retrograde flow rates that were reduced by 76% compared to DMSO control condition (Mean flow rates ± SEM; n=11 growth cones; Student's t-test; **** P<0.0001). (D) NADPH oxidase inhibition by 1µM celastrol between day 0 and 1 reduced neurite outgrowth irreversibly when compared with DMSO-containing medium. The drug was washed out between day 1 and day 2. Mean values of total neurite length per cell ± SEM are given for different times in culture: before drug application (day 0); 24h after drug treatment (day 1); and 24h after drug washout (day 2). n=number of neurons; Student's t-test; * = P<0.05, **** = P<0.0001. Scale bar: 10µm.

3.2.2 Localization of NOX2-type NADPH oxidase in neuronal growth cones

Although NOX1, NOX2, and NOX4 have been previously detected in cultured cerebellar granule neurons (Coyoy et al., 2008) and NOX2 additionally in hippocampal neurons (Tejada-Simon et al., 2005; Park and Jin, 2008), sympathetic neurons (Tammariello et al., 2000; Hilburger et al., 2005), and DRG neurons (Cao et al., 2009), None of these studies investigated the localization of these enzyme complexes specifically in neuronal growth cones. A previous lab member identified a NOX2-type NADPH oxidase complex in growth cones using antibodies raised against human homologs of the membrane-bound NOX2 (Quinn et al., 1989) and cytosolic $p40^{phox}$ subunits (Gauss et al., 2002). Western blotting of *Aplysia* CNS protein extracts with these antibodies detected a major band at the expected molecular weights of 75 kDa and 40 kDa, respectively (Fig. 3.3A). NOX2 proteins run between 73 and 91 kDa on SDS-PAGE depending on the species (Krijnen et al., 2003). The variations in molecular weight are believed to be caused by differences in glycosylation (Quinn et al., 1989; Gauss et al., 2002).

To confirm the specificity of the NOX2 antibody, I preincubated the rabbit anti NOX2 antibody with either the human peptide used for raising the antibody or the corresponding *Aplysia* peptide. Preincubation with either of these peptides significantly reduced the fluorescence intensity in the growth cone periphery (Fig. 3.3B). Immunolabeling of growth cones with NOX2 and $p40^{phox}$ antibodies revealed a punctate pattern of both proteins within growth cones (Fig. 3.3C-D). NOX2 labeling in the P domain is more uniform and dense than $p40^{phox}$ labeling, which is expected for a plasma

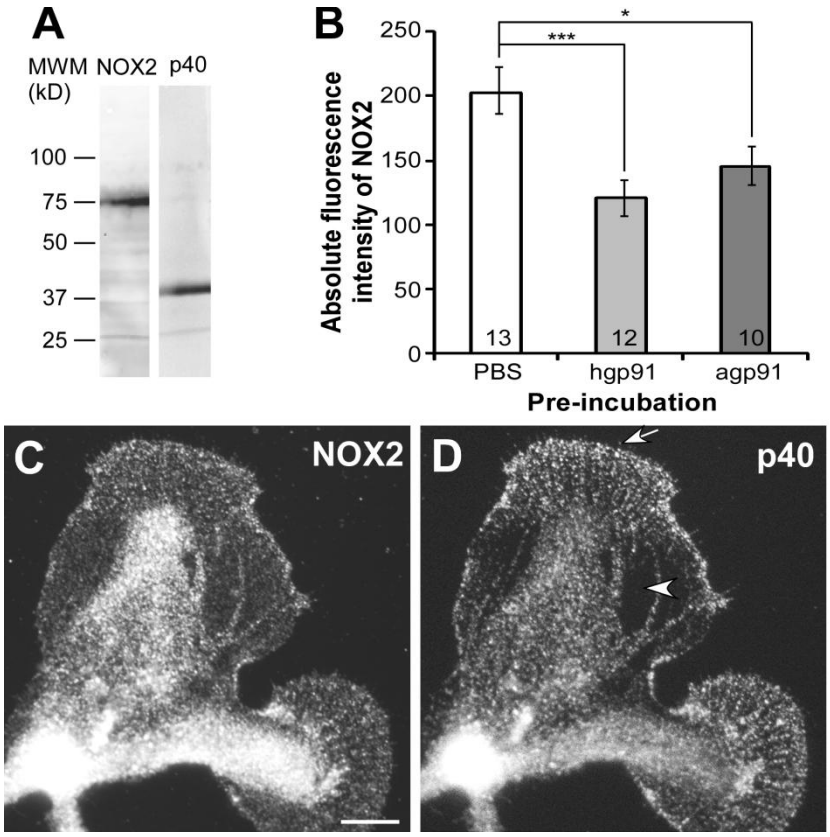

Figure 3.3: Localization of NOX2-type NADPH oxidase complex in *Aplysia* growth cones (A) Western blot of *Aplysia* CNS proteins detected by NOX2 and p40 antibodies. Each antibody detects a major band at the expected molecular weights of 75 kDa and 40 kDa, respectively. (B) Preincubation of the polyclonal rabbit anti-NOX2 antibody with either the human (hgp91) or the corresponding *Aplysia* peptide (agp91) reduced NOX2 labeling in the P domain of *Aplysia* bag cell growth cones by 40% and 28%, respectively, when compared to PBS preincubation. (C) Immunolocalization in cultured *Aplysia* bag cell growth cones revealed homogeneous NOX2 distribution in the P domain, suggesting plasma membrane-association, while the strong C domain labeling is indicative of vesicular association. (D) $p40^{phox}$ immunolocalization is somewhat less dense than NOX2 labeling. $p40^{phox}$ is prominent in the growth cone periphery including in filopodia (arrow). No labeling is found in very flat portions of the P domain (arrowhead). (D-G) VAS2870 lowers Number of growth cones are indicated; Student's t-test; * $P<0.05$, *** $P<0.001$. Scale bars: 10 µm.

membrane-associated protein. NOX2 signals were markedly higher in the C domain of the growth cone (Fig. 3.3C) compared to the P domain, which can be attributed to NOX2's association with vesicles. In the growth cone, localization of the cytosolic $p40^{phox}$ subunit differed from NOX2 in a few ways. First, $p40^{phox}$ exhibited a striking array-like localization (Fig. 3.3C), very similar to F-actin bundles in the P domain. Second, the labeling in the C domain was not increased as in the case of NOX2. Third,

hardly any $p40^{phox}$ was found in very thin growth cone regions that were clearly NOX2 positive (arrowhead in Fig. 3.3C and 3.6C).

NOX2 is expected to associate with the plasma membrane. Due to the thinness of growth cones, it is difficult to differentiate membrane associated and cytosolic proteins using immunolabeling. Instead, we found evidence for the expected plasma membrane association of NOX2 in unstimulated *Aplysia* neurons by confocal imaging of the large neuronal cell body (Fig. 3.4A). $p40^{phox}$ labeling was not enriched at the membrane in the cell bodies of unstimulated cells (Fig. 3.4B). NOX2 and p40phox positive structures also colocalized with actin in some cases (arrowheads in Fig3.4A'-F'). Collectively, these results demonstrate the presence of a NOX2-like and a $p40^{phox}$-like proteins in Aplysia neurons that can be detected with specific antibodies either by Western blot or immunolabeling.

3.2.3 NOX2 produces reactive oxygen in neuronal growth cones

NADPH oxidase produces superoxide, which can be converted quickly into H_2O_2, a ROS that has a longer half-life than superoxide and is likely involved in many ROS-mediated signaling processes (Bedard and Krause, 2007; Winterbourn, 2008). We used Peroxyfluor-6 acetoxymethyl ester (PF-6) as a H_2O_2-specific fluorescent dye (Dickinson et al., 2011) in combination with Calcein Red-Orange AM as a volume marker in order to perform ratiometric quantification of H_2O_2-levels in the growth cone P domain following activation and inhibition of NADPH oxidase (Fig. 3.5A-D). PF-6 signals were the highest in the C domain, specifically in mitochondria, a well-known intracellular ROS source, as

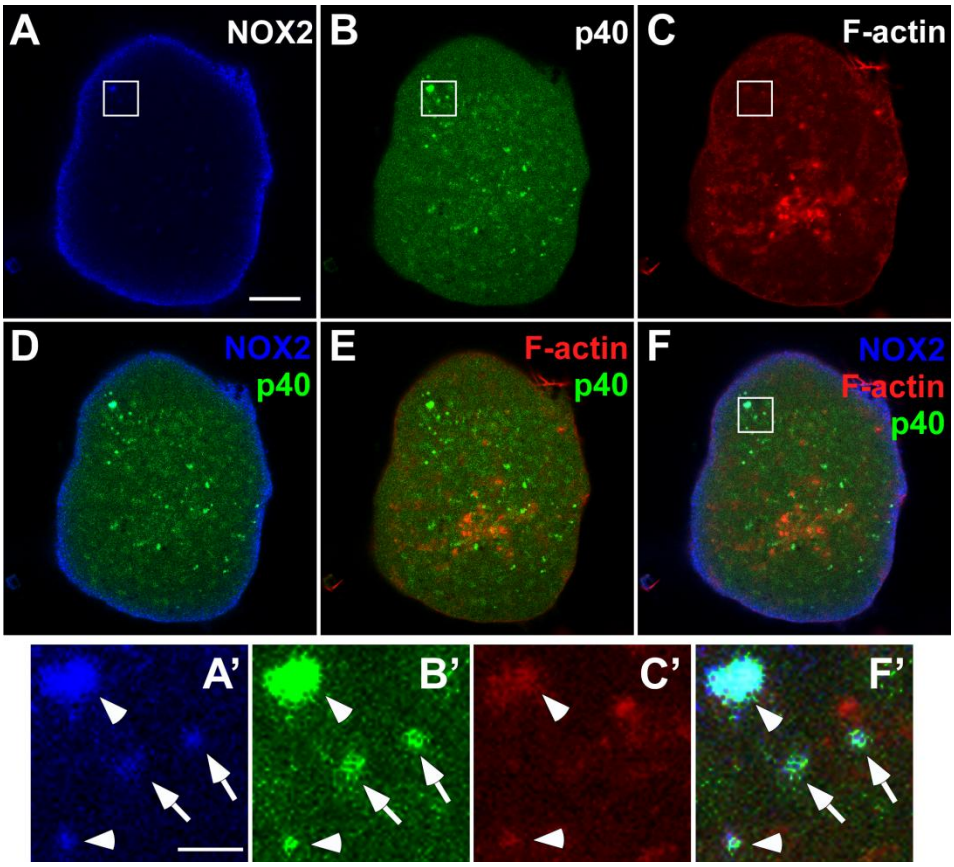

Figure 3.4: NOX2 and p40 exhibit distinct subcellular localizations in the cell body (A-C) Immunolabeling of Nox2 (A) and p40 (B) with phalloidin labeling of f-actin (C) in the cell body 10µm above the focal plane of the growth cone. (D and E) Dual-channel overlays of the images in A-C. (F) Triple-channel overlay of the images in A-C. (A', B', C' and F') Magnified views of the red boxes in A-C and F showing triple-labeled (arrowheads) and Nox2/p40-labled (arrows) puncta. Scale bar in A: 10µm, A': 2µm.

well as in T zone ruffles. NADPH oxidase inhibition with 5µM VAS2870 reduced H_2O_2 levels more than the control treatment with DMSO alone after 15 min (Fig. 3.5E; 30% reduction by VAS2870 vs. 16% reduction by DMSO), although these reductions were not significantly different (Student's t-test; P=0.12). Conversely, we used the phorbol ester phorbol 12,13-dibutyrate (PDBu) to activate PKC, which is known to stimulate activity of NADPH oxidase through phosphorylation of $p47^{phox}$ (Fontayne et al., 2002). Within 30 sec of PDBu application, H_2O_2-levels increased by 12±3%. This PDBu-induced rise in H_2O_2-levels could be significantly decreased by co-incubation with 5µM VAS2870 to

levels that were similar to basal H_2O_2-levels (Fig. 3.5F). In summary, these data confirm that NOX is functional in neuronal growth cones.

3.3 Discussion

This is the first report on subcellular localization of NOX in neuronal growth cones. Expression of NOX1-NOX4 family members at the RNA and protein levels has been shown for various brain regions including cortex, cerebellum, hippocampus, as well as for peripheral ganglia (Sorce and Krause, 2009; Hernandes and Britto, 2012). NOX2 subunits have been localized in cultured neurons, such as hippocampal (Tejada-Simon et al., 2005; Park and Jin, 2008), cerebellar granule (Coyoy et al., 2008), sympathetic (Tammariello et al., 2000; Hilburger et al., 2005), and DRG neurons (Cao et al., 2009). However, most of these studies did not investigate the detailed subcellular distribution of NOX complex proteins. Here, we have shown that a NOX2-type protein is localized to the plasma membrane of *Aplysia* neuronal growth cones (Fig. 3.4A). Whether another type of NOX is also present in *Aplysia* growth cones remains to be investigated. NOX inhibition with VAS2870 or celastrol impaired actin organization and dynamics as well as neurite outgrowth, confirming our previous findings (Fig. 3.1 & 3.2; (Munnamalai and Suter, 2009). NOX activation increased H_2O_2 levels in the growth cone P domain, and this was partially blocked by a NOX inhibitor (Fig. 3.5F).

Since $p40^{phox}$ exhibited an F-actin-like distribution, previous lab members performed triple labeling with phalloidin, $p40^{phox}$, and NOX2 antibodies to determine a potential colocalization between $p40^{phox}$ and F-actin. Upon analyzing this raw data, I

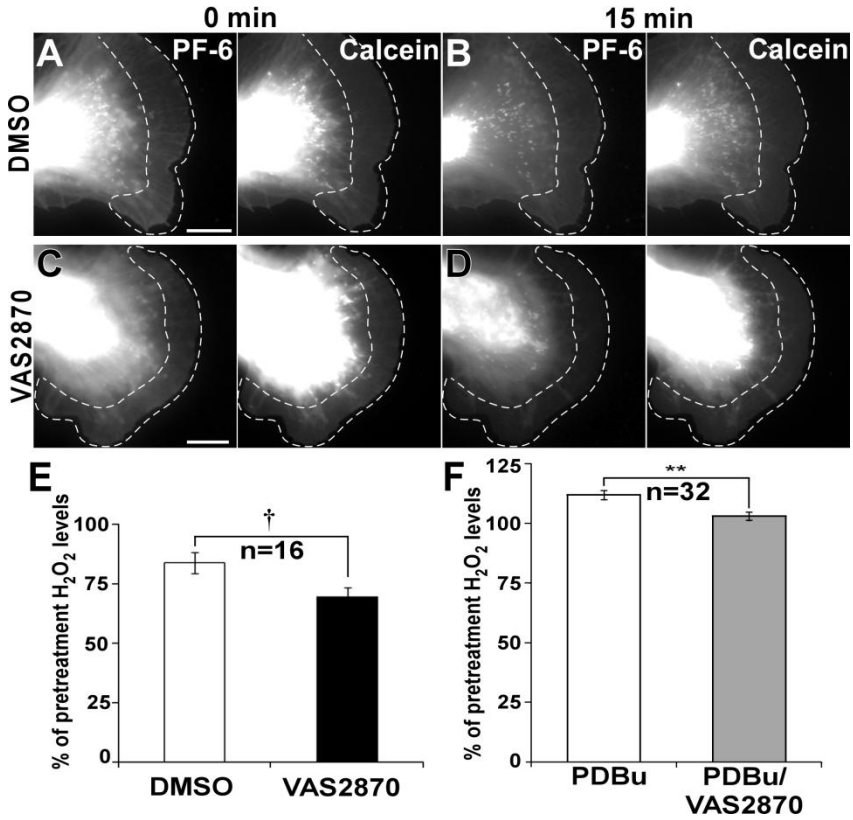

Figure 3.5: *Aplysia* growth cones produce reactive oxygen via NOX (A-D) VAS2870 lowers H_2O_2 levels in the P domain (indicated with dashed line). PF-6 signals were reduced in growth cones treated with 5 □M VAS2870 for 15 min when compared to DMSO control. Calcein red signals were used for volume correction. (E) Volume-corrected PF-6 signals after 15 min are shown as % of the pretreatment levels. DMSO: 84±4%; VAS2870: 70±8% (Mean values ± SEM; n=16 growth cones; Student t-test; †P=0.12). (F) Activation of NADPH oxidase increases H_2O_2 levels. Growth cones were treated with the protein kinase C activator PDBu (0.1 µM) to activate NADPH oxidase, or a combination of 0.1 µM PDBu and 5 µM VAS2870. Volume-corrected PF-6 signals measured after 30 sec were normalized against DMSO control values and presented as % changes of pretreatment values. PDBu increased H_2O_2 in the growth cone periphery to levels that were significantly higher than in growth cones treated with a combination of PDBu and VAS2870 (Average % changes in H_2O_2-levels ± SEM are given; n=32 growth cones; one-way ANOVA followed by Dunnett's T3 post-hoc test; **P<0.01). Scale bars: 10 µm.

found that in the growth cone P domain, $p40^{phox}$ signal exhibited only a partial overlap with NOX2. 38±2% of $p40^{phox}$ colocalized with NOX2, while 22±1% of NOX2 overlapped with $p40^{phox}$. The highest colocalization between $p40^{phox}$ and NOX2 was found in the neck of the growth cone, which consolidates into the axon, as well as in contact areas between two adjacent growth cones. $p40^{phox}$ exhibited higher colocalization

with filopodial F-actin bundles in the growth cone periphery, when compared to NOX2-colocalization with F-actin.

Additional work performed by other lab members was included in the original publication, but I will summarize it here. They observed variations in $p40^{phox}$ levels between growth cones, which correlated with F-actin content. Cytochalasin B significantly reduced the amount of $p40^{phox}$, but not NOX2, in the growth cone periphery. Cell fractionation and actin co-immunoprecipitation experiments confirmed a partial association of $p40^{phox}$ with F-actin. The cell fractionation studies were performed on total CNS lysates suggesting that the differential association of NOX2 and $p40^{phox}$ not only occurs in the growth cone but also in other regions of the cell. This was supported by my data showing the differential localization of NOX2 and $p40^{phox}$ in the cell body of Aplysia neurons (Fig. 3.4). Finally, these additional experiments found increased $p40^{phox}$/NOX2 co-localization at adhesion sites during apCAM-evoked neuronal growth. In summary, all of these findings provide evidence for a bidirectional functional relationship between NADPH oxidase activity and the actin cytoskeleton in neuronal growth cones, which may contribute to the control of neurite outgrowth.

Very little is known about NADPH oxidase signaling in neuronal development, particularly in axonal growth and guidance. Previous work from our lab and others suggested a role for NADPH oxidase-derived ROS in regulating neurite outgrowth (Suzukawa et al., 2000; Ibi et al., 2006; Munnamalai and Suter, 2009). A recent study showed that tail wound-derived H_2O_2 can promote regeneration of sensory axons in Zebrafish embryos (Rieger and Sagasti, 2011). Furthermore, we have shown that NADPH oxidase inhibition in *Aplysia* growth cones results in reduced F-actin content

(this study; Munnamalai and Suter, 2009). ROS have also been implicated in Rac1-dependent Ca^{2+} -release in *Aplysia* growth cones (Zhang and Forscher, 2009). Due to the short half-life and high reactivity of ROS, target proteins need to be close to the ROS source to establish signaling specificity (Ushio-Fukai, 2006). Consistent with this idea, we found NADPH oxidase localized in the growth cone periphery at sites where actin assembly occurs.

The present study is also interesting from an evolutionary point of view. While ancestral NOX2-, $p22^{phox}$ -, $p47^{phox}$ -, and $p67^{phox}$ -homologs have been identified for several invertebrate species including *Monosiga brevicollis*, *Nematostella vectensis*, *Strongylocentrotus purpuratus*, as well as the snail *Lottia gigantea*, no $p40^{phox}$ homolog has been identified in these species thus far, which has led to the conclusion that $p40^{phox}$ may have evolved later with the chordata (Kawahara et al., 2007a; Sumimoto, 2008). Very recently several predicted *Aplysia* NADPH oxidase-like sequences have been released to the NCBI database, including NOX2-like (XP_005090645), NOX5-like XP_005101964), DUOX1-like (XP_005108327), and DUOX2-like (XP_005106629). Our antibody results suggest that a NOX2-type NADPH complex with all membrane and cytosolic subunits including the regulatory subunit $p40^{phox}$ already evolved with the appearance of the molluscan clade. Other available antibodies against NOX2-type subunits did not detect proteins with high enough specificity (data not shown); thus, because of this limitation we were unable to detect other subunits of the NOX2-type complex in *Aplysia* growth cones thus far.

Our quantification of H_2O_2-levels following PKC activation revealed that the NADPH oxidase is functionally active in growth cones. VAS2870 abolished the fast

PDBu-stimulated increase in H_2O_2-levels in the growth cone periphery within 30 sec (Fig. 3.5I). Treatment of growth cones with VAS2870 alone for 15 min resulted only in a modest decrease of H_2O_2-levels (Fig.3.5H). These findings are in line with another study demonstrating that VAS2870 significantly blocked the increase of ROS levels in endothelial cells activated by oxidized low-density lipoprotein, but had minimal effect on the basal ROS levels without stimulation (Stielow et al., 2006). There are several possible reasons why VAS2870 treatment alone did not lower basal H_2O_2-levels more significantly. First, NADPH oxidases are not the only source for superoxide/hydrogen peroxide. Second we are measuring hydrogen peroxide in this assay and not superoxide, which is the primary product of NADPH oxidase. Third, ROS are highly reactive, act locally, and are tightly regulated; thus, it might be difficult to optically detect local changes in ROS levels induced by NADPH oxidase inhibition with sufficient temporal resolution, despite the fact that such changes can affect cellular physiology and morphology.

Cytoskeletal association of regulatory NOX subunits has been previously reported for $p40^{phox}$, $p47^{phox}$, and $p67^{phox}$ in non-neuronal cells. All three cytosolic subunits associate with the Triton X-100-insoluble cytoskeleton as well as the membrane cytoskeleton in neutrophils and endothelial cells (Nauseef et al., 1991; el Benna et al., 1994a; El Benna et al., 1999; Li and Shah, 2002). Furthermore, $p40^{phox}$ and $p47^{phox}$ associate with the neutrophil cytoskeleton through a PX-domain-dependent interaction with the actin-associated protein moesin (Wientjes et al., 2001; Zhan et al., 2004), while $p40^{phox}$ also interacts with the actin-binding protein coronin (Grogan et al., 1997), as well as directly with the actin cytoskeleton via its PX domain (Shao et al., 2010). These

findings suggested that actin-association of cytosolic NADPH oxidase subunits may have a regulatory function by keeping the complex in an inactive state until a stimulus releases the subunits from the cytoskeleton during the activation process. In agreement with this idea, COS-7 expression experiments revealed that $p40^{phox}$ is associated with actin and moesin, and that a mutated form of $p40^{phox}$ shows higher actin association and inhibits NOX2 activity (Chen et al., 2007). Furthermore, the actin-binding protein cortactin has been suggested to regulate NOX2 activation in lung endothelial cells trough an interaction with $p47^{phox}$ (Usatyuk et al., 2007). Thus, actin rearrangements could also deliver cytosolic NADPH oxidase subunits to the plasma membrane. Does NOX2 localization show actin-dependence? In migrating endothelial cells, NOX2 colocalizes with F-actin along the leading edge in an IQGAP1-dependent manner, while manipulating the actin cytoskeleton with latrunculin and jasplakinolide alters NOX2 localization (Ikeda et al., 2005). Our growth cone studies presented here also suggest a certain actin-dependence of NOX2 localization as indicated by the reduction of NOX2 following cytochalasin treatment and the co-localization of NOX2 with actin along the leading edge and in transition zone ruffle/intrapodia (not shown). Thus, a fraction of NOX2 along with $p40^{phox}$ appears to undergo retrograde flow together with the actin cytoskeleton. In summary, our present work in neuronal growth cones is consistent with previous findings made with leukocytes and endothelial cells indicating that the actin cytoskeleton may play a role in NADPH oxidase activation through localization of its subunits.

On the other hand, NADPH oxidase-derived ROS regulate actin organization and dynamics, growth cone motility, and neurite growth (this study; Munnamalai and Suter,

2009) and actin organization and migration of non-neuronal cells including leukocytes, keratinocytes, endothelial, smooth muscle, and HeLa cells (Nimnual et al., 2003; Wojciak-Stothard et al., 2005; Schroder et al., 2007; Kim et al., 2009; Kim et al., 2011a; Kuiper et al., 2011). Thus, together with these findings, our current study suggests an interesting bi-directional relationship between NADPH oxidase and F-actin. We propose that the regulatory cytosolic NADPH oxidase subunits such as p40 are associated with actin structures in unstimulated growth cones. Upon growth cone stimulation by guidance cues, cytosolic subunits $p47^{phox}$, $p67^{phox}$, $p40^{phox}$, and Rac1 translocate to the plasma membrane (either with or without F-actin) and activate the membrane bound subunits NOX2/$p22^{phox}$. NADPH oxidase-produced superoxide (or most likely hydrogen peroxide) diffuses back into the growth cone for local regulation of the cytoskeleton and related directional growth. In agreement with this hypothesis, we found increased $p40^{phox}$/NOX2 levels and co-localization at growth cone contact sites with apCAM beads (not shown) and interacting growth cones, where apCAM exhibits increased density as well (Thompson et al., 1996; Suter et al., 1998). These results indicate that apCAM-clustering can trigger actin remodeling as well as NADPH oxidase activation related to neurite outgrowth. The details of the functional relationship and order of events of apCAM clustering, actin reorganization, and NADPH oxidase activation are unclear at this point. apCAM clustering could first activate NADPH oxidase followed ROS-mediated actin reorganization; or apCAM-mediated actin remodeling could activate NOX2 by translocating cytosolic subunits close to plasma membrane. Thus, additional studies will be necessary to address the important question whether NADPH oxidase activation plays a functional role in directional axonal growth triggered by apCAM or other guidance cues

CHAPTER 4. NOX EXPRESSION DYNAMICS IN ZEBRAFISH

This work described in this chapter was previously published. The text presented here is adapted, with permission, from the original publication (Weaver et al., 2015).

4.1 Introduction

Reactive oxygen species (ROS) are a class of small molecules that can oxidize many biomolecules including proteins and lipids. Overproduction of ROS has been implicated in a number of diseases including hypertension, neurodegenerative conditions, and cancer (Montezano and Touyz, 2014; Nakanishi et al., 2014; Nayernia et al., 2014). However, when produced in a controlled fashion in response to a specific stimulus, ROS also act as critical signaling intermediates in a growing number of cellular signaling pathways regulating multiple biological processes including cell differentiation, migration, and death (Finkel, 2011; Forman et al., 2014). Although there are several sources of ROS within the cell, one class of enzymes called nicotinamide dinucleotide phosphate (NADPH) oxidases (commonly abbreviated NOX) are especially interesting in the context of cellular signaling, because these enzymes can be activated and inactivated by a variety of mechanisms, including by cytosolic proteins and signaling molecules as

well as by controlling expression (Bedard and Krause, 2007; Lambeth et al., 2007; Brown and Griendling, 2009; Brandes et al., 2014). Thus, a comprehensive knowledge of NOX soform expression could inform future studies on regulation and function of different NOX isoforms.

NOX2 is the first isoform to be identified and characterized. It is expressed in phagocytes, which use NOX2-derived ROS for bacterial killing (Nauseef, 2004). Following the initial discovery of NOX2, several additional isoforms have been identified in multicellular organisms, including NOX1, NOX3, NOX4, NOX5, DUOX1, and DUOX2 in humans (Fig. 1.1) (Kawahara et al., 2007b). In the human cardiovascular system, NOX1, NOX2, NOX4, and NOX5 are expressed in vascular smooth muscle cells (Jay et al., 2008; Zimmerman et al., 2011; Xu et al., 2014) as well as in endothelial cells (BelAiba et al., 2007; Drummond and Sobey, 2014). NOX activity is involved in blood pressure regulation and can lead to hypertension if out of control (Bedard and Krause, 2007). In the reproductive systems, NOX1 and 5 have been detected in human uterine tissue (Cheng et al., 2001; Brown and Griendling, 2009), while testis and ovary express NOX2, NOX4, and NOX5 (Cheng et al., 2001; Banfi et al., 2004b). NOX isoforms are also found in several other tissues including rabbit fibroblasts (NOX2), fish keratinocytes (DUOX), human kidneys (NOX1/2/4/5), human epithelial tissues of the colon (NOX1) and lung (DUOX), and in human thyroid tissue (DUOX) (Pagano et al., 1997; De Deken et al., 2000; Harper et al., 2006; Bedard and Krause, 2007; Rokutan et al., 2008; Rieger and Sagasti, 2011; Holterman et al., 2015; Zhu et al., 2015).

Of particular interest to the present study is the expression of NOX in the nervous system. NOX1, NOX2, and NOX4 have been identified in cultured neurons derived from

both peripheral and central nervous system (Hilburger et al., 2005; Tejada-Simon et al., 2005; Coyoy et al., 2008; Cao et al., 2009; Sorce and Krause, 2009; Choi et al., 2012; Kallenborn-Gerhardt et al., 2012; Munnamalai et al., 2014; Wilson et al., 2015). NOX3 is expressed in inner ear neurons (Banfi et al., 2004a) and has been implicated in balance based on swimming defects observed in NOX3 mutant mice (Paffenholz et al., 2004). Not surprisingly, NOX1 and NOX2 are also expressed in microglia, the phagocyte-like cells with immune function in the central nervous system (Wu et al., 2006; Cheret et al., 2008; Fischer et al., 2012). With respect to neuronal functions, NOX proteins have been implicated in neuronal stem cell maintenance in the brain (Dickinson et al., 2011), cerebellar development (Coyoy et al., 2013), neuronal differentiation (Tsatmali et al., 2006), neuronal polarity and neurite outgrowth (Munnamalai and Suter, 2009; Munnamalai et al., 2014; Olguin-Albuerne and Moran, 2015; Wilson et al., 2015), and synaptic plasticity (Kishida et al., 2006).

As detailed above, different NOX enzymes are found in many tissue types including in the nervous system and perform critical functions in these cells. In several cases, different NOX isoforms have been identified in the same tissue or even cell types; however, the functional relationship of the individual isoforms is often unclear. NADPH oxidase appears to have important roles in neuronal development; however, a systematic, tissue-scale characterization of NOX isoform expression throughout development of the nervous system has not been performed so far. In part, this is due to the limited availability of antibodies against several NOX isoforms in a number of species including zebrafish (*Danio rerio*) (Altenhofer et al., 2012). Furthermore, the current expression data from antibodies lacks validated support from other methods such as *in situ*

hybridization (ISH) (Nayernia et al., 2014). Tissue-specific NOX expression has often been reported in the form of Western blot data involving mixed cell populations. Some studies have shown cell-type specific expression of NOX in cultured cells, but these are often limited to specific isoforms (Kishida et al., 2006; Munnamalai et al., 2014; Wilson et al., 2015) and therefore fail to show the contributions, if any, of other NOX isoforms in the same cell type. In addition, immunolocalization studies using cell cultures often focus on a specific cell type. Thus, there are only a few studies that investigated NOX isoform expression in a broad range of tissues during development and into adulthood (Cheng et al., 2001). Here, researchers found that NOX5 is expressed in all human fetal tissues but later becomes restricted to specific adult tissue such as uterus (Cheng et al., 2001). In summary, a comprehensive NOX isoform expression analysis in the developing nervous system is missing. Expression data would not only confirm/identify the neuronal source of ROS for established functions but potentially unveil new functions of ROS signaling in neurons.

Here, we analyzed expression of Nox isoforms during early zebrafish development. Zebrafish have been used to study several NOX functions including neutrophil migration, wound healing, and axon regeneration (Niethammer et al., 2009; Rieger and Sagasti, 2011; Yoo et al., 2011; Yan et al., 2014; de Oliveira et al., 2015). Sequences for *nox1*, *nox2* (also called cytochrome B-245 or *cybb*), *nox4*, *nox5*, and *duox* genes have been identified in the zebrafish genome. *nox4*, however, is not well annotated, consists of multiple transcripts, and the suggested mRNA sequence does not align well with other known *nox4* gene sequences; therefore, we decided to focus our expression analysis on the other four isoforms. Humans express two distinct isoforms of *duox* (1/2)

while zebrafish express only a single isoform (Niethammer et al., 2009; Rigutto et al., 2009). To expand the current knowledge of NOX function in zebrafish nervous system development and regeneration, it is critical to know the spatiotemporal expression pattern of NOX genes. We used quantitative PCR (qPCR) along with ISH to characterize expression of *nox1*, *nox2/cybb*, *nox5*, and *duox* in the embryonic zebrafish during the first forty-eight hours after fertilization, which coincides with the development of major aspects of the zebrafish central nervous system (Schmidt et al., 2013). We identified dynamic changes in expression levels among three of the four isoforms studied. Furthermore, we found broad expression of all NOX isoforms during early development, which becomes more enhanced in specific regions of the brain at later developmental stages.

4.2 Results

4.2.1 *nox1*

In the present study, we investigated the expression of *nox1*, *cybb*, *nox5*, and *duox* genes at the mRNA level during the first forty-eight hours after fertilization in developing zebrafish embryos. The molecular compositions of the respective NADPH oxidase complexes for each of these isoforms are shown in Fig. 1.1. Quantitative PCR performed on mRNA extracted from whole zebrafish embryos showed that *nox1* expression is the highest at 12 hpf among all four isoforms investigated (Fig. 4.1B). After this time point,

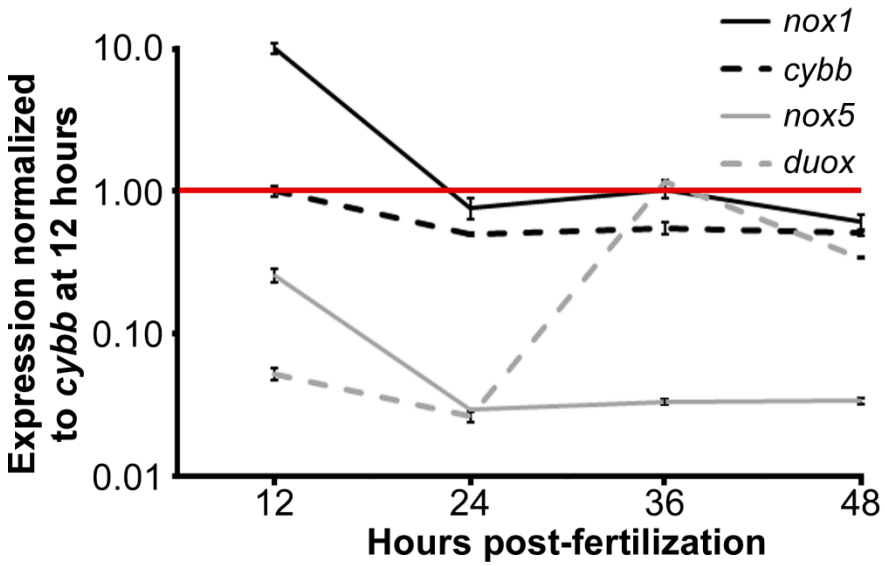

Figure 4.1: *nox* genes are expressed during early zebrafish development Relative expression levels derived via quantitative PCR from each of the 4 zebrafish NOX genes normalized to cybb at 12 hpf. cybb was chosen to normalize the data set as it was the most consistently expressed isoform. n = 6 for each data point. Error bars = SEM from all 6 data points.

the *nox1* expression decreases nearly ten-fold and remains consistent at this level throughout the next 36 h ($p < 0.0001$ at 12 hpf versus 24, 36 and 48 hpf). We next used ISH with single-stranded, antisense RNA probes to investigate *nox1* gene expression in the nervous system of developing zebrafish embryos at 24, 36, and 48 hpf (Fig. 4.2). We did not use 12 hpf embryos for ISH because our main focus was on the nervous system and no significant nervous system development has occurred at this stage. Images of whole-mount embryos demonstrate that *nox1* expression is broad in the head and anterior spinal cord (Fig. 4.2A-C). Next, we made 10 µm-thick transverse tissue sections from *in situ* hybridized embryos to provide a higher spatial resolution profile of *nox1* expression in the forebrain (Fig. 4.2E-H), eye (Fig. 4.2I-L), midbrain (Fig. 4.2M-P), hindbrain (Fig. 4.2Q-T), and anterior spinal cord (Fig. 4.2U-X). At 24 and 36 hpf, *nox1* expression is relatively uniform in all of these regions. By 48 hpf, *nox1* expression is

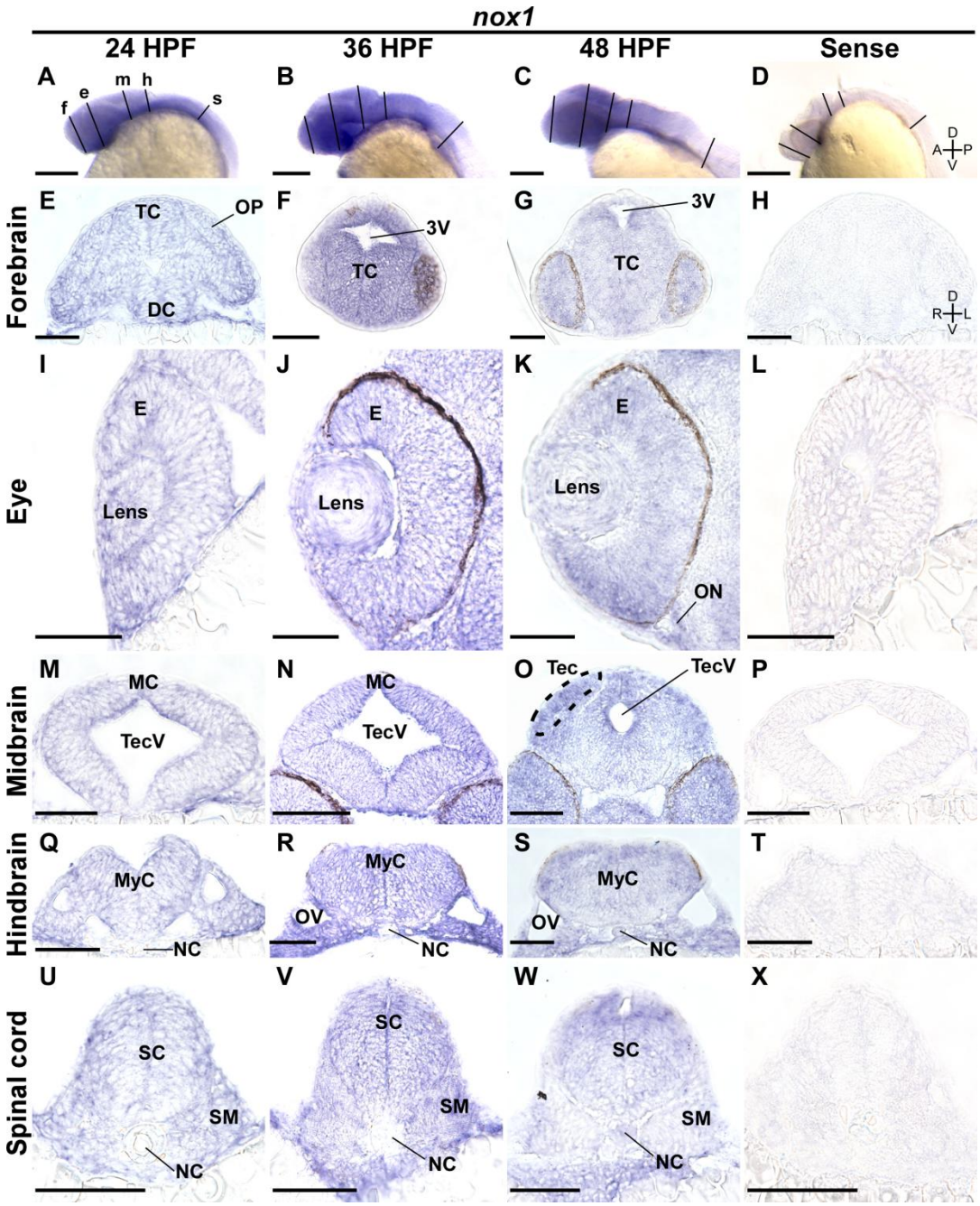

Figure 4.2: Broad *nox1* expression through the first two days of development (A-D) Lateral views of whole-mount ISH embryos probed with antisense (A-C) and sense control (D) riboprobe against zebrafish *nox1* mRNA. Lines represent the position of sections shown in E-X. E-H. 10 µm thick transverse sections through the forebrain (line labeled 'f' in A) of 24, 36, 48 hpf embryos incubated with antisense probes (E-G, respectively) and 24 hpf embryo incubated with a sense control probe (H). (I-L) Transverse sections through the eye (line labeled 'e' in A). (M-P) Corresponding midbrain sections (line labeled 'm' in A). (Q-T) Corresponding hindbrain sections (line labeled 'h' in A). (U-X) Corresponding spinal sections (line labeled 's' in A). Scale bar: 0.5 mm (A-D), 100 µm (E-X). 3V = third ventricle, DC = diencephalon, E = eye, MC = mesencephalon, MyC = myelencephalon, NC = notochord, ON = optic nerve, OV = Otic vesicle, SC = spinal cord, SM = somites; TC = telencephalon, Tec = tectum, TecV = tectal ventricle.

slightly elevated in the region corresponding to the optic tectum (Fig. 4.2O) and the dorsal region of the spinal cord (Fig. 4.2W).

4.2.2 *nox2/cybb*

Nomenclature for NOX2 varies among species. In zebrafish, it is commonly referred to as cytochrome b-245 beta polypeptide (*cybb*; GenBank ID 393386). As assessed via qPCR, *cybb* expression levels display marked consistency during the first two days of development in comparison to the other NOX isoforms (Fig. 4.1B). Images of whole-mount ISH embryos show broad expression of *cybb* throughout the head and spinal cord (Fig. 4.3A-D). Similarly to *nox1*, *cybb* is broadly expressed in all tissues examined during the first 36 h (Fig. 4.3 E-F, I-J, M-N, Q-R, U-V). By 48 hpf, the region of the midbrain corresponding to the optic tectum shows a slight increase in *cybb* expression (Fig. 4.3O). *cybb* remains broadly expressed in the forebrain, eye, hindbrain and spinal cord.

4.2.3 *nox5*

qPCR results indicate that *nox5* has a similar expression profile as *nox1* but at a significantly lower level (Fig. 4.1B). *nox5* reaches peak expression at 12 hpf, but exhibits lower expression levels by 24 hpf, which remain constant until 48 hpf ($p < 0.0001$ at 12 hpf versus 24, 36 and 48 hpf). By 36 hpf, *nox5* exhibits the lowest expression levels of

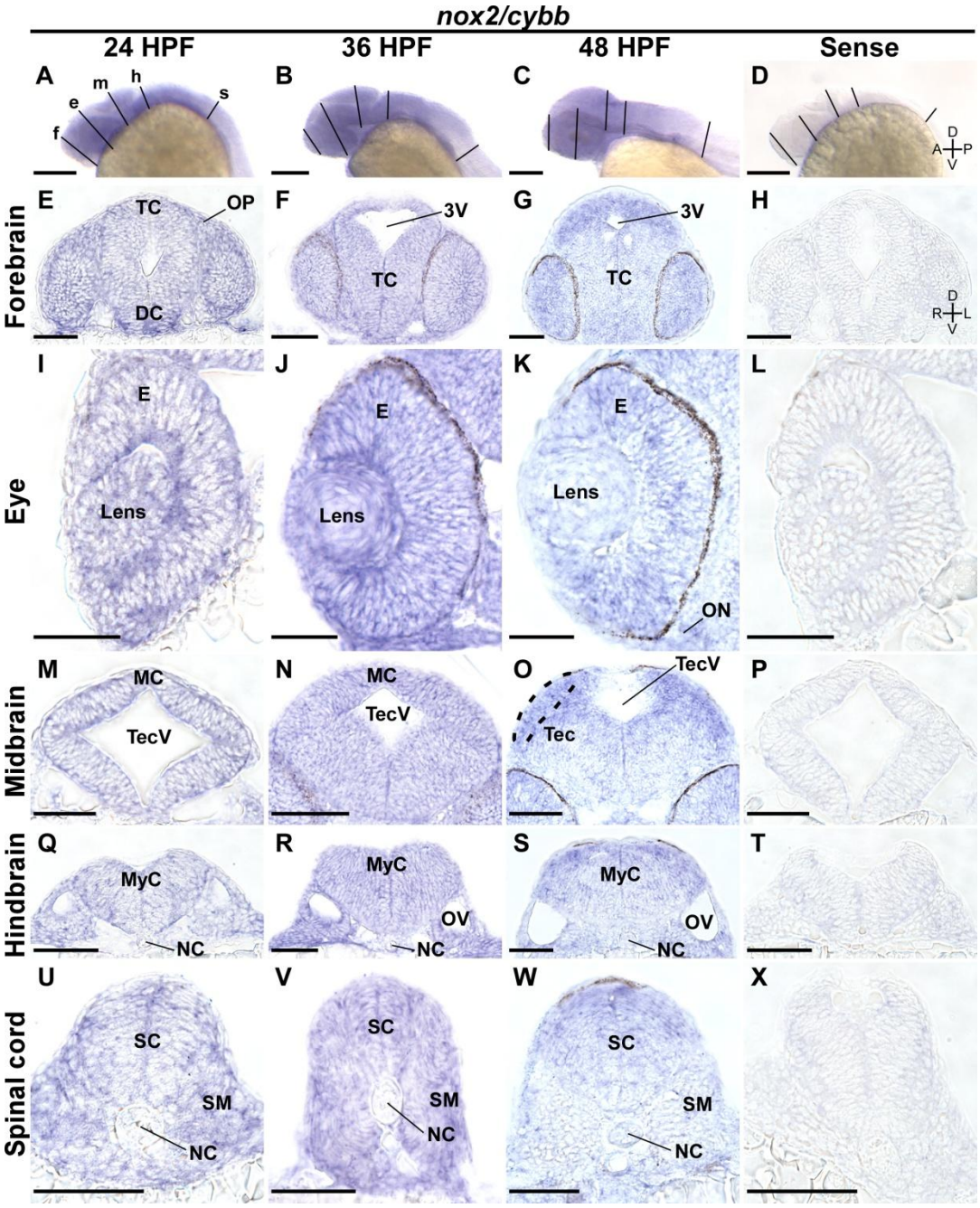

Figure 4.3: Broad *nox2/cybb* expression through the first two days of development (A-D) Lateral views of whole-mount ISH embryos probed with antisense (A-C) and sense control (D) riboprobe against zebrafish *nox2/cybb* mRNA. Lines represent the position of sections shown in E-X. E-H. 10 µm thick transverse sections through the forebrain (line labeled 'f' in A) of 24, 36, 48 hpf embryos incubated with antisense probes (E-G, respectively) and 24 hpf embryo probed with a sense control (H). (I-L) Transverse sections through the eye (line labeled 'e' in A). (M-P) Corresponding midbrain sections (line labeled 'm' in A). (Q-T) Corresponding hindbrain sections (line labeled 'h' in A). (U-X) Corresponding spinal sections (line labeled 's' in A). Scale bar 0.5 mm (A-D), 100 µm (E-X). 3V = third ventricle, DC = diencephalon, E = eye, MC = mesencephalon, MyC = myelencephalon, NC = notochord, ON = optic nerve, OV = Otic vesicle, SC = spinal cord, SM = somites, TC = telencephalon, Tec = tectum, TecV = tectal ventricle.

any NOX isoform during zebrafish development. Both whole-mounts and transverse tissue sections of ISH embryos demonstrate that *nox5* is broadly expressed throughout the nervous system at 24 and 36 hpf similarly to *nox1* and *nox2* (Fig. 4.4 A-B, E-F, I-J, M-N, Q-R, U-V). By 48 hpf, *nox5* shows a small increase in expression levels dorsally along the anterior-posterior axis from the forebrain (Fig. 4.4G) to the spinal cord (Fig. 4.4W).

4.2.4 *duox*

At 12 hpf, total *duox* expression is lower than any other NOX isoform. *duox* remains at this low level until 36 hpf, when expression increases by more than 10-fold ($p = 0.0001$ at 36 hpf versus 12 and 24 hpf). High expression levels similarly to *cybb* and *nox1* are maintained from 36 hpf to 48 hpf (Fig. 4.1B). *duox* is the only NOX isoform to undergo such a significant increase in expression during the first 48 h of development. Similarly to the other three NOX isoforms, whole-mount ISH embryos and tissue sections through the head and spinal cord at 24 and 36 hpf demonstrated that *duox* expression is relatively broad (Fig. 4.5 A-B, E-F, I-J, M-N, Q-R, U-V). By 48 hpf, *duox* expression domains become more unique. In the midbrain of 48 hpf fish, *duox* demonstrated a unique expression pattern that clearly deviates from any other NOX isoforms. *duox* is highly expressed in small regions surrounding the tectal ventricle, rather than broadly expressed in the dorsal region as found for *nox5* (Fig. 4.5O). Furthermore, *duox* expression is not increased in the tectum unlike the other three isoforms. In the spinal cord, *duox* is expressed throughout the neural tissue of 48 hpf fish with a slight increase on the dorsal side (asterisk in Fig. 4.5W). In summary, similarly to

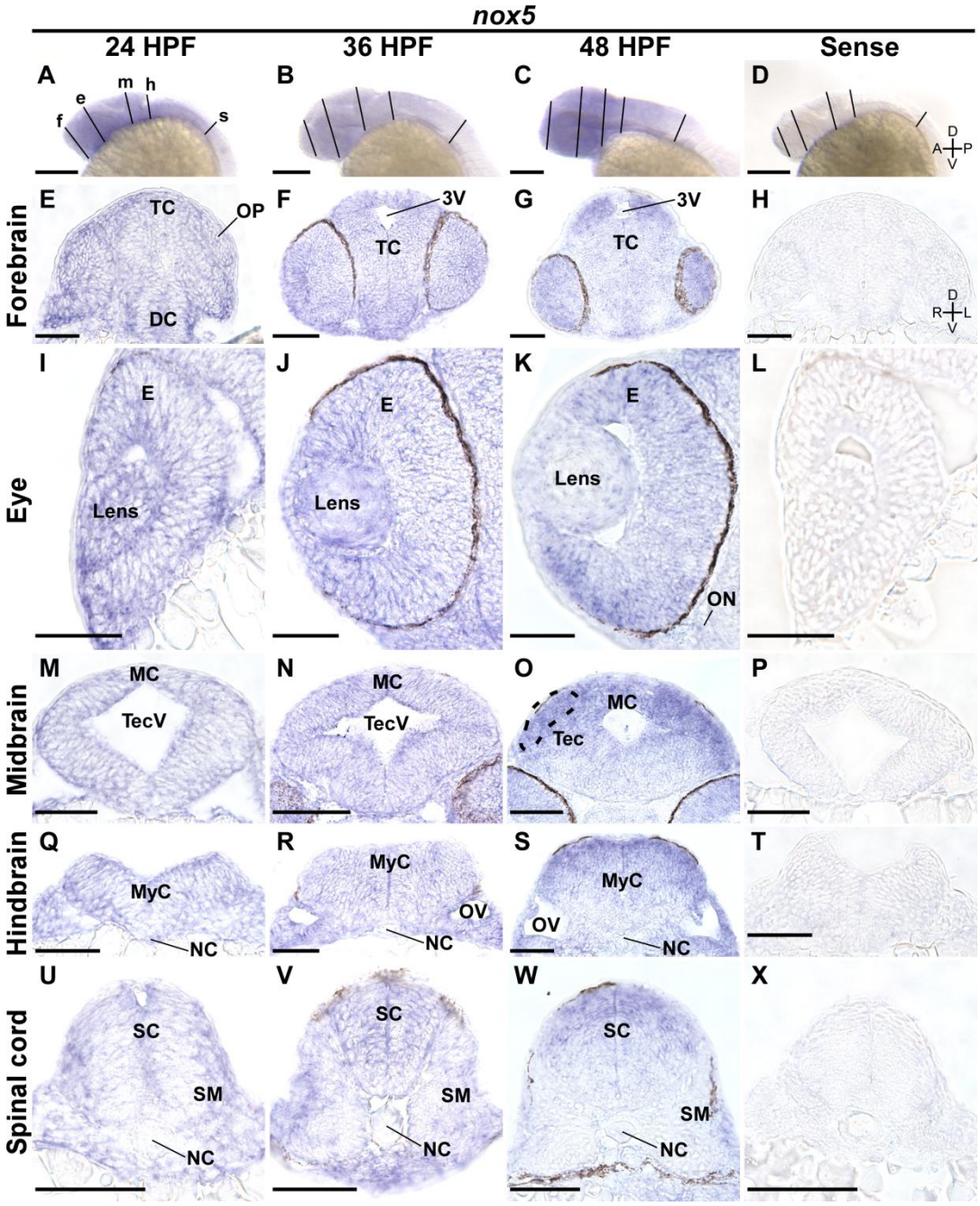

Figure 4.4: Broad *nox5* expression through the first two days of development (A-D) Lateral views of whole-mount ISH embryos probed with antisense (A-C) and sense control (D) riboprobe against zebrafish *nox5* mRNA. Lines represent the position of sections shown in E-X. (E-H) 10 µm thick transverse sections through the forebrain (line labeled 'f' in A) of 24, 36, 48 hpf embryos incubated with antisense probes (E-G, respectively) and 24 hpf embryo probed with a sense control (H). (I-L) Transverse sections through the eye (line labeled 'e' in A). (M-P) Corresponding midbrain sections (line labeled 'm' in A). (Q-T) Corresponding hindbrain sections (line labeled 'h' in A). U-X. Corresponding spinal sections (line labeled 's' in A). Scale bar 0.5 mm (A-D), 100 µm (E-X). 3V = third ventricle, DC = diencephalon, E = eye, MC = mesencephalon, MyC = myelencephalon, NC = notochord, ON = optic nerve, OV = Otic vesicle, SC = spinal cord, SM = somites, TC = telencephalon, Tec = tectum, TecV = tectal ventricle.

the other NOX isoforms *duox* exhibits a relatively broad expression pattern in the developing zebrafish nervous system until 48 hpf, when more distinct expression domains appear.

4.3 Discussion

NOX enzymes are a family of multi-subunit enzyme complexes, and each NOX isoform is subject to a unique type of regulation. This makes NOX enzymes excellent candidates to participate in cellular signaling in response to specific upstream stimuli. Within the nervous system, NOX isoforms have been shown to function in astrocytes, microglia, and neurons (Sorce and Krause, 2009; Fischer et al., 2012; Nayernia et al., 2014). NOX hyperactivity plays a role in the development and progression of neurodegenerative diseases such as Alzheimer's, Parkinson's, and amyotrophic lateral sclerosis (Bedard and Krause, 2007). Despite these well-publicized deleterious roles, NOX enzymes also have important functions in normal central and peripheral nervous system development and function (Sorce and Krause, 2009; Nayernia et al., 2014). These include neuronal stem cell maintenance (Dickinson et al., 2011), cerebellar development (Coyoy et al., 2013; Olguin-Albuerne and Moran, 2015), neuronal differentiation (Tsatmali et al., 2006), neuronal polarity and neurite outgrowth (Munnamalai and Suter, 2009; Munnamalai et al., 2014; Wilson et al., 2015), and synaptic plasticity (Kishida et al., 2006). However, comprehensive analyses of NOX expression in the nervous system, such as the current study, are crucial to better understand the role these enzymes plays in development, disease, and regeneration.

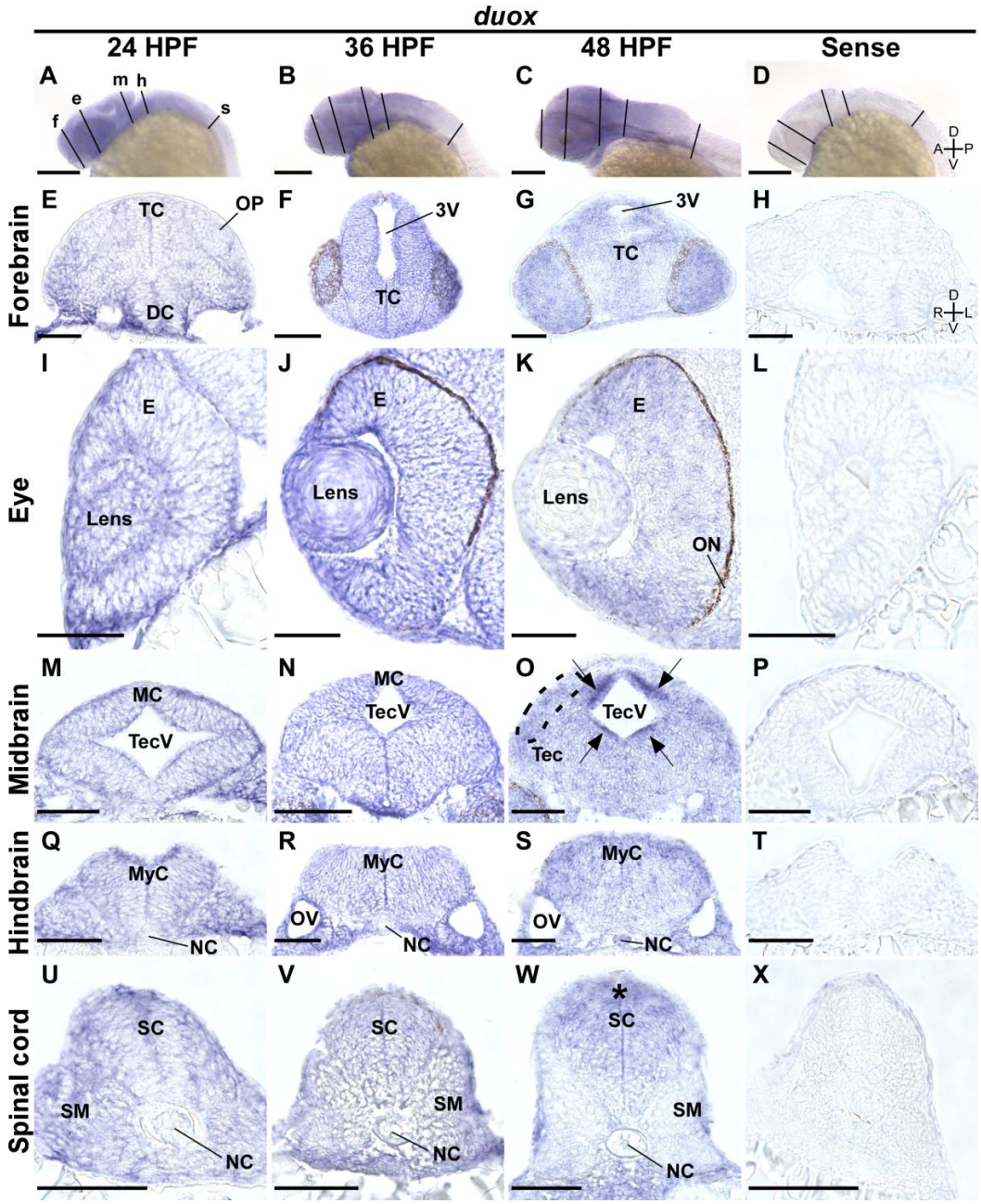

Figure 4.5: *duox* is highly expressed around tectal ventricle at 48 hpf (A-D) Lateral views of whole-mount ISH embryos probed with antisense (**A-C**) and sense control (**D**) riboprobe against zebrafish *duox* mRNA. Lines represent the position of sections shown in E-X. (**E-H)** 10 µm thick transverse sections through the forebrain (line labeled 'f' in A) of 24, 36, 48 hpf embryos incubated with antisense probes (**E-G**, respectively) and 24 hpf embryo probed with a sense control (**H**). (**I-L**) Transverse sections through the eye (line labeled 'e' in A). (**M-P**) Corresponding midbrain sections (line labeled 'm' in A). High *duox* expression was detected around the tectal ventricle (arrows in O). (**Q-T**) Corresponding hindbrain sections (line labeled 'h' in A). (**U-X**) Corresponding spinal sections (line labeled 's' in A). Asterisk and arrows represent regions and small areas of increased *duox* expression in the spinal cord and midbrain, respectively. Scale bar 0.5 mm (**A-D**), 100 µm (**E-X**). 3V = third ventricle, DC = diencephalon, E = eye, MC = mesencephalon, MyC = myelencephalon, NC = notochord, ON = optic nerve, OV = Otic vesicle, SC = spinal cord, SM = somites, TC = telencephalon, Tec = tectum, TecV = tectal ventricle.

In this study, we provide a detailed characterization of NOX expression within the nervous system of the developing zebrafish embryo. Sequences for *nox1, cybb, nox5,* and *duox* genes have been identified in the zebrafish genome; however, when and where individual NOX genes are expressed in fish embryos is currently unknown. We used qPCR (Fig. 4.1B) and ISH (Figs. 2-5) to characterize the expression of *nox1, cybb, nox5,* and *duox* in the developing fish nervous system between 12 and 48 hpf. qPCR data shows dynamic changes in *nox1*, *nox5* and *duox* expression while *cybb* levels are remarkably consistent from 12 to 48 hpf. Whole-mount ISH data is overall qualitatively in agreement with the qPCR data; however, it is important to keep in mind that ISH is not a quantitative method. Thus, proper quantification of ISH is difficult if not impossible between different time points and within tissues. All four NOX isoforms are broadly expressed in the early nervous system at 24 and 36 hpf. Whereas the broad expression continues, subtle differences in midbrain expression are visible by 48 hpf. *nox1*, *cybb,* and *nox5* show slightly elevated expression in the dorsal regions of the midbrain corresponding to the optic tectum. In contrast, *duox* expression was enriched in the regions adjacent to the tectal ventricle by this time. Increased labeling in dorsal and ventricle-adjacent regions was not observed in other samples using tissue of comparable thickness. Therefore we believe that the small increases in *nox1*, *cybb,* and *nox5* expression in the dorsal midbrain is real and not due to a technical artifact caused by incomplete probe penetration or probe trapping. Nonetheless, in most cases these increases are subtle and may not necessarily suggest functional significance.

One might wonder why the four zebrafish NOX isoforms show a very similar expression pattern early in development. A few points should be considered here. First,

we have not assessed protein levels, since isoform-specific antibodies are still sparse and not well validated in the zebrafish model system. It is possible that different NOX isoforms show more distinct expression patterns at the protein level during first 2 days of zebrafish development depending on translational regulation. MicroRNAs have been shown to effect the activity of NOX4, the constitutively active isoform of NOX (Gordillo et al., 2014; Wang et al., 2014). Based on this, it is plausible that other NOX isoforms could be post-transcriptionally regulated. Thus, it will be important to investigate the levels of protein expression in the developing nervous system. Second, broad NOX expression during early development is not without precedent as NOX5 expression is present in all human fetal tissues but more restricted in adult tissue (Cheng et al., 2001). Because of broad expression of all NOX isoforms early during development, knocking out one isoform might result in functional compensation by another NOX isoform and therefore not generate strong phenotypes. This idea is supported by the fact that ROS levels in cultured cerebellar granule neurons derived from NOX2 knockout mice were not different from wild type control neurons (Olguin-Albuerne and Moran, 2015). In addition, there is not much information in the literature about strong nervous system phenotypes of existing NOX knockout mouse models, besides the mild impairments in hippocampus-dependent memory in NOX2 knockout mice (Kishida et al., 2006). Lastly, it is important to keep in mind that the different NOX isoforms have unique activation mechanisms, and the resulting ROS are expected to act locally close to the source. Thus, even if multiple isoforms are expressed in the same cell type at any given time, different upstream signals could activate distinct NOX isoforms, which act in specific functions such as cell differentiation, adhesion, or migration.

Our current data on broad expression of NOX genes suggest that NOX activity may be a central contributor during nervous system development. We are aware that the present expression data of the main enzymatic subunit of the NOX complex is not sufficient to make any conclusions about ROS levels in different regions of the nervous system. However, we believe that the results from this study will provide important information when interpreting results of future studies addressing the function of NOX enzymes in embryonic zebrafish nervous system development and neurogenesis using pharmacological and molecular manipulations of activity and expression levels of NOX isoforms

CHAPTER 5. FUNCTION OF NOX IN ZEBRAFISH RETINAL DEVELOPMENT

5.1 Introduction

Reactive oxygen species (ROS) readily oxidize many biomolecules, including proteins, DNA, and lipids. Like other post-translational modifications, oxidation can have a significant impact on biological functions such as cell migration (Hung et al., 2011; Yoo et al., 2011; Tauzin et al., 2014). Thus, there is a need to tightly control the production of ROS in the cell. Unlike other cellular sources of ROS, some isoforms of an enzyme family called nicotinamide dinucleotide phosphate (NADPH) oxidases (Nox) produce a burst of ROS only upon activation. This makes Nox enzymes ideal candidates to be involved in ROS-mediated signaling. Nox activity has now been linked to various cellular signaling pathways involving Src tyrosine kinase, Wnt, and tumor necrosis factor alpha. Specifically, Nox-derived ROS are shown to be key signaling molecules in multiple biological processes (Brown and Griendling, 2009; Yoo et al., 2011; Choi et al., 2012; Kajla et al., 2012; Spencer et al., 2013; Weaver and Taylor-Fishwick, 2013; Nayernia et al., 2014; Tauzin et al., 2014).

Nox-derived ROS have also been shown to mediate signaling in the nervous system (Nayernia et al., 2014). Nox activity in adult mouse brains is essential for

neuronal plasticity in the hippocampus and long-term potentiation (Tejada-Simon et al., 2005; Kishida et al., 2006). Studies using cultured rat hippocampal neurons have shown that Nox2 is critical for the establishment of neuronal polarity (Wilson et al., 2015). Nox2 activity also regulates neurite outgrowth and actin dynamics in cultured neurons from *Aplysia californica* (Munnamalai and Suter, 2009; Munnamalai et al., 2014). Additionally, Nox inhibition causes defects in rat cerebellar development (Coyoy et al., 2013) and reduced neurite outgrowth of cerebellar neurons (Olguin-Albuerne and Moran, 2015). Furthermore, neural stem cells retain a high level of ROS that is critical for their self-renewal, and ROS production in these cells has been linked to Nox2 (Dickinson et al., 2011; Le Belle et al., 2011; Ren et al., 2015). Taken collectively, these studies show that Nox-derived ROS are critical components of normal signaling in the nervous system. However, the detailed functions of Nox during normal nervous system development *in vivo* are not well understood.

The goal of the present study was to determine the role of Nox in the development of axonal tracts in the nervous system. We used zebrafish embryos as a model system since they are a well-validated model of vertebrate neurodevelopment and compatible with *in vivo* imaging, immunolabeling, and molecular genetics. Gene sequences for five *nox* isoforms have been identified in the zebrafish genome (*nox1*, *nox2* also called *cybb* in zebrafish, *nox4*, *nox5*, and *duox*). Since the *nox4* gene is not well annotated in zebrafish, it was excluded from the current study. A series of studies showed that Nox-derived ROS mediate leukocyte and macrophage recruitment and promote wound healing in zebrafish (Yoo et al., 2011; Yoo et al., 2012; Tauzin et al., 2014). With respect to the nervous system, one study found that DUOX is important for peripheral axon

regeneration (Rieger and Sagasti, 2011). We have recently shown that zebrafish express *nox1*, *cybb*, *nox5* and *duox* broadly throughout the central nervous system during early development (Weaver et al., 2015). However, whether or not specific Nox isoforms play a functional role in zebrafish neurodevelopment remains unclear.

Here, we report that Nox2 is critical for the development of retinotectal connections. We show that transient pharmacological Nox inhibition during early development leads to an expansion of the ganglion cell layer (GCL), thinning of the optic nerve (ON), and decreased innervation of the optic tectum (OT). To determine which Nox isoforms are involved in retinal development, we generated isoform-specific *nox* mutant fish using CRISPR/Cas9. We found that homozygous *nox2/cybb* mutations caused an expansion of the GCL and mistargeted retinal axons in the OT. Taken together, these results demonstrate a novel role for *nox2/cybb* in the developing zebrafish visual system.

5.2 Results

5.2.1 Nox inhibition leads to defects in retinal development

In order to study the role of Nox function in nervous system development, we applied a pan-Nox inhibitor, celastrol (Jaquet et al., 2011), to zebrafish embryos and screened for neuroanatomical defects. This compound was chosen because it shows no antioxidant effects common in other Nox inhibitors like apocynin (Heumuller et al., 2008). We observed defects specifically in the formation of the ganglion cell layer (GCL)

and the optic nerve (ON) when celastrol was applied between 32 and 36 hpf (Figure 5.1) as well as the formation of anterior forebrain commissures when the inhibitor was applied between 20 and 24 hpf (data not shown). Since the zebrafish visual system is well characterized anatomically, functionally, and developmentally, we chose to focus this study on the development of the retinal ganglion cells (RGCs) and ON. In zebrafish, the retina begins to differentiate at 28 hours post-fertilization (hpf). At this time, RGCs differentiate in the GCL medial to the lens of the eye (Hu and Easter, 1999). At a point in the middle of the eye called the optic disk, axons throughout the GCL fasciculate into a single bundle called the ON. The left and right ONs then grow toward the midline of the embryo where they cross at a point called the optic chiasm at ~36 hpf (Burrill and Easter, 1995; Stenkamp, 2015). From the chiasm, ON axons grow dorso-caudally toward a midbrain region called the optic tectum (OT) where they form synapses with tectal neurons by 48 hpf (Kita et al., 2015).

To assess the effects of Nox inhibition on retinal and ON development, celastrol was applied at 2.5 μM during the period of ON fasciculation and growth toward the chiasm (32–36 hpf). The inhibitor was then washed out and the embryos were allowed to develop until ON axons reached the OT (48 hpf). Embryos were then fixed and immunostained with zn-8, an antibody that labels the GCL and ON (Avanesov and Malicki, 2010). We observed an expansion of the zn-8-positive GCL and a thinning of the ON in celastrol-treated fish embryos (Figure 5.1A, B). We quantified GCL width and ON thickness as measures of retinal development (Figure 5.1D, E). Differences in GCL width were found to be statistically significant ($F(2, 35) = 66.6$, $p < 0.0001$). Control GCLs had an average width of 100 ± 10.6 μm (mean ± SD, Figure 5.1A, D). Inhibitor-

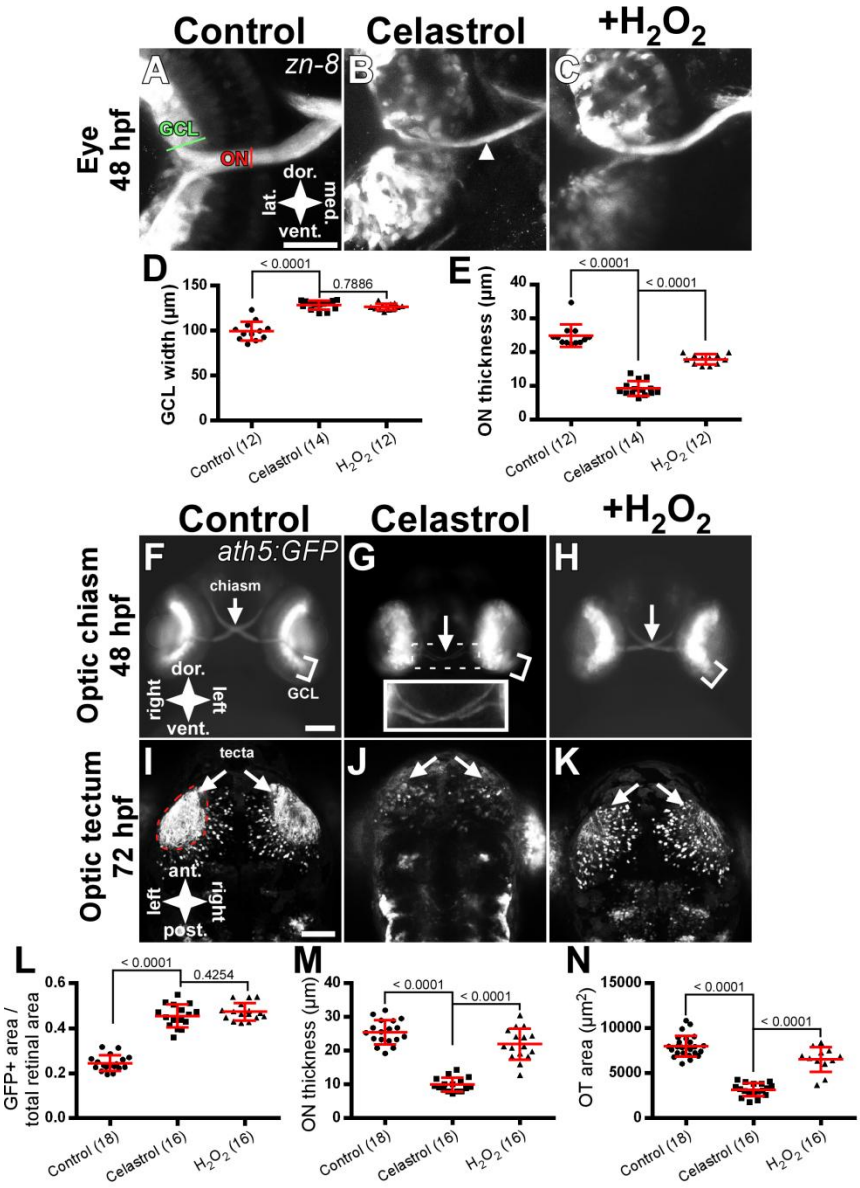

Figure 5.1: Nox inhibition causes defects in retinal development and tectal innervation **(**A-C) Retinal micrographs of 48 hpf embryos labeled with the RGC marker zn-8 following a 4 hour treatment with 0.1% DMSO (A) or 2.5 µM celastrol (B–C). Embryo in C was incubated with 2 mM H_2O_2 following drug washout. White arrowhead in B indicates ON thinning. (D) Graph of GCL width in zn-8 labeled embryos treated with celastrol. (E) Graph of ON thickness in zn-8 labeled embryos treated with celastrol. (F–H) Anterior views of 48 hpf *Tg(ath5:GFP)* embryos after treatment with DMSO (F) or celastrol with (H) or without (G) subsequent H_2O_2 incubation. Inset in G shows the optic chiasm. (I–K) Dorsal views of control (I), inhibitor-treated (J) and H_2O_2 rescue (K) embryos at 72 hpf of embryos showing optic tectum innervation. White arrows indicate the optic chiasm (F-H) or optic tecta (I-K). (L) Graph of GFP-positive area corresponding to the GCL divided by total retinal area in *Tg(ath5:GFP)* embryos treated with celastrol. (M) Graph of ON thickness in *Tg(ath5:GFP)* embryos treated with celastrol. (N) Graph of OT area in *Tg(ath5:GFP)* embryos treated with celastrol. Scale bars = 50µm (A–C) and 100µm (F–K). All graphs show mean ± standard deviation. Number in parenthesis indicates the number of embryos analyzed. p-values from Tukey HSD tests are reported above comparison bars.

treated embryos displayed a significant increase in GCL thickness compared with control (128 ± 5.0 µm, $p < 0.0001$, Figure 5.1B, D). Previous studies have shown that Nox loss-of-function can be rescued via the addition of hydrogen peroxide (H_2O_2) (Le Belle et al., 2011; Rieger and Sagasti, 2011). Therefore, we optimized a rescue approach using several concentrations of H2O2 applied continuously throughout the first 48 hpf (Figure 5.2). We found that 2 mM H2O2 did not have any impact on embryonic survival or any visible effect on visual system development (Figure 5.2). Therefore, we applied 2 mM H_2O_2 immediately following celastrol treatment; however, this did not affect the width of the GCL compared to celastrol only-treated embryos (127 ± 3.6 µm, $p = 0.7886$, Figure 5.1C, D). Differences among mean ON thickness were also found to be significant ($(F2, 35) = 133.5$, $p < 0.0001$). Control embryos treated with 0.01% DMSO displayed a mean ON thickness of 25 ± 3.4 µm (Figures 1A, E). ONs of celastrol-treated embryos were significantly thinner (9 ± 2.2 µm, $p < 0.0001$ versus control, Figure 5.1B, E). Here, H_2O_2 application caused a marked recovery of ON thinning (17.9 ± 1.5 µm, $p < 0.0001$ compared to celastrol alone, Figure 5.1C, E).

We then used the *Tg(ath5:GFP)* transgenic line to label RGCs and the ON in live embryos. Using this strategy, we were able to image retinal development and OT innervation at different time points in the same embryo. In response to the Nox inhibitor treatment, the GCL again appeared wider (Figure 5.1G). To determine if this wider GCL represented an expansion of RGCs within the retina, we calculated the ratio of the GFP-positive area divided by the total area of the retina, and found significant differences

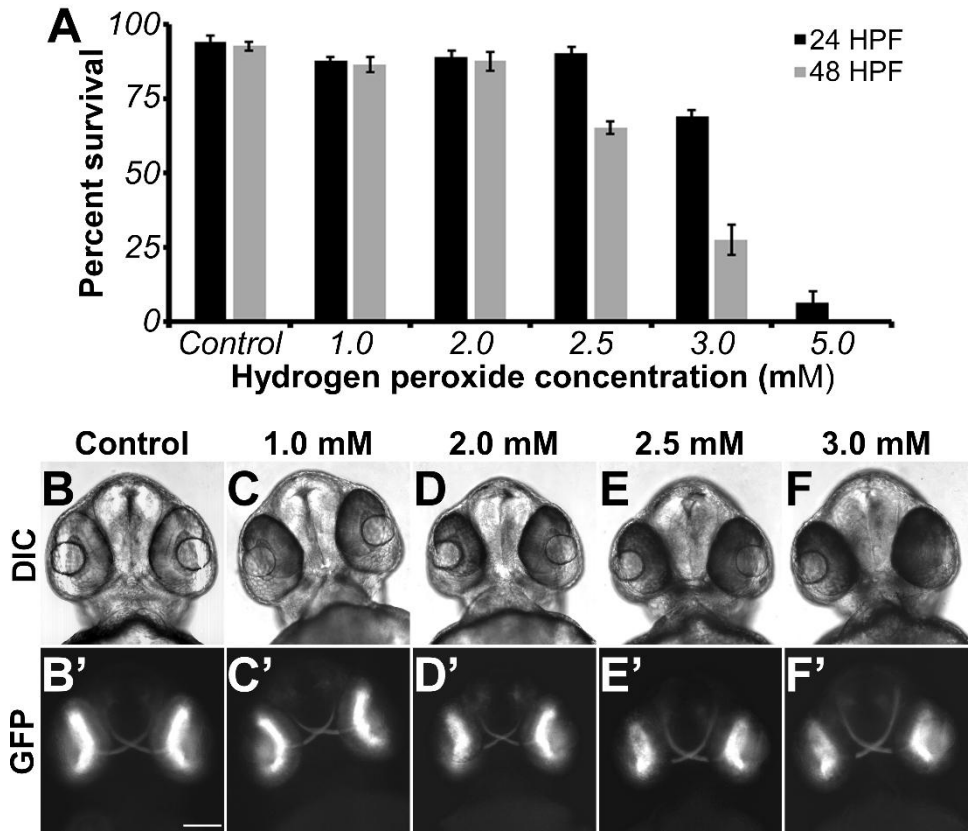

Figure 5.2: Optimization of H_2O_2 rescue (A) Percent survival versus hydrogen peroxide concentration measure at 24 and 48HPF. Embryos were maintained in the solution from 0-48HPF. n = 80 individuals per condition. Error bars represent SEM. (B-F) DIC images of 48HPF *Tg(ath5:GFP)* embryos following hydrogen peroxide treatment. (B'-F') Corresponding images of the GFP signals. Scale bar = 100µm.

among groups ($F(2, 47) = 159$, $p < 0.0001$). The GCL in inhibitor-treated embryos occupied a greater proportion of the retina versus controls (Figure 5.1L; 0.45 ± 0.05, 0.24 ± 0.03, respectively, $p < 0.0001$). Similarly to our findings with zn-8 labeling (Figure 5.1D), treatment with H_2O_2 did not significantly diminish the ratio of the retina occupied by GFP-positive RGCs versus celastrol treatment (0.47 ± 0.04, $p = 0.43$). We again found a significant difference among mean ON thickness the three treatment groups ($F(2, 47) = 85.6$, $p < 0.0001$). Control embryos had ONs with a mean thickness of 25.5 ± 3.4 µm (Figure 5.1F, M) whereas ONs of inhibitor-treated embryos were significantly thinner compared to controls (9.9 ± 2.0 µm, $p < 0.0001$, Figures 1G, M). The addition of H_2O_2

partially rescued ON thickness compared to celastrol treatment (22.0 ± 4.6 μm, $p < 0.0001$, Figures 1H, M).

We next investigated the innervation of the OT in response to Nox inhibition. No differences in axon targeting were observed as all GFP signals localized to the presumptive OT as determined by visual comparison to control embryos. However, we measured the area of the OT innervated by GFP-positive axons and found significant differences among groups ($F(2, 53) = 105.3$, $p < 0.0001$). Controls displayed a mean area of 7998 ± 1154 μm^2 at 72 hpf (Figure 5.1I, N). Celastrol-treated embryos showed a significant decrease in OT innervation (3164 ± 721 μm^2, $p < 0.0001$ versus control, Figures 1J, N). Like ON thickness, OT innervation was partially rescued by the 2 mM H_2O_2 applied immediately following inhibitor treatment (6538 ± 1384 μm^2, $p < 0.0001$ versus celastrol, Figures 1K–N). Collectively, these results demonstrate that pharmacological Nox inhibition results in GCL expansion, ON thinning, and reduced OT innervation, indicating a role for Nox in normal retinal development.

5.2.2 *nox2/cybb* chimeric mutants display retinal defects

To determine the specific Nox isoform involved, we used the clustered regularly-interspaced short palindromic repeats (CRISPR)/Cas9 genome editing technique to generate isoform-specific mutations in zebrafish embryos. We designed two guide RNAs (gRNAs) per Nox isoform, and injected these gRNAs into 1-cell stage embryos to generate site-specific mutations in the *nox* genes. The locations of the gRNA target sites with respect to full-length Nox proteins are shown in Figure 5.3A. We first calculated the

efficiency of the gRNAs by quantifying the percentage of mutant embryos generated by each gRNA (Table 4). All of the gRNAs produced mutations in at least 65 percent of the injected embryos. Some (e.g. *nox1* gRNAI and *nox5* gRNAII) generated mutations in greater than 90 percent of the injected embryos. We also genotyped the predicted off-target sites, shown in Table 2, for each gRNA and found no mutations at these locations in the genome (data not shown).

Table 5.1. gRNA efficiency

	gRNA I			**gRNA II**		
	mutant	*total*	*%*	*mutant*	*total*	*%*
nox1	50	55	**91**	46	61	**75**
nox2/cybb	40	60	**67**	49	58	**84**
nox5	35	52	**67**	50	55	**91**
duox	49	55	**89**	42	50	**84**

Embryos were genotyped as described in Methods. Total refers to the total number of embryos that were injected and genotyped. Mutant refers to the number of embryos found to carry mutations.

Using this validated set of Nox isoform-specific gRNAs, we investigated which Nox isoforms contribute to retinal development. Therefore, we co-injected both gRNAs against a given *nox* gene into *Tg(ath5:GFP)* embryos which generated a set of novel mutations in each embryo. Due to the random incorporation of insertions and deletions in the early cells, these embryos are chimeric. Therefore, these chimeric embryos retain an unknown percentage of wild-type *nox* genes in certain tissues. The implications of this will be addressed in the Discussion. The injected embryos were genotyped at both gRNA loci, and resulting phenotypes were assessed only in individuals carrying mutations at both gRNA sites. Restricting the analysis to double-site mutants maximizes the probability of producing a loss-of-function mutation. At least 20 chimeric mutants were

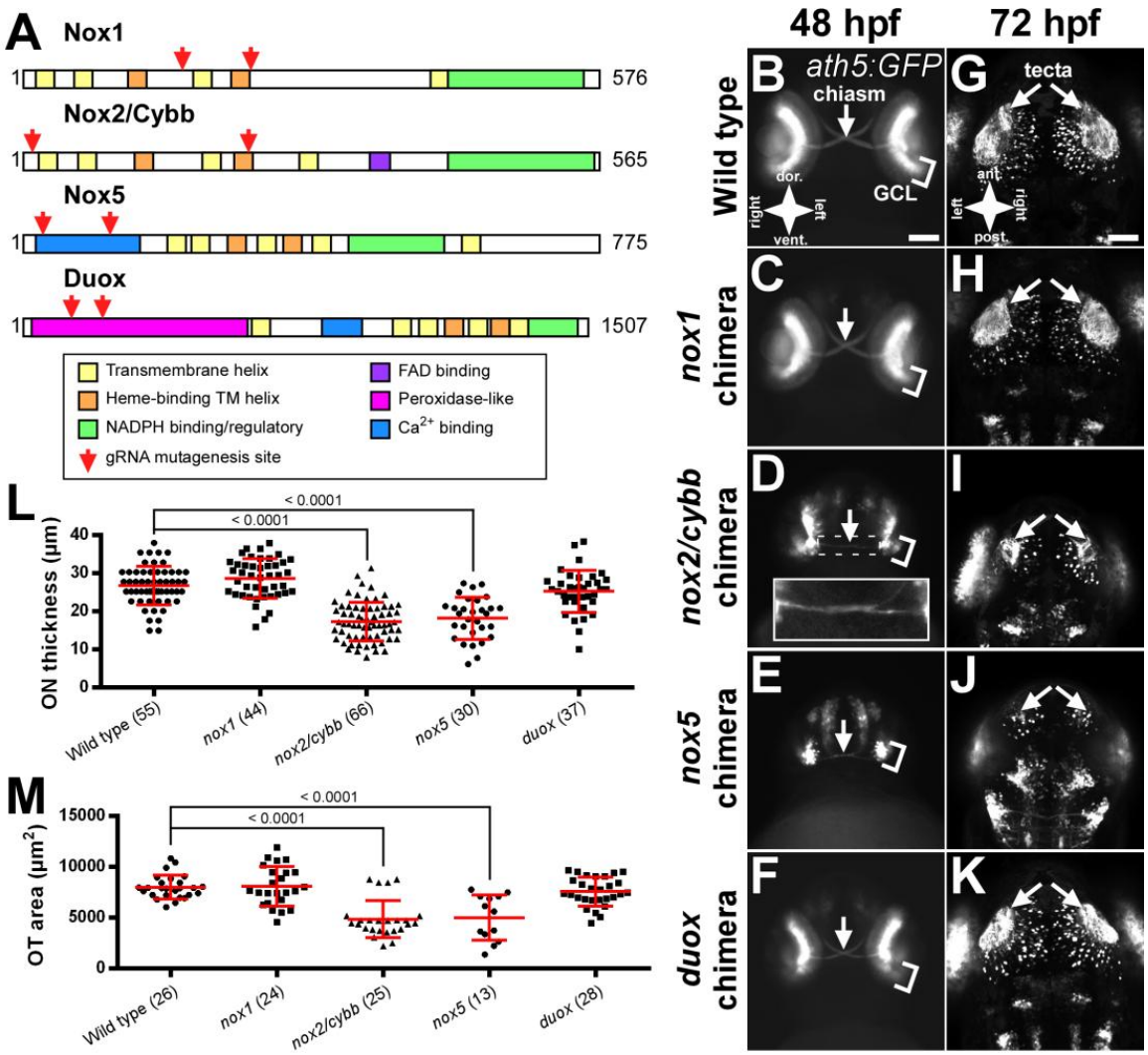

Figure 5.3: *nox* mutants show optic nerve and tectal defects (A) Schematic of zebrafish NOX protein domains as determined by alignment to the human protein sequences. Red arrows indicate the relative location of gRNA target sites. (B–F) Anterior views *Tg(ath5:GFP)*-positive, *nox* chimeras at 48 hpf. White arrows indicate the optic chiasm. Inset in D shows in enlarged and enhanced view of the optic chiasm. (G–K) Dorsal views of chimeric embryos showing the innervation of the optic tecta (white arrows). GFP-positive cells not indicated with arrows represent non-tectal early neurons from the hindbrain and eye. Scale bars = 100 µm (B–F) and 50 µm (G–K). (L) Graph of ON thickness in *Tg(ath5:GFP)* positive, chimeric mutants. (M) Graph of OT area in *Tg(ath5:GFP)* positive, chimeric mutants. Number in parenthesis indicates the number of embryos analyzed. Graphs show mean ± standard deviation. p-values from Dunnett's tests are reported above comparison bars.

analyzed for each gene, and representative ON and OT images are shown in Figure 5.3 along with measurements of ON thickness at 48 hpf and OT area at 72 hpf. Injected embryos that did not carry mutations at either gRNA site served as wild-type controls for

these experiments (Figure 5.3B, G). None of the nox chimeric mutants showed expansion of the GCL as in the case of inhibitor-treated embryos (Figure 5.3B-F) or significant mistargeting of GFP-positive axons within the midbrain (Figure 5.3G–K). Importantly, ON thickness and OT innervation in controls were similar to what was found previously in DMSO-treated embryos (26.8 ± 5.0 μm and 7998 ± 1154 μm^2, respectively, Figure 5.3B, G, L, M). ONs of *nox1* mutants are not significantly different from wild-type controls (28.7 ± 5.2 μm, $p = 0.24$, Figure 5.3C, L). OT innervation was similarly unaffected in these mutants (8063 ± 1946 μm, $p = 1.00$, Figure 5.3H, M). Similar to what was observed in response to pharmacological Nox inhibition, *nox2/cybb* mutants displayed thin ONs (17.4± 5.1 μm, $p < 0.0001$ versus control, Figure 5.3D, L). The OT of *nox2/cybb* mutant larvae showed sparse GFP signals indicating a reduced number of ON axons innervating the tissue (4840 ± 1835 μm^2, $p < 0.0001$ versus control, Figure 5.3I, M). *nox5* mutants also displayed ON thinning (18.2 ± 5.5 μm, $p < 0.0001$ versus control, Figure 5.3E, L) and decreased tectal innervation (4995 ± 2243 μm^2, $p < 0.0001$ versus control, Figure 5.3J, M). However, *nox5* mutants have severe general morphological defects early in development that might interfere with the formation of the brain and retina (data not shown). Since *nox2/cybb* mutants better phenocopied our inhibitor-treated embryos, we chose to focus on *nox2/cybb* in subsequent experiments. Finally, *duox* mutants displayed insignificant ON thinning (25.3± 5.5 μm, $p = 0.44$ versus control, Figure 5.3F, L) and decreased tectal innervation (7556 ± 1417 μm^2, $p = 0.74$ versus control, Figure 5.3K, M). In summary, these results showed that among the different *nox* isoforms, *nox2/cybb* plays a critical the development of the zebrafish visual system.

5.2.3 Optic nerve projection is delayed in *nox2/cybb* mutants

The effect of *nox2/cybb* mutation is a thin, underdeveloped ON at 48 hpf, whose axons fail to properly innervate the OT by 72 hpf (Figure 5.3D, I). To address whether these defects in retinotectal connectivity persist at later time points, we leveraged the live-imaging capability of the *Tg(ath5:GFP)* line to capture ON and OT images from *nox2/cybb* chimeric embryos at multiple time points. We also included a set of *nox2/cybb* chimeric mutants that were incubated with 2 mM H_2O_2 as a rescue control condition. As shown in Figure 5.4B and C, we observed characteristic ON thinning in *nox2/cybb* mutants at 48 hpf (14.7 ± 3.7 μm, $p < 0.0001$ versus control, Figure 5.4I). ONs from *nox2/cybb* mutants incubated with H_2O_2 were significantly thicker than untreated mutants (19.8 ± 3.4 μm, $p = 0.0035$ versus mutant, Figure 5.4D, I), indicating that the phenotype observed in *nox2/cybb* mutants is likely due to reduced H_2O_2 levels. We then imaged the same embryos at 72 hpf to assess the persistence of ON thinning. By this time point, *nox2/cybb* mutants recovered (35.7 ± 7.8 μm, Figure 5.3B'-C') such that they were nearly identical to controls (39.9 ± 6.9 μm, Figure 5.4A'). H_2O_2-treated larvae were similar to controls with a thickness of 37.3 ± 5.2 μm (Figure 5.4D'). No significant differences were detected among groups suggesting that the ON phenotypes observed in response to *nox2/cybb* mutation could be transient, and likely due to developmental delays ($F(2, 57) = 2.086$, $p = 0.7842$).

We then turned our attention to the effects of *nox2/cybb* mutations on OT innervation. Imaging the same samples over three days, we saw a progressive increase in

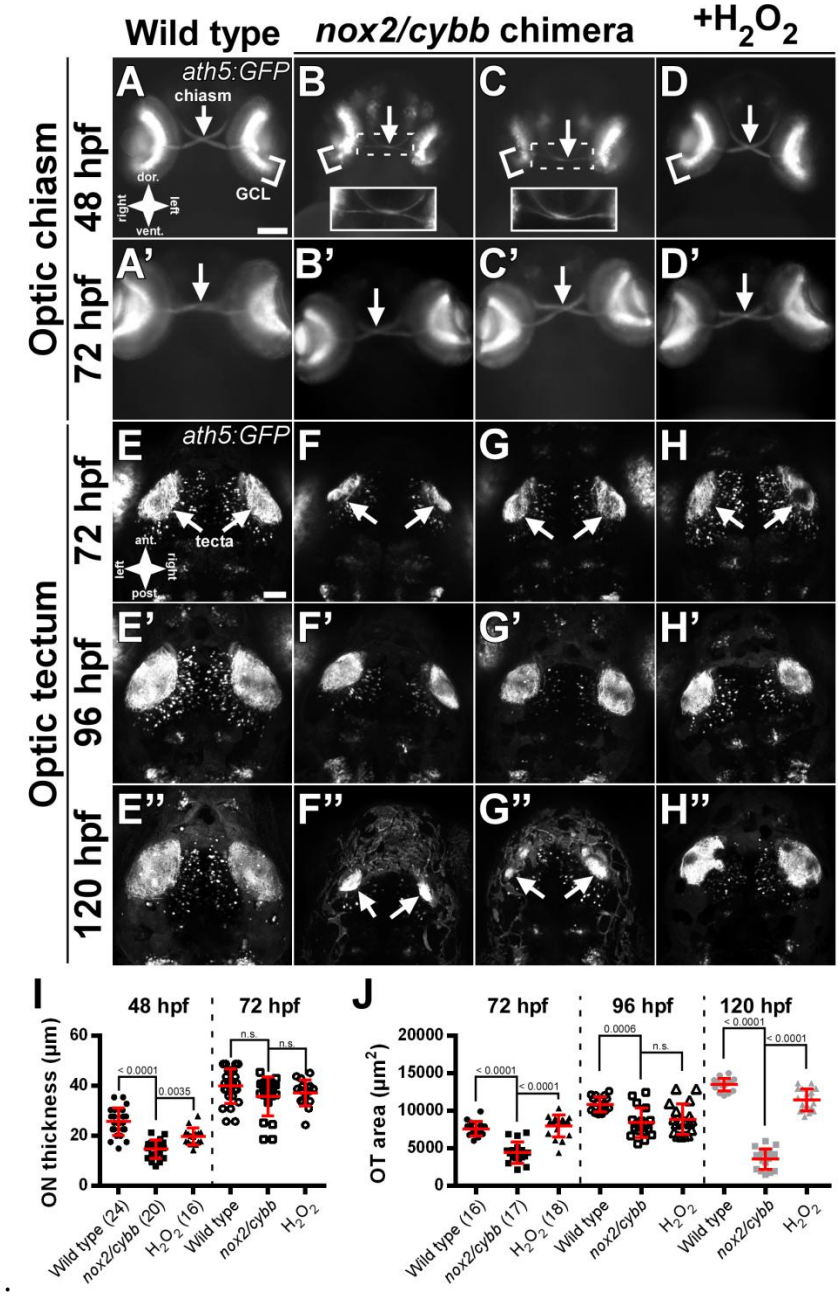

Figure 5.4: ON extension and OT innervation are delayed in chimeric *nox2/cybb* mutants (A–D) Anterior views of *nox2/cybb* chimeras at 48 hpf showing the formation of the optic chiasm. Insets in B & C show enlarged and enhanced views of the chiasm. (A'–D') The same samples as A–D imaged at 72 hpf showing recovery of ON outgrowth in chimeras. (E–F) Dorsal views of *nox2/cybb* chimeras at 72 hpf showing the innervation of the optic tecta. The same samples were imaged at 96 (E'–H') and 120 hpf (E"–H") to assess the extent of recovery. White arrows indicate the optic chiasm (A–D') or optic tecta (E–H"). Scale bars = 100 µm (A–D') and 50 µm (E–H") (I) Graph of ON thickness in *Tg(ath5:GFP)* positive, *nox2/cybb* chimeric mutants. (J) Graph of OT area in *Tg(ath5:GFP)* positive, *nox2/cybb* chimeric mutants. Number in parenthesis indicates the number of embryos analyzed. Graphs show mean ± standard deviation. p-values from Tukey HSD tests are reported above comparison bars. n.s. indicates no significant difference.

tectal innervation between 72 and 96 hpf in wild type controls (Figure 5.4E-H, E'-H', J). Significant differences among groups were identified at both time points ($F(2, 48) = 38.37$, $p < 0.0001$ for 72 hpf; $F(2, 48) = 9.106$, $p = 0.0004$ for 96 hpf). Innervated areas in the OT from *nox2/cybb* mutants were significantly smaller than control ($p < 0.0001$) and H_2O_2 rescue condition ($p < 0.0001$) at 72 hpf (Figure 5.4E-H, J). By 96 hpf, innervated tectal areas of mutants and H_2O_2-treated mutants were still smaller than controls ($p = 0.0006$ and 0.005, respectively), but were not different from one another ($p = 0.72$, Figure 5.4E'-H', J). A more severe loss of OT innervation was detected in *nox2/cybb* mutants by 120 hpf ($F(2, 48) = 291.9$, $p < 0.0001$). OT innervation in mutants drops to 3590 ± 1357 μm^2 ($p < 0.0001$ versus control, Figure 5.4F", G", J) compared to wild-type controls (13,505 ± 844 μm^2, Figure 5.4E", J), and is significantly different from H_2O_2 treated mutants (11,462 ± 1444 μm^2, $p < 0.0001$, Figure 5.4H"& J). These results suggest that OT innervation is initially delayed in *nox2/cybb* chimeras, whereas more severe defects arise later.

5.2.4 *nox2/cybb*$^{-/-}$ embryos show expansion of the GCL

To minimize the potential phenotypic variability of *nox2/cybb* mutant chimeras, we generated stable fish lines harboring homozygous *nox2/cybb* mutations at either site targeted by the *nox2/cybb* gRNAs (referred to as *nox2/cybb*$^{-/-}$). Two lines carrying mutations at different loci within the *nox2/cybb* gene were generated to confirm the convergence of phenotypes and ensure the specificity of mutagenesis. The mutant line generated from gRNA I had a 5 base-pair deletion while the line from gRNA II carried a

23 base-pair deletion (Figure 5.5A). Each line carries a premature stop codon early in the coding sequence for *nox2/cybb,* which results in a significant truncation of the Nox2/Cybb protein (Figure 5.5B). Both Nox2/Cybb mutant enzyme types have lost the C-terminal substrate binding domain. Four histidine residues within alpha helices III and V are essential for electron shuttling to the O_2 acceptor, and at least one of these critical histidines are missing in both mutant types (Kawahara and Lambeth, 2007; Brandes et al., 2014). Without these critical functional domains, the mutant Nox2/Cybb proteins are likely not functional.

Since *nox2/cybb*$^{-/-}$ mutant lines do not carry the *Tg(ath5:GFP)* transgene, we used zn-8 antibodies to visualize axons. Samples were also counterstained with the nuclear label DAPI to assess overall retinal development and lamination. In these experiments, wt clutch mates served as controls. In contrast to chimeras, *nox2/cybb*$^{-/-}$ embryos exhibited significant expansion of the zn-8-positive GCL at 48 hpf ($F(2, 41) = 63$, $p < 0.0001$). The GCL in gRNAI (0.49 ± 0.06, Figure 5.5D–D”, I) and gRNAII mutants (0.48 ± 0.04, Figure 5.5E–E”, I) occupies a greater proportion of the retina compared to controls (0.34 ± 0.03, Figure 5.5C–C”, I, $p < 0.0001$ versus mutants). Unlike the ON phenotypes observed in chimeric mutants, GCL expansion did not recover by 72 hpf in *nox2/cybb*$^{-/-}$ mutants, and many cells were pyknotic at this later stage (Figure 5.5G’–H’). In controls, the wt GCL occupied a similar percentage of the retina at 72 hpf compared to that at 48 hpf (0.31 ± 0.02, Figure 5.5F–F”, I) Mutant GCLs represented a significantly higher proportion of the retina compared with wild type controls (gRNA I 0.48 ± 0.05, gRNA II 0.45 ± 0.06, $p < 0.0001$, Figure 5.5G–H”, I). These results further confirm a role for Nox2/Cybb in GCL development. Interestingly, the ON was not significantly thinner in

the homozygous mutants compared to wt controls (data not shown). The phenotypic differences observed among inhibitor-treated, chimeric, and homozygous mutant embryos will be addressed in the discussion.

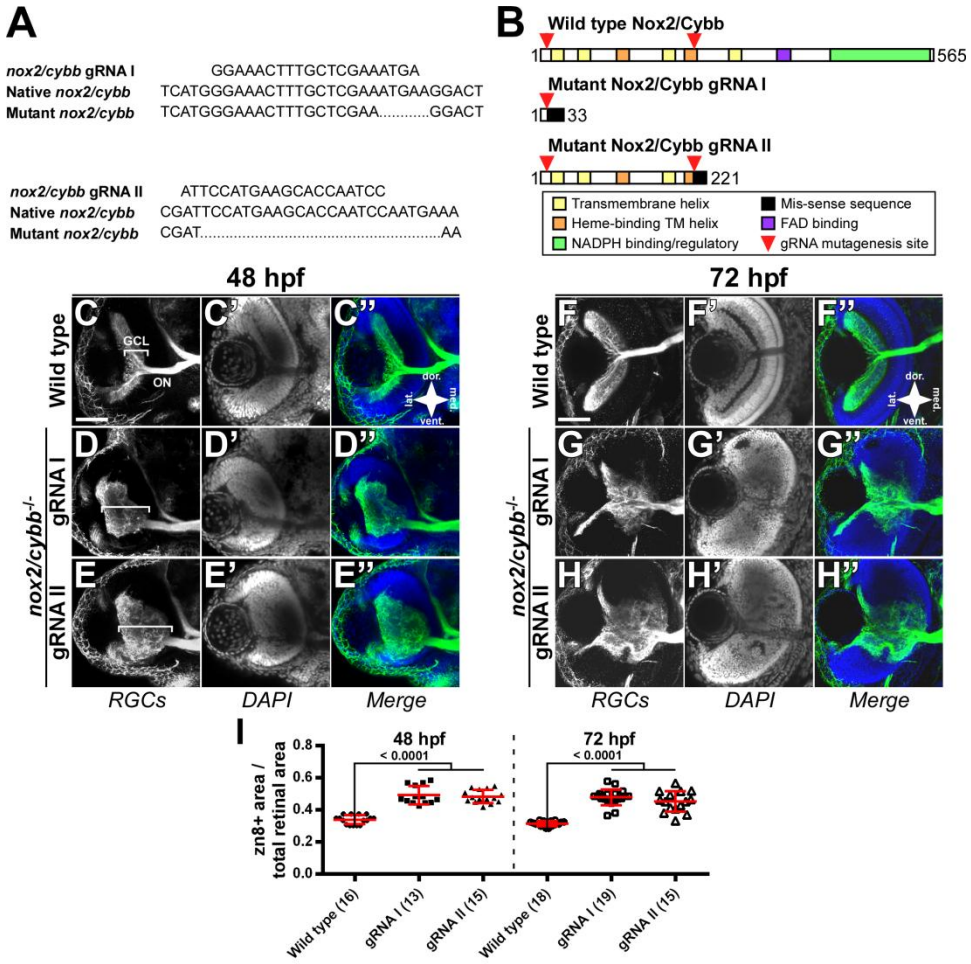

Figure 5.5: Homozygous *nox2/cybb* mutants exhibit GCL expansion (A) Genomic sequences of *nox2/cybb* mutants showing the 5 and 23 base pair deletions generated from gRNA I and II, respectively. (B) Schematic of the mutant Nox2/Cybb proteins based on translated mRNA sequences and alignment to the human protein sequence. (C–E") Micrographs of 48 hpf *nox2/cybb*$^{-/-}$ eyes labeled with the RGC marker, zn-8 (C–E), and DAPI (C'–E'). Mutants show defects in RGC outgrowth and retinal lamination. White brackets mark the ganglion cell layer. (F–H") *nox2/cybb*$^{-/-}$ eyes at 72 hpf labeled with zn-8 (F–H) and DAPI (F'–H') showing that the phenotype does not recover at later stages. Scale bars = 100 µm. (I) Graph of zn-8-positive area corresponding to the GCL divided by total retinal area in *nox2/cybb*$^{-/-}$ mutants. Number in parenthesis indicates the number of embryos analyzed. Graph shows mean ± standard deviation. p-values from Dunnett's tests are reported above comparison bars.

5.2.5 *nox2/cybb*$^{-/-}$ mutants exhibit mistargeted axons in the OT

We next investigated the effect of *nox2/cybb*$^{-/-}$ mutation on OT innervation. The area of the midbrain occupied by innervating ON axons in wt embryos is largely devoid of DAPI-positive cell bodies (Figure 5.6A–A"). This represents a prototypical morphology of the zebrafish OT (Kita et al., 2015). In *nox2/cybb*$^{-/-}$ mutants, zn-8-positive axons are mistargeted to adjacent midbrain regions outside of the presumptive OT (Figure 5.6B–C). Additionally, there is no area devoid of DAPI-positive cell bodies in the presumptive location of the OT suggesting the absence of a single nerve bundle entering the midbrain (Figure 5.6B'–C'). To better evaluate the changes in tectal innervation, we used line scans visualizing the changes in labeling intensity across the tectum. In wt embryos at 72 hpf, fluorescent intensity is highest in the area corresponding to the OT, and falls precipitously in adjacent regions (Figure 5.6B–C"). In contrast, line scans through tectal areas of *nox2/cybb*$^{-/-}$ mutants reveal lower signals in presumptive tectal areas, whereas zn-8-positive axons can be found in extra-tectal areas (Figure 5.6B, C, G). By 120 hpf, a significant number of zn-8 positive axons in the midbrain of *nox2/cybb*$^{-/-}$ mutants were not targeted uniformly to the presumptive OT (Figure 5.6E, F). Again, DAPI staining in mutant embryos failed to show an area free of cell bodies indicative of an axon tract (Figure 5.6 E', F'). Line scans continued to show a reduced and more diffuse zn-8 signals in tecta of mutants when compared with wild type embryos (Figure 5.6H). Collectively, these results show that *nox2/cybb*$^{-/-}$ embryos exhibit defective ON development that results in improper axonal targeting within the OT.

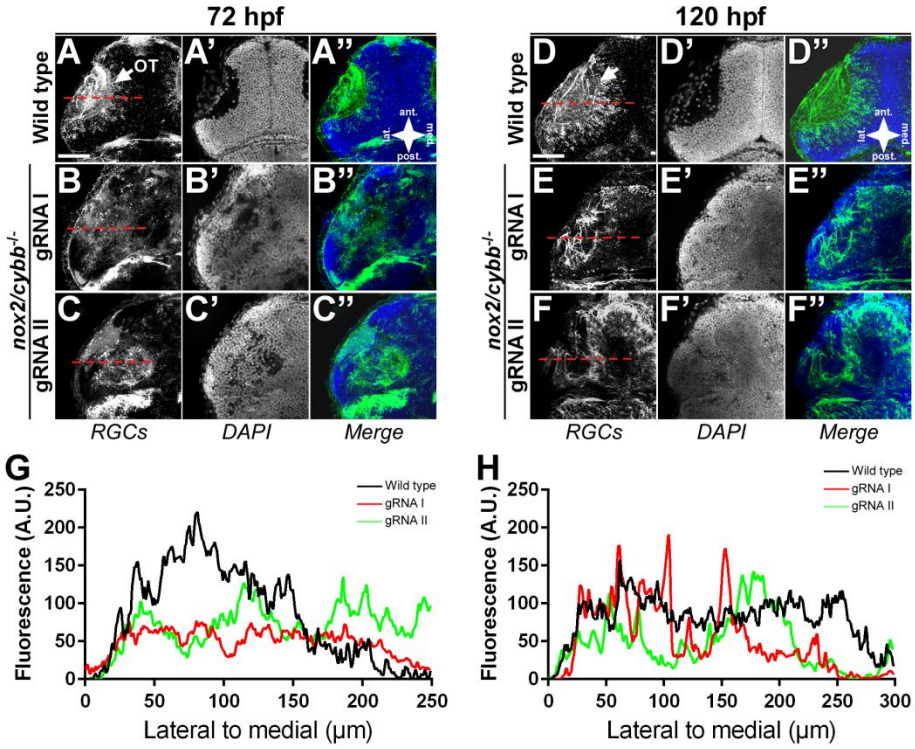

Figure 5.6: Axons are mistargeted in the OT of homozygous *nox2/cybb* mutants (A–C") Micrographs of 72 hpf *nox2/cybb*$^{-/-}$ midbrains labeled with zn-8 (A–C), and DAPI (A'–C'). Mutants show defects in tectal innervation. (D–F") Wild-type (D) and *nox2/cybb*$^{-/-}$ midbrains at 120 hpf labeled with zn-8 (E–F) and DAPI (E'–F') showing that the phenotype does not recover at later stages. White arrows indicate the optic tecta. Scale bars = 100 μm. (G–H) Line scans plotting fluorescent intensity of zn-8 signals versus position in the midbrain. Placements of the line scans are shown with red dashed lines in zn-8 panels.

5.3 Discussion

There is emerging evidence that NADPH oxidases play a role during nervous system development (Munnamalai and Suter, 2009; Dickinson et al., 2011; Le Belle et al., 2011; Coyoy et al., 2013; Munnamalai et al., 2014; Olguin-Albuerne and Moran, 2015; Ren et al., 2015; Wilson et al., 2015); however, the detailed functions of individual Nox isoforms in neuronal development are not well understood, especially *in vivo*. We have previously shown in cultured *Aplysia californica* neurons that cell autonomous Nox activity is critical for proper actin organization, actin retrograde flow, and neurite

outgrowth (Munnamalai and Suter, 2009; Munnamalai et al., 2014). The latter study, showed that Nox2 regulatory subunits co-localize at adhesion sites suggesting that Nox2 may be involved in adhesion-mediated axonal growth. A separate study identified Nox as a critical regulator of neuronal polarity and axonal growth of rat hippocampal neurons and mouse cerebellar granule neurons (Coyoy et al., 2013; Wilson et al., 2015).

Here, we investigated the role of Nox in zebrafish retinal development. We found that Nox inhibitors caused an expansion of the GCL, thinning of the ON, decreased OT innervation and mistargeting of axons within the OT. To investigate the role of specific Nox isoforms in this process, we used CRISPR/Cas9 mutagenesis to create chimeric mutants targeted to each of four zebrafish *nox* isoforms. Among all four *nox* isoform mutants, we observed that *nox2/cybb* chimeric mutant fish displayed a phenotype that was most similar to the one caused by pharmacological Nox inhibition. *nox2/cybb* chimeric mutants exhibited ON thinning and decreased tectal innervation caused by developmental delays, which were rescued by treatment with H_2O_2. In contrast to fish embryos treated with Nox inhibitor, the GCLs in these *nox2/cybb* chimeric mutants were not expanded when compared with wt embryos. To better characterize the impact of *nox2/cybb* mutation, we then bred chimeric mutants into stable lines carrying a truncated version of Nox2/Cybb for each of the two *nox2/cybb*-specific gRNAs (*nox2/cybb*$^{-/-}$). Homozygous mutants displayed GCL expansion, alterations in retinal morphology and mistargeting of axons in the OT. None of these phenotypes improve at later stages suggesting that they are not the result of developmental delays.

We can divide the phenotypes observed in this study into two broad classes. First, we found developmental delays that recovered at later developmental stages and could be

rescued by H_2O_2. These included ON thinning and a decrease in the area of OT innervation. Since both of these phenotypes respond to H_2O_2, it seems that they are generally sensitive to ROS and not absolutely dependent on Nox2/Cybb. Phenotypes of the second class did not improve with time or respond to the addition of H_2O_2. These include GCL expansion and the mistargeting of axons in the OT. This OT phenotype is distinct from the decrease in OT innervation described above. Here, axons reach the midbrain without delay, but extend outside of the presumptive OT. The absence of H_2O_2-mediated rescue for this second class of phenotypes suggests that they specifically require Nox2/Cybb, and alternative sources of ROS will not suffice. The presence or absence of some of these phenotypes with the different experimental approaches can be explained by inherit differences among the experimental techniques as further explained below. Whereas the individual phenotypes (GCL expansion, ON formation, area of OT innervation and targeting of axon in the OT) are likely functionally linked to one another, the current strategy of global Nox inhibition and knockout approach does not allow us to conclude that the observed effects are solely due to Nox2/Cybb activity in RGCs. Nonetheless, our current study clearly demonstrates a functional role for Nox2/Cybb in zebrafish retinal development and outgrowth of RGC axons towards the OT.

Embryos injected with CRISPR/Cas9 components display chimerism. This is due to the time required for CRISPR/Cas9 complex formation after injection. During this time, cells of the embryo continue to divide, leading to the generation of unique mutations in each cell. This results in chimeric animals carrying multiple mutations along with wild-type alleles. Since the type of mutation generated at the target site is variable, it is impossible to determine the net result on protein function. This means that chimeras

typically have less severe phenotypes, owing to the presence of an unknown percentage of functional enzyme. *nox2/cybb* chimeric mutants express both functional and non-functional Nox2/Cybb, leading to a global decrease in Nox2/Cybb activity. This decrease would be expected to diminish, but not completely inhibit propagation of Nox2/Cybb-mediated signals. This means that Nox2/Cybb-dependent events such as GCL development and targeting of axons in the OT still occur, but may happen more slowly. This explains the presence of developmental delays in chimeras characterized by ON thinning and decreased OT innervation that recover at later time points.

nox2/cybb$^{-/-}$ embryos on the other hand are not expected to express any functional protein, and thus, experience a strong, persistent loss of Nox2/Cybb activity. Given that Nox isoforms are known to compensate for one another, it is reasonable to speculate that *nox2/cybb*$^{-/-}$ mutants might activate compensatory mechanisms to survive. These mechanisms may include increased expression of other Nox isoforms, a decrease in cellular antioxidants or activated regulatory subunits binding to a different Nox isoform (Yang et al., 2001; Banfi et al., 2003; Frantz et al., 2006; Pendyala and Natarajan, 2010). Any of these alternative sources of ROS would be expected to mask developmental delays in much the same way that H_2O_2 can rescue these phenotypes. This fits our observations since *nox2/cybb*$^{-/-}$ mutants do not exhibit delays characterized by ON thinning or a decrease in OT innervation. However, compensatory sources of ROS might not be able to rescue phenotypes specifically requiring Nox2/Cybb, just as H_2O_2 cannot rescue these phenotypes. Again, this fits with our observation of GCL expansion and mistargeting of axons in the OT in *nox2/cybb*$^{-/-}$ samples. Compensation to mask

developmental delays is not expected in chimeras since functional Nox2/Cybb is still present in these embryos.

Differences in the timing and extent of interfering with Nox activity among the approaches used in our study might also explain the observed response to pharmacological Nox inhibition. Celastrol treatment is expected to completely inhibit all Nox isoforms temporally restricted to a few hours during ON development. These embryos display phenotypes of both classes such as GCL expansion, ON thinning and a decrease in the area of OT innervation likely stemming from the temporary but complete loss of Nox activity.

We would predict that *nox2/cybb*$^{-/-}$ mutants have localized decreases in ROS that impact signaling. ROS biosensors such as HyPer3 (Bilan et al., 2013) and ro-GFP (Meyer and Dick, 2010) allow *in vivo*, ratiometric imaging of ROS. However, it is unlikely that macro-scale changes in ROS production might be observed due to possible compensation by non-mutant Nox isoforms and mitochondria that contribute to global redox homeostasis. Our current approach of CRISPR/Cas9 mutagenesis does not allow for spatial or temporal control. However, newly developed techniques allow for restricted expression of Cas9 using cell-type specific (Ablain et al., 2015) or heat-shock promoters (Yin et al., 2015). Cell-type specific mutagenesis will provide insight into cell-autonomous functions of Nox, whereas temporally controlled mutagenesis will reveal the role of Nox at specific developmental stages. Additionally, these new technologies will allow for the dissection of molecular signaling pathways in specific cell types that underlie the phenotypes we report here.

In conclusion, we report that Nox2/Cybb is involved in the development and differentiation of RGCs in the zebrafish retina, the timing of ON outgrowth and the targeting of RGC axons within the OT. This finding advances the role of Nox-mediated signaling to include neurodevelopmental events in the retina. Lastly, we believe that the *nox2/cybb*$^{-/-}$ fish line generated in the present study will be a valuable resource for future investigations of Nox2/Cybb function not only in the nervous system, but also in other organ systems and cell types.

.

CHAPTER 6. CONCLUSIONS FROM NEURONAL CULTURE STUDIES

6.1 NOX2 and p40^{phox} in *Aplysia* neurons

In Chapter 3, I presented a series of experiments demonstrating the presence and function of a NOX2-like protein in *Aplysia* neuronal growth cones. I demonstrated that NOX activity is necessary for neurite extension, actomyosin-driven retrograde flow and actin organization. Treatment with NOX inhibitors, VAS2870 or celastrol, decreased retrograde flow rates and stalled neurite outgrowth (Figures 3.1 & 3.2). The effect was reversed when inhibitors were washed out after 20 minutes, but the effects of overnight application were irreversible. In cell bodies, NOX2 and p40phox were rarely colocalized. NOX2 localized to the plasma membrane, and p40^{phox} displayed a cytosolic, punctuate distribution (Figure 3.4). Some puncta were stained positive for NOX2, p40^{phox} and actin (Figure 3.4F'). VAS2870 caused a subtle decrease in ROS levels under basal growth conditions, but was able to block spikes in ROS production caused by the NOX activator phorbol 12, 13-dibutyrate (PDBu, Figure 3.5). In growth cones, antibody labeling for NOX2 and p40^{phox} revealed a punctuate distribution for both proteins (Figure 3.3). I then showed that NOX2 and p40^{phox} puncta colocalize with f-actin in the growth cone periphery (Figure 3.6). Additional experiments included in the published version of this work showed the dependence of peripheral NOX2 and p40^{phox} localization on actin and

the enrichment of NOX2/p40^{phox} colocalization at artificially-induced adhesion sites (Munnamalai et al., 2014). Collectively, this work identified NOX2 and p40^{phox} in *Aplysia*, and showed a direct interaction between the NOX subunits and actin. These results showed that NOX activity is necessary for proper actin dynamics and neurite outgrowth.

It is still unclear how exactly NOX-derived ROS are involved in growth cone signaling. In this chapter, I will introduce additional evidence from our lab suggesting that NOX may be involved in cell adhesions in neuronal growth cones and in zebrafish RGC neurite outgrowth. Additionally, I will briefly review upstream signals and downstream effectors that have been associated with NOX and are relevant to growth cone guidance. Finally, I will propose approaches to extend our current work addressing the function of NOX in axonal growth and guidance.

6.2 Evidence for NOX in neuronal cell adhesions

Compared to other species, neurites from *Aplysia* bag cell neurons grow slowly. The large size of the growth cone, which is excellent for imaging, makes turning assays difficult. Therefore, it is challenging to observe guidance in these cells. However, we can induce artificial adhesion sites that mimic turning responses by applying 5µm beads coated with a cell adhesion molecule (apCAM) directly to P domain of the growth cone (Suter et al., 1998; Suter and Forscher, 2001; Suter, 2011). The beads are carried retrogradely via actomyosin-driven flow. If the bead is restrained with a microneedle, the growth cone will respond by extending the microtubule-rich central domain and apply

additional force to pull the bead (Suter et al., 1998). This process is largely analogous to the turning and steering responses in smaller growth cones that direct axon growth and guidance

Additional work from our lab showed that NOX2/ $p40^{phox}$ colocalization is enriched at sites of bead interactions (Munnamalai et al., 2014). Whether NOX is activated in response to apCAM binding is still unknown, however the assembly of subunits would suggest this is the case. Future experiments will determine whether NOX activity is necessary for apCAM-meditated responses, but the finding of NOX2/ $p40^{phox}$ colocalization suggests that NOX2 may be activated by apCAM binding, and may play a role in downstream signaling that leads to growth cone turning.

6.3 Nox function in zebrafish retinal neurons

Cultured neurons with smaller, faster growing neurites would allow us to perform growth cone turning assays that are not possible with *Aplysia* neurons. Since my *in vivo* studies focus on retinal nerves from zebrafish, I decided to culture these cells for *in vitro* assays. I performed preliminary experiments on neurons derived from 36 hpf zebrafish retinas (AB strain) on coverslips coated with 20µg/mL laminin. Retinal neurons exhibited processes extending >50µm after 12 hours in culture growing at 10 ± 1.3µm/hr (Figure 6.1A-E). This growth rate is similar to what has been observed for retinal neurons *in vitro* (Chen et al., 2013) and *in vivo* (Kita et al., 2015). I then tested the response of retinal neurons to the application of growth factors and cues including nerve growth factor (NGF, 20ng/mL), netrin-1 (Netrin, 250ng/mL) and semaphorin 3E (Sema3E, 5µg/mL,

Figure 6.1E). Neurite growth rates were no different in response to NGF, but netrin-1 caused a slight, but not statistically significant decrease in growth rate (Figure 6.1E). This could be due to the relatively low number of cells analyzed (n = 12) in this preliminary study. The response to sema3E was a robust retraction of neurites. This pilot study showed that we could culture zebrafish retinal neurons in our lab and that neurite growth rates respond to growth factors and guidance cues.

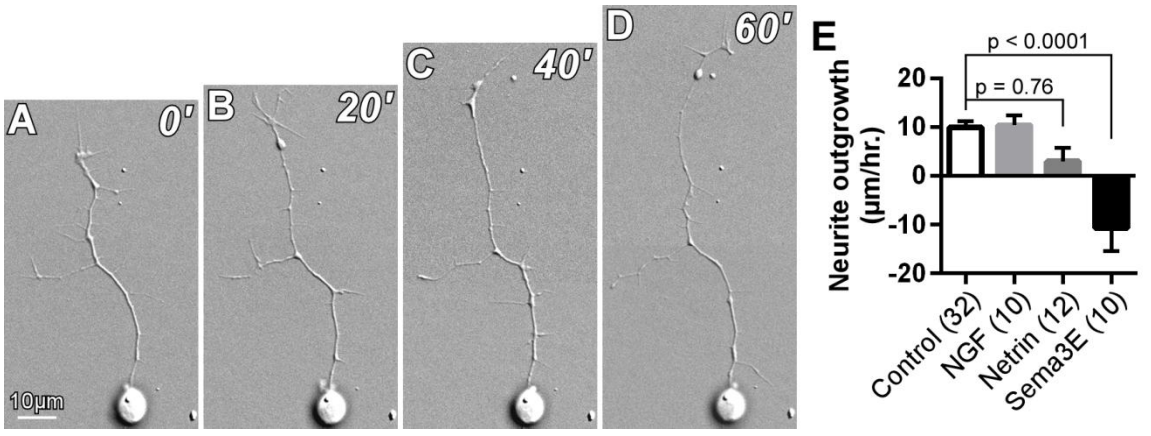

Figure 6.1: Cultured zebrafish retinal neurons respond to soluble cues (A-D) Time-lapse image series showing neurite outgrowth from a retinal neuron harvested from a wild type zebrafish at 36 hpf. Cells were cultured on laminin for 12 hours prior to imaging. Images were captured at 20 minute intervals for 1 hour. (E) Graph showing mean neurite growth rates ± SEM under control conditions (serum-free media) and in response to global application of the indicated guidance cue. Numbers in parenthesis represent the numbers of cells analyzed. Significant differences were identified with one-way ANOVA ($F(3, 60) = 13.72$, $p < 0.0001$). p-values for Dunnett's multiple comparison tests versus controls are shown above comparison bars. $p < 0.05$ was considered significant.

Since my preliminary trials, use of the zebrafish neuronal culture system has been extended by others in the lab. We now culture neurons derived from the *Tg(ath5:GFP)* transgenic line to restrict our analysis to RGCs. We have also moved from global application of growth factors and guidance cues to directional applications that allow for quantification of neurite turning in addition to measurements of growth rate.

We also turned to the *in vitro* culture system to test the effect of Nox inhibitors on RGC neurite outgrowth. The *in vivo* studies described in Chapter 5 present a complex set of phenotypes that likely stem from the global manipulations of Nox activity with inhibitor applications and CRISPR mutants. To focus specifically on Nox in RGCs, we applied the inhibitors VAS2870 or celastrol to retinal neurons in culture. We saw a dose-dependent reduction in RGC neurite outgrowth following a 15 minute pre-incubation with the inhibitors. The sensitivity of these cells to the drugs suggests that RGCs express one or more NOX isoforms, and that Nox activity is necessary for neurite outgrowth. Additional experiments are needed to uncover the isoforms expressed and the mechanistic details of Nox-mediated signaling in RGCs. The experiments proposed in section 6.6 may be performed using *Aplysia* bag cell neurons or zebrafish RGCs.

6.4 Upstream activators of NOX

From our studies, NOX appears to be important for neurite outgrowth in multiple species. Additionally, preliminary work suggests that NOX may be activated at adhesion sites in *Aplysia* neurons. If NOX is to act as a signal in axon growth and guidance, it is practical to consider what upstream signals might be using NOX-derived ROS as an intermediate. At present, there is little evidence for the involvement of NOX in traditional guidance cue signaling pathways like semaphorins, netrins, and slits. However, the finding that Mical-derived ROS is necessary for semaphorin-mediated axon guidance in *Drosophila* (see Chapter 1) leaves open the possibility that NOX may be involved in some of these pathways as well. Axons are also guided by morphogens, mitogens,

extracellular matrix proteins, proteoglycans and cell adhesion molecules (Fadool and Dowling, 2008; Stenkamp, 2015). While the involvement of NOX in these cellular signals has not been well studied in neurons, there is overwhelming evidence that NOX mediates these signals in other cell types. To provide a basis for further experiments, the following sections introduce NOX-mediated signaling pathways that are known to induce cell motility. Additional NOX and ROS-related cellular signals involved specifically in the development of the optic nerve are presented in Chapter 7

6.4.1 Platelet-derived growth factor

Shortly after their discovery, NOX enzymes were found in the cells of the vasculature, and much of what is known about NOX-mediated cell signaling comes from this field (Drummond and Sobey, 2014). The cells lining the walls of the vasculature control blood circulation and blood pressure. In particular, the misregulation of two cell types, vascular smooth muscle cells (VSMCs) and endothelial cells, contribute to the onset and progression of atherosclerosis and hypertension (Hadrava et al., 1991; Castellon and Bogdanova, 2016). Both cell types respond to platelet-derived growth factor (PDGF). VSMCs treated with PDGF become proliferative and motile, and it is well-established that PDGF stimulation of VSMCs is accompanied by H_2O_2 production (Sundaresan et al., 1995). In the same study, authors found that application of ROS scavengers blocks PDGF-stimulated kinase activity and chemotaxis, demonstrating that ROS production was necessary for signal propagation. Subsequent studies found that the NOX inhibitor VAS2870 also blocked PDGF-induced ROS production and VSMC

migration (ten Freyhaus et al., 2006). Interestingly, the authors found that VAS2870 did not affect PDGF-stimulated DNA synthesis or cell cycle progression, suggesting that these processes are not dependent on NOX. Finally, NOX1 was identified as the source of ROS downstream of PDGF in VSMCs (Maheswaranathan et al., 2011).

Aortic smooth muscle cells (ASMCs) also produce ROS and become proliferative in response to PDGF. Unlike VSMCs, ROS produced by human ASMCs in response to PDGF is dependent on NOX5 (Jay et al., 2008). It is unclear exactly how PDGF signaling pathways are divergent in VSMCs versus ASMCs in other aspects, but these studies reveal that the source of ROS varies with cell type. Since NOX1 and NOX5 are activated by very different types of upstream signals, these results suggest that PDGF signals are propagated very differently in these two cell types

Endothelial cells also become proliferative in response to PDGF, and this is dependent on the production of ROS via NOX. PDGF-induced cell migration in endothelial cells is specifically dependent on NOX1 (Garrido-Urbani et al., 2011). Authors found that endothelial cells express NOX1, 2 and 4, but PDGF signal propagation is dependent on NOX1. This is one example of a cell type coexpressing multiple NOX isoforms but maintaining functional specificity for each. This is relevant to the results I presented in Chapter 4 of overlapping expression domains for multiple *nox* genes in the zebrafish central nervous system.

6.4.2 Additional NOX-mediated growth factors

Vascular endothelial growth factor (VEGF) is a potent mitogen that promotes angiogenesis. VEGF stimulation of endothelial cells causes proliferation and migration. Like PDGF, VEGF stimulation is accompanied by an increase in ROS. Preincubation with NOX inhibitors blocks the VEGF-mediated spike in ROS along with cell migration and proliferation demonstrating that all of these responses are NOX dependent (Abid et al., 2000). A subsequent study showed that VEGF stimulation induced that translocation of $p47^{phox}$ to sites of membrane ruffling (Wu et al., 2003). Translocation was accompanied by $p47^{phox}$ phosphorylation, Rac1 activity and ROS production, and this suggests that NOX2 is responsible for VEGF-induced ROS production.

Angiotensin II (AngII) is a growth promoting mitogen for smooth muscle cells (Fyhrquist et al., 1995). One study identified expression of NOX1, 2 and 4 in VSMCs, but found that NOX1 specifically contributed to AngII signaling and proliferative responses (Lassegue et al., 2001). A separate study found that NOX4 was responsible for basal ROS production in rat ASMCs, but NOX1 was specifically activated in response to AngII (Dikalov et al., 2008). Authors of a different study found NOX1 and NOX4 activity downstream from insulin-like growth factor 1 in VSMCs (Meng et al., 2008). However, the primary isoform responsible for ROS production in this pathway is still unknown.

NGF-mediated signaling has also been linked to NOX. Treatment of PC12 cells with NGF causes neurite extension that is accompanied by a rise in ROS levels. NGF exposure leads to an increase in *nox1* and decrease in *nox2* mRNA transcripts.

Accordingly, NOX inhibitors and *nox1*-targeted ribosymes block NGF-induced ROS production (Ibi et al., 2006). However, the researchers found that blocking ROS enhanced NGF-induced neurite outgrowth. They went on to speculate that NOX1 may prevent excessive growth of neurites when cells are exposed to NGF.

Collectively, these results show that several growth factors induce the production of ROS via NOX and rely on ROS-mediated signal transduction for some functions. It should be noted that VSMCs, ASMC and endothelial cells all express multiple NOX isoforms. However, specific isoforms seem to be involved in the transduction of signals. Upstream signals are even able to differentiate between the NOX1 and NOX2, which are regulated in very similar ways. How growth factor signaling cascades target individual NOX isoforms is an open question that deserves further study.

6.4.3 Cell adhesions

Focal adhesions (FAs) are multi-protein complexes linking the cytoskeleton to the extracellular matrix. Formation and turnover of FAs is critical for cell motility, and has been implicated in cellular behaviors ranging from cancer metastasis to axon guidance (Wozniak et al., 2004; Myers et al., 2011). Treatment of endothelial cells with H_2O_2 causes the formation of stress fibers and phosphorylation of the FA-associated proteins focal adhesion kinase (FAK) and paxillin (Vepa et al., 1999). Subsequent studies showed a direct interaction between the NOX2 subunit $p47^{phox}$ and another FA protein, TRAF4 (Wu et al., 2005). TRAF4 binding helped localize $p47^{phox}$ to the FA site. In this case, ROS generated at FAs oxidized a protein tyrosine phosphatase, PTP-PEST, and likely

inhibited function. This is similar to what was discussed in Chapter 1 wherein oxidation inhibits the function of PTP-1B (Salmeen et al., 2003). A separate study suggested the involvement of NOX4 in FAs due to the colocalization of NOX4 with vinculin, an FA complex protein (Hilenski et al., 2004). While this work was solely based on immunolabeling, additional evidence has shown that NOX4 mediates FA turnover and migration in VSMCs (Datla et al., 2014). More recent studies continue to support for the role of NOX-derived ROS in establishment and turnover of FAs during cell migration (Basuroy et al., 2010; Abdelsaid and El-Remessy, 2012). However, much of the current work is focused on NOX1/4 in spite early reports showing NOX2 in FA complexes.

Vascular CAM (VCAM) regulates the maintenance of stem cell populations in the subventricular zone of adult mice. VCAM signaling is accompanied by ROS production via NOX2 (Kokovay et al., 2012). The results of this study are particularly relevant to my work since they demonstrate a role for NOX2-mediated CAM signaling in the central nervous system.

NOX is known to mediate growth factor signals, focal adhesions dynamics and CAM-based adhesions (summarized in Table 6.1). The role of these signals in axon guidance is well established, and NOX enzymes are known to be expressed in neurons. Further, our work demonstrates the importance of NOX activity to neurite outgrowth. Therefore, it is reasonable to hypothesize that NOX-derived ROS may be involved in axon growth and guidance downstream of one or more of these signals. I propose experiments designed to test this hypothesis and extend our current results in section 6.6.

Table 6.1: Growth factors and adhesion molecules involving NOX

Protein	Function(s)	Section	Source of ROS
PDGF	growth factor: proliferation, chemotaxis	6.4.1	NOX1/5
VEGF		6.4.2	NOX2
AngII			NOX1
NGF			NOX1
TRAF4	focal adhesions: migration	6.4.3	NOX2
Vinculin			NOX4
Integrin			NOX2/4
VCAM			NOX2

6.5 Downstream targets of NOX-derived reactive oxygen

Axon and neurite outgrowth is driven by cytoskeletal dynamics. In Chapter 1, I introduced what is known about redox regulation of actin and microtubules. It is tempting to speculate that NOX-derived ROS in *Aplysia* growth cones and zebrafish acts directly on the cytoskeleton to effect dynamics, organization and neurite outgrowth. However, there are several other redox-sensitive effectors that are involved in cytoskeletal remodeling and cell motility. Many of these have been previously studied in our lab, and thus, are even more relevant to consider for future experiments.

6.5.1 Src

Src is a non-receptor tyrosine kinase activated downstream of growth factors, adhesion molecules and other cellular signals. Src signaling is commonly implicated in cancer and has also been shown to be involved in growth cone guidance (Suter and Forscher, 2001; Suter et al., 2004; Buday and Downward, 2007; He et al., 2015). Our lab

has previously shown that Src activation promotes lamellipodial protrusion and filopodial stability in *Aplysia* growth cones (He et al., 2015). With regard to NOX, early studies showed that $p47^{phox}$ was a Src substrate, making Src an upstream activator of NOX2 in VSMCs (Touyz et al., 2003). However, subsequent studies showed that Src is activated by H_2O_2 oxidation via the formation of a C-terminal disulfide bond (Giannoni et al., 2005; Mills et al., 2007; Basuroy et al., 2010). Eventually, it was discovered that Src and NOX1 form a positive feedback loop in response to inflammatory cytokines in beta cells (Weaver et al., 2012; Weaver and Taylor-Fishwick, 2013).

Like developing axons, neutrophils and leukocytes are highly motile. These cells infiltrate wound margins to facilitate healing. In zebrafish, H_2O_2 is produced at wound margins by DUOX, and this ROS acts as a signal to recruit leukocytes to the damage tissue (Niethammer et al., 2009). A zebrafish Src family kinase member, Lyn, was found to be responsible for redox sensitivity in neutrophils. Oxidation of cysteine 466 mediates Lyn activation and neutrophil migration into the ROS gradient (Yoo et al., 2011). This work was extended to show that NOX-derived ROS and Src are necessary for tail regeneration and, surprisingly, the reduction of post-injury inflammation (Yoo et al., 2012; Tauzin et al., 2014). Our lab has significant experience studying Src in *Aplysia* growth cones. Therefore, we are uniquely equipped to investigate a possible NOX/Src signaling axis in this model system.

6.5.2 Cortactin

Cortactin is an f-actin binding protein and a Src substrate (Decourt et al., 2009; He et al., 2015). Our lab has also found that cortactin is involved in lamellipodial and filopodial dynamics in *Aplysia* growth cones (He et al., 2015). It has been shown that H_2O_2 treatment of endothelial cells caused an increase in Src-dependent cortactin phosphorylation (Li et al., 2000). This is expected since Src activity is increased in response to ROS application. However, later studies revealed that $p47^{phox}$ is localized to f-actin filaments, and this interaction is mediated by direct interaction with cortactin (Touyz et al., 2005). $p47^{phox}$ has also been linked to the regulation of cytoskeletal dynamics via cortactin (Patel et al., 2013). However, this study posited a NOX-independent function for $p47^{phox}$ so the exact connection between cortactin and NOX-derived ROS remains unclear.

6.5.3 Slingshot/cofilin

Actin depolymerizing factor (ADF)/cofilin is an actin filament severing protein that regulates actin dynamics. ADF/cofilin activity is involved in several axon guidance pathways including netrins, ephrins and slits (Marsick et al., 2010; Marsick et al., 2012). ADF/cofilin binds and severs existing f-actin filaments. This causes f-actin to depolymerize and creates new actin nucleators to facilitate polymerization (Bamburg and Bernstein, 2010). The phosphorylated form of ADF/cofilin is inactive, therefore activation is mediated by a phosphatase called Slingshot (Niwa et al., 2002; Kaji et al.,

2003). Slingshot is regulated by binding to a 14-3-3 protein, which maintains Slingshot in the inactive state. NOX-derived ROS oxidize the 14-3-3 protein inducing the release of Slingshot and subsequent activation of cofilin (Kim et al., 2009). Redox regulation of Slingshot/14-3-3 binding has been observed in VSMCs (Lee et al., 2009; Maheswaranathan et al., 2011) and keratinocytes (Kim et al., 2011b). The study in keratinocytes found NOX-mediated Slingshot regulation in response to neuregulin, a growth factor known to be involved in neurodevelopment.

6.5.4 WAVE and moesin

The WASP-family verprolin homologous protein-1 (WAVE1) is an actin binding protein involved in the regulation of actin lamellipodial networks via the nucleator Arp2/3 (Pollitt and Insall, 2009). In response to VEGF, WAVE1 is localized to membrane ruffles and mediates actin reorganization. One study found that WAVE1 directly interacts with $p47^{phox}$, and this interaction is necessary for cytoskeletal modification (Wu et al., 2003).

Early but promising research implicates another actin binding protein, moesin, in NOX-mediated signaling. Moesin is one of a family of proteins shown to link f-actin to the plasma membrane (Tsukita and Yonemura, 1997). Cell-free studies have shown that moesin binds to the PX domain of both $p47^{phox}$ and $p40^{phox}$ (Wientjes et al., 2001). There is no functional data to link moesin to NOX activity, but it is noteworthy given that other actin binding proteins, like cortactin and WAVE, have been found to be regulated by NOX-derived ROS.

6.6 Future directions for the growth cone project

The studies discussed in sections 6.4 and 6.5 show that NOX is involved in growth factor and adhesion-based signaling, and downstream signals in these pathways are redox sensitive. While the bulk of this evidence is derived from non-neuronal cells, the basic mechanisms of signal propagation and regulation of dynamics may translate to many motile cells. My work, discussed in Chapters 3, shows the requirement for NOX activity in *Aplysia* bag cell neurons, and the preliminary studies in section 6.3 extend this into cultured zebrafish RGCs. In addition, we have evidence that suggests NOX2 may be active at adhesion sites in *Aplysia* growth cones (Munnamalai et al., 2014). Moving forward, I propose to investigate the specific function of NOX-derived ROS during axon growth and guidance. I would then screen for soluble guidance cues and substrate molecules that modulate the production of ROS in the neuronal growth cone. Next, I would dissect the molecular signaling pathways downstream of the cues that lead to NOX activation. Finally, I would investigate the direct effectors of NOX-derived ROS that contribute to growth cone turning.

An essential part of all of these studies would be to monitor cellular ROS levels in real time. In the past, we have used cell-permeable dyes like 2',7'-dichlorofluorescin (DCF) and Peroxyfluor-6 (PF6) to monitor ROS levels (Dickinson et al., 2011). These dyes require the addition of a volume indicator dye, and are subject to ROS-mediated autofluorescence. Therefore, they are not optimal for long-term, dynamic ROS imaging of single cells. Better suited for these experiments are the latest generation ROS biosensors: roGFP2-Orp1 and HyPer3 (Meyer and Dick, 2010; Bilan et al., 2013).

Table 6.2: Downstream effectors targeted by NOX-derived reactive oxygen

Protein	Function(s)	Section	Source of ROS
Actin	cytoskeletal remodeling	1.2.1	Unknown
Src	tyrosine kinase	6.5.1	NOX1/3
Lyn			NOX
Cortactin	actin adaptor protein	6.5.2	NOX2
Slingshot	regulation of actin dynamics	6.5.3	NOX2
WAVE		6.5.4	NOX2
Moesin	actin-membrane anchor		NOX2

'ROS' refers to redox sensitive targets where no source has been identified. 'NOX' indicates that no specific isoform has been identified.

roGFP2-Orp1 relies on the peroxidase activity of yeast Orp1 to oxidize the redox sensitive roGFP2 (Gutscher et al., 2009). The H_2O_2-specific HyPer3 is based on a circularly permutated yellow fluorescent protein inserted into the regulatory domain of a naturally occurring, redox sensitive protein called OxyR (Bilan et al., 2013). Both probes provide a quantitative method of detecting ROS in live cells, and are preferable to cell-permeable dyes. One potential drawback is the pH sensitivity of HyPer, but this is not a concern for roGFP (Roma et al., 2012). However, newly developed pH biosensors like pHusion make it possible to measure pH changes and control for their effects on HyPer3 signals (Gjetting et al., 2012).

6.6.1 Correlating reactive oxygen with neurite outgrowth

Having shown that NOX inhibitors decrease basal ROS levels and cause neurites to stall, it is now imperative to correlate ROS production and neurite outgrowth. We have HyPer3 and roGFP2-Orp1 in our lab, and I propose using both biosensors, independently, to quantify changes in growth cone ROS during neurite outgrowth. In the past, we have

used dye-based measurements to correlate ROS levels with neurite growth rates. In these experiments, we measured ROS at the end of 12 or 24 hours and compared this to overall outgrowth. The major drawback of this approach is that ROS is a very short-lived signal, and a single measurement is unlikely to correlate with long-term outgrowth. Instead, I would predict that transient spikes and troughs in ROS production would precede changes in growth rate. To capture these effects, we can use time-lapse imaging of *Aplysia* or zebrafish neurons expressing ROS biosensors to determine whether or not ROS levels correlate with or even predict changes in growth rate.

A newly developed set of cell-permeable actin and microtubules probes based on silicon rhodamine dyes allow live-imaging of the cytoskeleton. Called SiR-actin and SiR-tubulin, these probes use far-red fluorescent wavelengths that would be compatible with either roGFP2 or HyPer3 (Lukinavicius et al., 2014). We have used these probes to label NIH/3T3 fibroblasts for a separate project (Figure 6.1). Both SiR-actin and SiR-tubulin provide stable, uniform signals in live cells, but additional validation experiments are necessary to confirm the extent of labeling. However, preliminary results are promising given that the tubulin probe even appears to label the primary cilia (Figure 6.1B). Combining the cytoskeletal probes with ROS biosensors we could simultaneously measure ROS levels, cytoskeletal restructuring and neurite outgrowth.

To directly determine the impact of changing ROS levels on neurite outgrowth, we can manipulate ROS concentrations by adding H_2O_2 or ROS scavengers to the media. More specifically, we can determine the role of NOX by treating cells with specific NOX inhibitors (VAS2870, celastrol or apocynin) or activators (phorbol 12-myristate 13-acetate or phorbol 12 13-dibutyrate). With the ROS biosensors, we can directly

investigate the spatiotemporal relationships between intracellular ROS, cytoskeletal organization and neurite outgrowth.

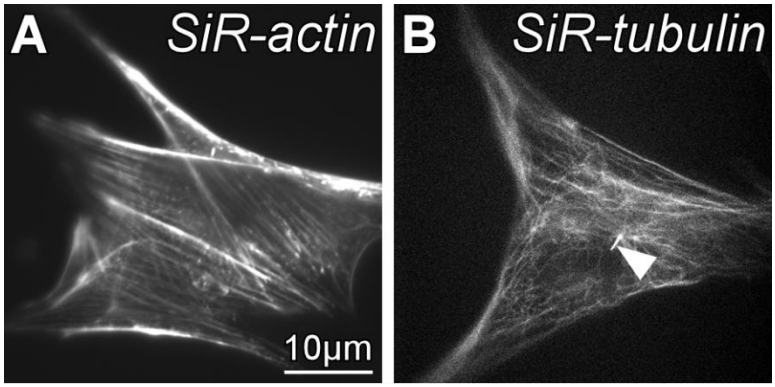

Figure 6.2: SiR-actin and SiR-tubulin label cytoskeletal structures in fibroblasts NIH/3T3 fibroblasts were incubated with 100nM probes in normal media overnight. A primary cilia-like structure is visible with SiR-tubulin (arrowhead). Scale bar = 10µm.

We could then investigate the ability of asymmetric gradients of ROS across the growth cone to generate turning responses. Directional application of exogenous H_2O_2, ROS scavengers, NOX activators or inhibitors would be expected to generate gradients of ROS across the growth cone. We can verify this using the ROS biosensors. Simultaneously, we can quantify changes in the cytoskeleton, growth cone morphology and neurite outgrowth in response to the ROS gradients. This would be the first demonstration of ROS levels predicting growth cone steering. Combined with quantitative measurements of intracellular ROS and cytoskeletal dynamics, this type of experiment would provide excellent evidence for the importance of NOX-mediated redox signaling in axon guidance.

6.6.2 Identification of upstream guidance cues

The experiments proposed above focus on the direct effect of ROS, but do not provide any physiological relevance. Even if NOX-mediated ROS can be shown to alter neurite outgrowth and guidance *in vitro* that it does not prove their function *in vivo*. If redox signaling plays a role in axon patterning, ROS production must be controlled by an upstream guidance cue. Earlier in this chapter, I detailed what is known regarding NOX-mediated growth factor and adhesion signaling. Given this, I predict that some growth factors, guidance cues or substrate proteins will modulate NOX activity in growth cones. Applied asymmetrically, cues should induce a gradient of ROS that can be measured with the ROS biosensors. Cues can be presented to the cell in various ways. The protein coated, 5µm silica beads, discussed earlier, work well in Aplysia. Traditional pipet assays or the development of patterned substrates would be more suitable for zebrafish neurons.

Initial experiments would be aimed at identifying cues that asymmetrically alter intracellular ROS concentrations. This would be accomplished by combining directional application of cues with ROS biosensor imaging. Once a suitable set of cues is identified, necessity of ROS generation in cue-mediated turning can be tested by applying low concentrations of ROS scavengers to block spikes in ROS. Further, the involvement of NOX can be verified using the small-molecule inhibitors and activators presented in earlier sections. For example, if cue-mediated turning requires the production of NOX-derived ROS, pretreatment with a low concentration of scavenger or NOX inhibitor should block turning responses. The relationship between ROS generation and growth cone turning may be complex, and the response may vary among cues. Combining ROS

measurements, cytoskeletal imaging and neurite guidance in response to specific cues would provide physiologically relevant evidence for the necessity of NOX-derived ROS in axon guidance.

6.6.3 Characterization of downstream targets

A more difficult problem is identifying downstream targets of NOX-derived ROS. The simplest possible situation would be if NOX-derived ROS acted directly on the cytoskeleton, likely actin, to mediate changes in stability and dynamics. However, given the number of redox sensitive targets involved in growth cone steering, discussed in section 6.5, it is unlikely that actin is the only effector of ROS. Time-lapse imaging with SiR-actin and ROS biosensors would provide adequate temporal resolution to make this determination. Direct effects of ROS on the cytoskeleton would happen rapidly while effects controlled by intermediate signals would take longer to propagate. Careful dissection of the timecourse of cytoskeletal rearrangements in response to ROS-generating cues would delineate direct versus indirect effects, and inform subsequent studies.

The next step would be to directly assess protein oxidation in response to cues. There is a comprehensive review of methods to detect all forms of oxidation, and I will not discuss them extensively here (Shacter, 2000). Instead, I will briefly mention methods that would be most relevant to NOX-mediated protein oxidation in growth cones. S-glutathionylation, cysteine/methionine oxidation and disulfide crosslinking are the most common protein modifications caused by H_2O_2, the primary signal produced by NOX

(Brandes et al., 2014). These can be detected by high performance liquid chromatography, SDS-PAGE and mass spectroscopy (Shacter, 2000; Verrastro et al., 2015). However, this is not a straightforward procedure since cultured neurons are typically plated at low densities and are non-proliferative. This makes it challenging to obtain enough protein for analysis. Alternative methods such as harvesting from cue-treated explant cultures would provide higher amounts of protein, but reduce the cell type specificity since non-neuronal cells may be included. This compromise may be necessary, however, to perform direct analysis of protein oxidation.

Another strategy would be to look for proteins that are activated in response to ROS. Biosensors for Src and FAK, both known to be redox sensitive, are available (Gulyani et al., 2011; Seong et al., 2011), and our lab has done significant work with a novel Src biosensor in *Aplysia*. Using these tools, we could look for changes in activation of either protein in response to ROS-generating cues. More importantly, we could dissect the time course of activation to determine if either protein is the direct effector of NOX-derived ROS. Unfortunately, the Src/FAK and ROS biosensors have similar excitation and emission spectra, and are therefore not compatible. However, we can establish a time course of ROS production and Src/FAK activation in separate experiments

In some of the studies listed in the previous sections, authors developed oxidation-insensitive mutants such as SrcC245A and SrcC487A (Giannoni et al., 2009). We could develop redox-insensitive mutants for targets we suspect are oxidized in response to cues, and the mass spectroscopy experiments described above would identity putative oxidation sites in the target proteins. Done correctly, this approach would produce effectors that cannot be oxidized, but otherwise maintain their normal function.

Cells expressing these redox-insensitive mutants would not be expected to exhibit turning in response to cues that require oxidative signaling.

Using the described combination of approaches we can extend the current work to directly identify cues that use NOX-derived ROS as intermediate signals and characterize the spatiotemporal parameters of ROS generation. We can measure the time course of cytoskeletal rearrangements, growth cone turning and neurite outgrowth in response to cue-induced ROS production. We can also specify the downstream effectors of ROS that lead to growth cone turning and drive neurite outgrowth. Collectively, the proposed experiments would allow us to characterize an entire ROS-mediated signaling pathway in neurons induced by specific cues.

CHAPTER 7. CONCLUSIONS FROM ZEBRAFISH STUDIES

7.1 Summary of current work on zebrafish neurodevelopment

In Chapter 5, I described a series of experiments designed to investigate the functions of NOX enzymes in zebrafish neurodevelopment. I began applying NOX inhibitors to developing embryos. From these early screens, I identified defects in the optic nerve and anterior forebrain commissures (Figure 5.1 & 7.1). I chose to focus subsequent studies on the optic nerve because of the potential functional implications of this system. Treatment with the NOX inhibitor celastrol caused an expansion of the glial cell layer (GCL), thinning of the optic nerve (ON) and a decrease in ON axons reaching their targets in the optic tectum (OT, Figure 5.1). ON thickness and OT innervation was rescued by the addition of 2mM H_2O_2, but GCL expansion was not (Figure 5.1) Generation of chimeric, isoform-specific *nox* mutants showed that mutations of *nox2/cybb* resulted in ON thinning and a decrease in OT innervation comparable to inhibitor treatments (Figure 5.2). No GCL expansion was observed in chimeric *nox2/cybb* mutants (Figure 5.2). Time-lapse imaging of *nox2/cybb* chimeras revealed that ON thinning was transient and recovered by 72 hours post-fertilization (hpf, Figure 5.3). Similarly, the area of OT innervation increased between 72 and 96 hpf in *nox2/cybb* chimeras (Figure 5.3) indicating that both phenotypes were the result of developmental

delays. In addition, both phenotypes were partially rescued by the addition of 2mM H_2O_2.

Surprisingly, homozygous *nox2/cybb* mutants (*nox2/cybb*$^{-/-}$) did not show significant ON thinning like *nox2/cybb* chimeras. Instead, these homozygous mutants displayed GCL expansion (Figure 5.4) and defects in axon targeting within the OT (Figure 5.5). In addition, *nox2/cybb*$^{-/-}$ embryos had defective retinal lamination visualized with DAPI nuclear staining. None of the observed phenotypes improved at later stages.

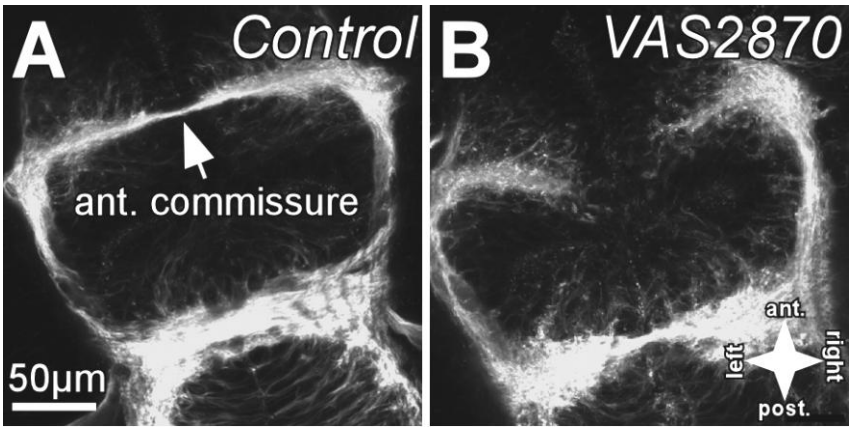

Figure 7.1: Forebrain development in zebrafish treated with a Nox inhibitor (A-B) Dorsal views of a 24 hpf embryo immunolabeled with an anti-acetylated tubulin antibody. Embryos were treated with 0.1% DMSO (A) or 2µM VAS2870 (B) from 18-22 hpf to coincide with forebrain commissure development. The anterior commissure is indicated with a white arrow in A. Commissures of inhibitor-treated embryos fail to close at the midline.

In all cases, ON thinning and decreased OT innervation recovered at subsequent developmental stages and was rescued by H_2O_2. Therefore, both of these phenotypes can be regarded as symptoms of developmental delays. Further, that they can be rescued by global application of exogenous ROS may indicate that they are generally mediated by ROS, and do not specifically require NOX2/CYBB. That is to say that NOX2/CYBB may normally produce the ROS that signals in these pathways, but it can be substituted for with other sources of ROS. In contrast, GCL expansion and axon targeting in the OT

do not recover at later stages, and in the case of inhibitor treatments GCL expansion cannot be rescued by H_2O_2. This may indicate that these phenotypes are mediated specifically by NOX2/CYBB, and cannot be substituted for other sources of ROS.

Chimeras may not be expected to show GCL expansion or mistargeted OT axons because they carry some percentage of functional NOX2/CYBB. Therefore, NOX2/CYBB-mediated signaling would still occur, but may take more time due to the partial loss of protein function in chimeras. This simultaneously explains the presence of developmental delays and lack of permanent phenotypes. Conversely, *nox2/cybb*$^{-/-}$ embryos that have a complete loss of NOX2/CYBB may be forced to upregulate compensatory mechanisms in order to survive. Compensation among NOX enzymes has been evidenced in several studies (Yang et al., 2001; Banfi et al., 2003; Frantz et al., 2006; Pendyala and Natarajan, 2010), and this is not surprising given the similarities among isoforms. Upregulation of other NOX isoforms may not even be necessary. Recall that many cells in the central nervous system express multiple isoforms. Some of the studies cited above have shown that activated NOX2 regulatory subunits can bind and activate NOX1 (Bedard and Krause, 2007; Bedard et al., 2007; Sorce and Krause, 2009). Therefore the mere presence of other NOX isoforms in the cell could be enough to mediate compensation. Phenotypes caused by a general decrease in ROS, like developmental delays rescued by H_2O_2, would be masked by compensation in *nox2/cybb*$^{-/-}$ mutants. However, persistent phenotypes stemming specifically from the loss of NOX2/CYBB, which are not recued by H_2O_2, would persist even with compensation. This explains why *nox2/cybb*$^{-/-}$ mutants do not show developmental delays, but do have GCL expansion and defects on axon targeting in the OT.

Inhibitor treatments are a special case that induces both transient and permanent effects. Developmental delays are explained by the potent inhibition of all NOX isoforms over short time. Compensation could not have masked this because 1) all isoforms were inhibited and 2) the time was too short to upregulated alternative compensation. GCL expansion is likely due to the timing of application which coincided with RGC differentiation. Delayed application of the drugs would likely leave the GCL unaffected, but may cause defects in axon targeting in the OT.

The effects of NOX2/CYBB mutation extend beyond the eye. I also reported microphthalmia, pericardial edema and ventral body curling in both chimeric and homozygous NOX2/CYBB mutants. This suggests that NOX2/CYBB is involved generally in development, and implies that future work should be directed at discerning the role of NOX2/CYBB in specific cell and tissue types. These phenotypes may contribute to the defects in OT innervation observed at 120 hpf. By this stage, the worsening morphological defects may impact the health of the larva.

Given observations of GCL expansion, mistargeting of axons in the OT, and developmental delays, I predict that NOX2/CYBB has a specific role in retinal and/or ON development. This is supported by the work described below in section 6.3 which shows that cultured zebrafish RGCs are sensitive to NOX inhibitors. To design future experiments, it is important to identify signaling pathways involved in retinal and ON development that may be redox sensitive. Therefore, in this chapter I will provide a brief overview of eye and retinal development and highlight particular signals that have been shown to involve redox signaling. I will also point out developmental events that may explain the phenotypes observed in my experiments. In the final section of this chapter, I

will suggest future directions for the zebrafish work with an aim to the delineate tissue- and stage-specific functions of NOX isoforms.

7.2 Summary of eye and optic nerve development

NOX2/CYBB mutants display defects in the eye including GCL expansion and a lack of retinal lamination. Additionally, axons are mistargeted to the OT in mutant larva. Given this, it is reasonable to consider which developmental events that underlie these processes might involve NOX-mediated signaling. To this end, the subsections below describe the induction and development of the early eye, the specification of RGCs and the mechanisms of RGC axon guidance at several stages. Comprehensive reviews of these topics have previously been published (Fadool and Dowling, 2008; Erskine and Herrera, 2014; Stenkamp, 2015), and it is not pertinent to repeat all of those details here. Instead, I will provide a general description of development and focus specifically on events and signaling pathways that might involve NOX.

7.2.1 Early eye development

In vertebrates, the eye field is specified from the early neuroepithelium by expression of a suite of homoeodomain-containing transcription factors including *pax6, rx,* s*ix3,* s*ix6, lhx2* and *otx2* (Nornes et al., 1998; Loosli et al., 1999; Stenkamp, 2015; Samuel et al., 2016). Expression of these factors is restricted laterally by the presence of

sonic hedgehog (Shh) at the midline (Macdonald et al., 1995; Masai et al., 2000). The cells expressing these transcription factors evaginate from the neuroepithelium into presumptive eye masses. In zebrafish, the centers of these eye masses invaginate at ~20 hpf to form bilateral optic cups, double-layers of neuroepithelium (Fadool and Dowling, 2008). The distal layer is highly proliferative and produces all of the cells of the neural retina while the proximal layer differentiates into the retinal pigment epithelium (Stenkamp, 2015).

One redox-sensitive target involved in eye specification could be *pax6*. *pax6* is a transcription factor involved in eye field specification that is highly conserved among vertebrates (Fadool and Dowling, 2008). Misregulation of *pax6* leads to the formation of ectopic eyes in both zebrafish and *Drosophila* (Nornes et al., 1998). Two separate studies have shown that the DNA binding affinity of a related protein, Pax8, is dependent on the redox state of the protein (Kambe et al., 1996; Codutti et al., 2008). The latter study showed that the redox sensitive cysteine residues of Pax8 were conserved among several Pax family members. The authors went on to suggest that redox regulation could be conserved feature of all Pax family members (Codutti et al., 2008) making Pax6 a potential target for ROS-mediated signaling during eye development.

7.2.2 Ganglion cell fate determination

Following the formation of the optic cup, retinal progenitors begin to divide and terminally differentiate into RGCs. In all vertebrates, RGC differentiation occurs as a wave that passes through the early retina (Fadool and Dowling, 2008). The shape and

starting point of this wave varies among species, but in zebrafish the wave begins ventrally and extends nasally, dorsally and temporally until completed (Stenkamp, 2015). Fibroblast growth factor (FGF) secreted from the optic stalk, a layer of neuroepithelium connecting the eye to the forebrain, initiates RGC specification (Martinez-Morales et al., 2005). *atoh7*, also called *ath5*, a basic helix-loop-helix transcription factor is well-established as an early RGC-specifying gene (Kay et al., 2001; Kay et al., 2005). Expression of *atoh7* determines RGC cell fate and leads to the expression of additional RGC-specific genes including *isl1* and *brn3b* (Prasov and Glaser, 2012; Pacal and Bremner, 2014). The spatiotemporal characteristics of the RGC differentiation wave are coordinated by several signaling pathways including Shh, Wnt, retinoic acid and Notch/Delta (Bernardos et al., 2005; Masai et al., 2005; Meyers et al., 2012; Erskine and Herrera, 2014; Imai et al., 2014). Differentiated RGCs also secrete cell-autonomous signals to promote their survival. These include a neural epidermal growth factor-like protein and VEGF (Hashimoto et al., 2006; Nakamoto et al., 2014).

Several factors involved in RGC specification are potentially redox sensitive. The expansion of the GCL observed in *nox2/cybb*$^{-/-}$ mutants suggests misregulation of fate specification, so this is a particularly promising area for future studies. I detailed several examples of growth factor signaling that are mediated specifically by NOX in Chapter 6. It is no surprise that FGF signaling, responsible for the initiation of RGC specification, is also dependent on ROS production in other cell types. Treatment of smooth muscle cells with FGF induces migration, and this is dependent on NOX1-derived ROS (Schroder et al., 2007) The authors went on to shown that NOX1-mediated signaling was dependent on JNK oxidation.

VEGF, the cell-autonomous survival signal for newly differentiated RGCs, has also been shown to be NOX-dependent in other cell types. One study found that NOX2 activity was necessary for cell survival and proliferation in response to VEGF in leukemic cells (Maraldi et al., 2010). Another showed that FAK upregulation and cell migration in response to VEGF was mediated by oxidative inactivation of a protein tyrosine phosphatase (Abdelsaid and El-Remessy, 2012).

Notch/Delta signaling is also involved in the control of RGC fate determination. While not linked to NOX, studies have shown that Notch signaling in neuronal precursors is dependent on the activity of peroxyredoxin 4 (Prdx4) (Yan et al., 2015). Disruption of Prdx4, resulting in a lack of downstream protein oxidation, causes premature differentiation of neurons and a depletion of progenitors. It is known that neuronal precursors require elevated ROS levels to maintain potency. Depleting ROS in these cells causes premature differentiation (Le Belle et al., 2011). A second study has shown that disrupting Notch/Delta signaling during zebrafish retinal development leads to a phenotype similar to what was observed in the *nox2/cybb*$^{-/-}$ mutants (Bernardos et al., 2005). The morphology of the eye, disruption of retinal lamination and pattern of GCL expansion are strikingly similar between embryos with Notch/Delta impairment and Nox2/Cybb mutants. Therefore, it is reasonable to hypothesize a connection between Nox2/Cybb-derived ROS and Notch/Delta signaling in zebrafish retinal development.

This potential connection between ROS and Notch/Delta signaling is particularly important given the results presented in Chapter 5. Nox2/Cybb loss-of-function lead to disruption of inner retinal development that included an expansion of the GCL

A final candidate for NOX-mediated signaling is Wnt which is involved in the spatiotemporal control of the RGC differentiation wave. In developing vasculature, the propagation of Wnt5a signals have been show to rely on redox signaling (Murdoch et al., 2014). Additional studies revealed that redox controls the activation of canonical Wnt signaling during endodermal fate specification (Sandieson et al., 2014), and that Wnt signals in mouse colon epithelial cells and human colon cancers depend on NOX1. These reports show that Wnt is well-established as a redox controlled pathway. Therefore, it is possible that disruptions of Wnt signaling are responsible for some of the phenotypes observed in NOX2/CYBB mutants.

7.2.3 Early retinal axon guidance

RGCs undergo a terminal differentiation in the apical retina, adjacent to the retinal pigment epithelium. These non-polar cells then extend a process to the basal retina, and the nucleus migrates along this process until it reaches its terminal position at the vitreal surface (Fadool and Dowling, 2008). As the nucleus nears this final position, the trailing, apical process is retracted and the axon begins to emerge. Apical retraction is mediated by a coordination of slit and N-cadherin signaling (Erskine and Herrera, 2014). Axon emergence is dependent on Rac1 (Ruchhoeft et al., 1999), and early polarized axon growth is guided by cadherins (Riehl et al., 1996), integrins (Lilienbaum et al., 1995) and a peripheral gradient of chondroitin sulfate proteoglycans (CSPGs) (Erskine and Herrera, 2014). The expansion of the GCL observed in *nox2/cybb*$^{-/-}$ mutants could also be due to

disruptions in RGC migration or early axonogeneis. Therefore, it is important to discuss potential nodes for redox signaling during these events.

In Chapter 1, I introduced Rac1 as a critical component of NOX1, 2 and 3 enzyme complexes (Brown and Griendling, 2009). That initial RGC axon emergence is dependent on cytoskeletal rearrangements involving Rac1, makes this event a prime candidate for NOX-mediated signaling. In Chapter 6, I detailed the importance of NOX and ROS to the formation and turnover of integrin-based focal adhesions (section 6.4.3). Disruption of ROS production altered integrin-mediated motility in several cell types (Basuroy et al., 2010; Abdelsaid and El-Remessy, 2012; de Rezende et al., 2012; Datla et al., 2014). Not only does integrin guide early axons, but it also patterns the growth of axons at later stages. Since both Rac and integrin have strong connections to redox signaling, terminal RGC migration and early axonogeneis could be disrupted in *nox2/cybb*$^{-/-}$ mutants.

7.2.4 Intraretinal axon guidance

RGC axons extend along the vitreal surface directly toward the optic disc, the point at which axons turn and exit the eye. The layer containing RGC axons is known as the inner fiber layer. There are several cues and substrate molecules that help to guide axons toward the optic disc and simultaneously prevent axons from growing into adjacent retinal layers. Repulsive, peripheral gradients of slit2 and CSPGs coordinate to drive growth inward toward the optic disc (Brittis et al., 1992; Zolessi et al., 2006). A gradient of Shh along with the growth permissive substrate of neuronal cell adhesion molecule (NCAM) attracts growing axons to the disc (Brittis and Silver, 1995). Additionally, cells

at the optic disc express netrin-1 and the chemokine SDF-1 that act as attractive cues (Li et al., 2005; Stacher Horndli and Chien, 2012; Erskine and Herrera, 2014). Slit1/2 are strongly expressed by the lens and apical retinal layers to prevent axons from straying outside the IFL (Zolessi et al., 2006). All of these molecules act in concert to guide RGC axons to the optic disc. At this stage of our research, it is important to consider the redox regulation of all steps during eye and ON development to decide which events by be sensitive to NOX mutations. However, intraretinal axon guidance does not seem to be affected in *nox2/cybb*$^{-/-}$ mutants. This may be because disruptions in early developmental events mask a guidance phenotype, but the presence of normal appearing ONs in the mutants suggests otherwise. Nonetheless, I will briefly describe possible targets for redox regulation during intraretinal axon guidance.

Of the aforementioned guidance molecules, NCAM is a promising candidate for NOX-mediated signaling. As detailed in Chapter 6 and repeated above, some components of adhesion complexes are known to be redox sensitive. NOX2 subunits have been found to colocalize with focal adhesion proteins (Wu et al., 2005). While much of this work is focused specifically on integrin-based adhesions, our lab has found colocalization of NOX2 and p40^{phox} at apCAM-based adhesion sites in *Aplysia* (Munnamalai et al., 2014), and others have identified a connection between NOX2 and VCAM (Kokovay et al., 2012).

Another possible redox-mediated signal is cytokine SDF-1. Cytokines are a class of secreted, small molecules that are classically associated with inflammatory signaling (Zhang and An, 2007). NOX-derived ROS are a well-established component of the inflammatory response. While there is nothing to directly link SDF-1 with NOX-

mediated signaling, it is worth noting that cytokines and NOX are often identified in the same inflammatory signaling pathways (Brandes et al., 2014).

7.2.5 Axons exiting the eye

As RGC axons reach the optic disc they make a 45° turn and exit the back of the retina. As more axons reach this point, they fasciculate to form a single bundle, the ON (Stenkamp, 2015). As described above, netrin-1 acts locally to attract RGC axons to the optic disc (Deiner et al., 1997). Once axons reach the disc, netrin-1 converts from an attractive to a repulsive cue (Hopker et al., 1999). This conversion is mediated by the presence of laminin-1 at the optic disc which lowers the amount of cAMP in growth cones. This change in cAMP levels transforms the growth promoting netrin-1 signal into an inhibitory signal, and drives the axons toward the midline (Hopker et al., 1999). In addition to the netrin-1/laminin-1 signaling axis, the expression of *pax6* and surface presentation of NCAMs facilitate the bundling of axons into a single ON (Manuel et al., 2008; Tai et al., 2010). The phenotypes observed in *nox2/cybb*$^{-/-}$ mutants are not indicative of defects in optic disc turning or axon fasciculation. However, there are several signaling molecules with potential redox implication involved in this process.

I have detailed the involvement of ROS and/or NOX in the regulation of Pax6 and CAMs in previous sections. However, laminin is uniquely involved in optic disc turning, and therefore has not been mentioned. Laminins are large, extracellular matrix proteins that provide structural support for tissues as well as participate in cellular signaling (Beck et al., 1990). One group reported that treatment of tumor cells with H_2O_2 improved

adhesion efficiency to laminin (Vilas-Boas et al., 2016). While this study was not linked to NOX, it adds to the list of adhesion/matrix proteins whose signaling pathways involve ROS.

7.2.6 Guidance at the optic chiasm

After exiting the eye, RGC axons extend to the midline where, in zebrafish, the ONs completely cross and extend toward the contralateral tectum (Fadool and Dowling, 2008). This crossing event is mainly mediated by the restricted expression of repulsive slit and semaphorin to prevent axons from straying into adjacent tissues (Hutson and Chien, 2002; Fadool and Dowling, 2008; Erskine and Herrera, 2014). The establishment of repulsive slit-expressing regions within the tissue is mediated by the presence of heparin sulfate proteoglycans (HSPGs) and SDF-1 (Chalasani et al., 2007; Wright et al., 2012). In addition to the repulsive cues, VEGF acts as an attractive cue for RGC axons at the midline (Erskine et al., 2011). While we did not focus specifically on axons crossing at the chiasm, *nox2/cybb*$^{-/-}$ mutants do not appear to harbor any defects in this area. Nonetheless, there is at least one unique redox sensitive target involved in this event.

The protein core of some HSPGs can be directly modified by oxidation. The authors of one study reported that perlecan, an endothelial matrix component, can be modified by ROS derived from myeloperoxidase (Rees et al., 2010). Redox modification of this HSPG altered its ability to promote cell adhesion in epithelial cell culture models. This suggests yet another matrix adhesion protein whose signaling is redox sensitive.

Potential redox regulation of VEGF and SDF-1, also involved in chiasm crossing, was discussed in preceding sections, so that information will not be repeated here.

7.2.7 Guidance from the chiasm to the tectum

In teleost fish, axons that have completed midline crossing at the chiasm extend dorsorostrally toward their final targets in optic tectum. This distance between the chiasm and the tectum is known as the optic tract. Similar to other parts of ON development, growth through the optic tract is controlled by repulsive cues flanking the tract and attractive cues emanating from the target region. In this case, the repulsive cues include integrins (Stone and Sakaguchi, 1996), Tenascin-R (Becker et al., 2003), Shh , CSPGs and slits (Erskine and Herrera, 2014). FGF acts as a positive cue to attract RGC axons toward the tectum (Stenkamp, 2015). Once RGC axons reach the tectum, they form synapses in a retinotopic fashion (Fadool and Dowling, 2008). This means that axons from specific regions of the retina innervate specific regions of the tectum. Within the optic tract, dorsal and rostral RGCs axons are sorted, and this process is dependent on HSPGs (Poulain and Chien, 2013). Once in the tectum, opposing gradients of ephrins and Eph receptors refine target selection in a fashion that mimics retinal topography (Frisen et al., 1998). RGC axons are mistargeted in *nox2/cybb*$^{-/-}$ mutants. Axons are not confined to the OT and extend to adjacent midbrain regions. This could be due to defects in midbrain formation, but could also result from disruption of RGC axon guidance. Therefore, it is valuable to consider which signals that pattern tectal innervation may also be redox sensitive.

The involvement of ROS in integrin, FGF and HSPGs signaling has been detailed one or more of the previous sections. However, ephrin signaling is unique to the tectum, and has not been discussed previously. One study found that inhibition of integrin-based cell adhesion by ephrinA1 was dependent on the downregulation of Rac1. The authors went on to show that this was mediated by the redox-dependent inactivation of a protein tyrosine phosphatase (Buricchi et al., 2007). While this study does not directly implicate NOX, the involvement of Rac1 and the redox inactivation of a protein tyrosine phosphatase strongly suggest a role for NOX-derived ROS in ephrin-mediated signaling. This means that it is reasonable to speculate that Eph/ephrin-based target selection in the tectum could be disrupted in *nox2/cybb*$^{-/-}$ mutants.

7.2.8 Summary of potential redox signaling in optic nerve development

The preceding sections describe vertebrate, specifically zebrafish, ON development in some detail, and highlight signaling pathways that potentially involve NOX-derived ROS or redox signaling in general. Table 7.1 summarizes the cues and other proteins with potential connections to redox signaling for each section above. As stated previously, *nox2/cybb*$^{-/-}$ mutant phenotypes likely rule out the involvement of NOX2/CYBB in certain events (i.e. crossing at the chiasm). However, RGC fate determination, early axonogenesis and axon guidance in the tectum are good candidates based on the phenotypes observed and the presence of redox sensitive signaling pathways.

7.3 Future directions for the zebrafish project

Chapter 1 introduced a number of studies that show the involvement of NOX in neurodevelopment. Some focused on declines in cognitive ability (Pao et al., 2004; Kishida et al., 2006) while others detail the well-established role of ROS in stem cell maintenance or neuronal maturation (Dickinson et al., 2011; Forsberg et al., 2013; Forsberg and Di Giovanni, 2014; Olguin-Albuerne and Moran, 2015). One report

Table 7.1: Redox sensitive events during eye and optic nerve development

Develomental event	Cue/signal	Source of ROS	Section
Eye field specification	Pax6	Unknown	7.2.1
RGC differentiation	FGF	Unknown	7.2.2
	VEGF	NOX	
	Notch	Unknown	
	Wnt	NOX1	
Early RGC axon guidance	Rac1	NOX1/2/3	7.2.3
	Integrin	NOX2/4	
Intraretinal axon guidance	NCAM	NOX2	7.2.4
	SDF-1	Unknown	
Turning at the optic disc	Pax6	Unknown	7.2.5
	CAM	NOX	
	Laminin	H_2O_2	
Crossing at the optic chiasm	VEGF	NOX	7.2.6
	SDF-1	Unknown	
	HSPGs	Unknown	
Optic tract and tectal innervation	Integrin	NOX2/4	7.2.7
	FGF	Unknown	
	HSPGs	Unknown	
	Ephrin	Rac1*	

'Unknown' refers to redox-mediated pathways in which no source of ROS has been identified. 'NOX' indicates that no specific isoform has been implicated. *Ephrin signaling is mediated by Rac1-dependent generation of ROS. Rac1 is not a direct source of ROS.

addressed NOX-mediated axon guidance, but this was done in peripheral nerves (Rieger and Sagasti, 2011). Yet another investigated ROS in brain development, but did not establish a direct link to any NOX isoform (Coyoy et al., 2013). My study is the first to directly assess the impact of a specific NOX on neurodevelopment and axon outgrowth. The results suggest a functional role for NOX in this process. However, many questions remain regarding when, where and how NOX-derived ROS are involved the differentiation and/or growth of axons. The next section suggests strategies to address these questions. In addition, I propose approaches to study the impact of NOX on overall development and morphogenesis.

7.3.1 Further characterization of Nox mutant lines

In Chapter 5, I described the use of gRNAs against all four zebrafish Nox isoforms. However, I only detail the development and testing of *nox2/cybb* mutant lines. In fact, we have developed mutant lines for all of the Nox isoforms, and can predict the domains that remain in the mutant proteins (Figure 7.2). As these lines are already developed, future experiments should be designed to assess the impact of Nox1, 5 and DUOX mutants on development. The first steps would be to cross the heterozygous mutants, genotype the resulting embryos and look for morphological changes that appear only in heterozygous or homozygous mutants. From there, studies similar to those described in Figures 5.4 and 5.5 could be done to address the effect of Nox mutants on ON and OT development.

Further genetic and molecular characterization should be done on all of the lines. If the mutant lines are to be distributed to the community or placed in a repository, it will be necessary to sequence the genomes of each line. This can be done at the Purdue Genomics Core facility. A complete genome would also confirm the absence of any unpredicted off-target mutagenesis. There are still no suitable antibodies against zebrafish Nox proteins, but we have tested some potential antibodies with varying degrees of success. The identification of specific antibodies would allow for proper characterization of the mutant proteins via Western blot and/or immunoprecipitation. The presence or absence of co-precipitating regulatory subunits would address the binding capacity of mutant Nox proteins. This is an important question given that inactive mutant proteins that retain the ability to bind regulatory subunits could act as dominant negatives, and this could change the way we approach future experiments. The introduction of dominant negatives into cultured cells or whole embryos would also be a useful knockdown strategy in the future.

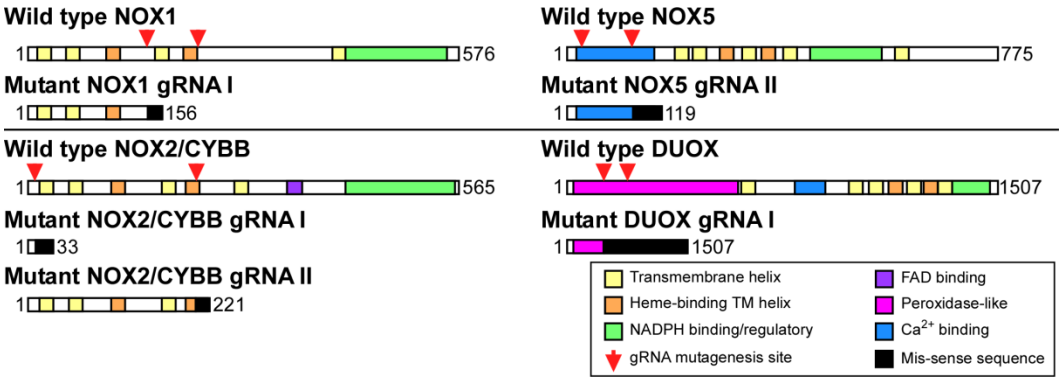

Figure 7.2: Protein domains from all Nox mutant lines Wild type and mutant domain structures for all of the Nox isoforms are shown. Elements are color-coded and the legend is shown at the bottom-right.

Functional characterization can be done by cloning and expressing wild type and mutant zebrafish Nox proteins in cultured eukaryotic cells. Standard ROS activation assays using luciferase reporters could be used to measure ROS production. One example is the ROS-Glo™ H_2O_2 Assay from Promega (Cat. G8820). The type of cells used in the assay would need to be chosen carefully. Eukaryotic cells would be necessary due to the glycosylation of NOX proteins (Brandes et al., 2014). Cell types that do not express endogenous NOX would require the co-transfection of additional subunits while cells expressing endogenous NOX might not be sensitive to the introduction of mutant NOX proteins. This is another reason to investigate the ability of mutant proteins to act as dominant negatives. While this series of experiments would be labor intensive, the wild type and mutant constructs would have may uses for other projects.

7.3.2 Specifying the role of Nox in retinal and optic nerve development

As described in the preceding sections, NOX-derived ROS may play a role in several events during RGC development and ON growth. The challenge is to determine which of these events is disrupted in *nox2/cybb* mutants and how Nox-derived ROS mediates this specific process. One approach to accomplish this would be to deactivate Nox during specific developmental stages and assess the impact on RGC differentiation and ON development. Application of Nox inhibitors allows for this type of precise temporal control, but lacks isoform specificity. A better method was recently introduced that allows for temporally controlled CRISPR-mediated mutagenesis (Yin et al., 2015). The authors describe the use of heat shock promoters to drive expression of Cas9 while

gRNAs are expressed ubiquitously. The result is the generation of mutations at discrete timepoints. The advantages are obvious, but this approach requires the construction of new fish lines that express specific gRNAs for each target gene. This can be laborious and time-consuming. However, I would recommend two approaches to improve efficiency. First, we can use our gRNAs that have already been proven to be specific and efficient. This saves time in validating a new set of tools. Second, I recommend initial screening experiments by injecting gRNAs into lines expressing heat shock-inducible Cas9. This would result in the ubiquitous expression of gRNA with temporally controlled expression of Cas9. However, this approach would not require extensive time and labor investment, and would allow the user to screen several gRNAs prior to constructing lines.

In addition to temporal control, it is also desirable to have spatial control of Nox function. One method to obtain spatial and temporal restriction would be intravitreal injection of Nox inhibitors. Since the RGCs lie at the vitreal surface of the retina, they are more sensitive to substances injected in the vitreous space. Intravitreal administration of ouabain has been shown to selectively impair the innermost retinal neurons (Fimbel et al., 2007). I suggest a similar approach to selectively inhibit Nox in RGCs. However, this would be limited to early developmental events since RGC axon pathfinding outside of the intraretinal space is unlikely to be affected by inhibitor treatment in the vitreal space.

Spatial or cell-type specificity is commonly achieved using transplantation assays (Detrich et al., 2010). I propose to transplant mutant RGCs or whole eye primordia into wild type hosts and track RGC specification and ON outgrowth throughout development. Depending on the methods used, we can eliminate potential interference from non-cell autonomous sources of Nox. This approach would require that donor cells be labeled, so I

suggest the use of mutant lines that have been crossed into *Tg(ath5:GFP)* backgrounds. The transplant could also be reversed, wild type RGCs into a mutant host, to assess the RGC-independent functions of Nox. A similar approach was used to study the function of zebrafish DUOX in regenerating peripheral nerves (Rieger and Sagasti, 2011).

A final method for achieving cell-type specificity is the generation of CRISPR mutants using a gene-specific promoter to drive Cas9 expression (Ablain et al., 2015). I propose to use this method to generate mutations in RGCs. However, it may also be useful to develop lines that express Cas9 in other retinal cell types. Again, I would recommend the use of our validated gRNAs for building the new lines, and screening the different gRNAs by injecting them into embryos that express Cas9 in a specific subset of cells. The drawback of this approach is the complete lack of temporal control. Mutations are generated early in development and carried throughout development. It is advisable to pair this approach with temporally controlled mutagenesis to achieve a more comprehensive set of results.

7.3.3 Nox in axon guidance

In Chapter 6, I introduced a number of ways to investigate the role of Nox in axonal growth and guidance. A simple way to enhance those studies would be to perform the experiments with neurons derived from Nox mutant embryos. This would eliminate the need for inhibitor applications, and would be especially useful for determining upstream guidance cues that use ROS as an intermediate signal. I would expect specific isoform mutants to be insensitive to redox-controlled cues.

While I propose that the initial experiments into axon guidance should be done using *in vitro* culture systems, there are some methods to address axon guidance *in vivo*. One way is to track single axons from transplanted RGCs (see above). Time-lapse imaging of transplanted mutant axons yields insights into the cell-autonomous role of Nox in axon guidance. However, this is very low throughput, and transplantations can be technically challenging. So this approach should be used in combination with more robust methods.

Previous studies have introduced approaches for labeling single axons *in vivo* without the need for difficult transplantations. The authors injected a small amount of plasmid encoding a neuron-specific EGFP into single-cell zebrafish embryos. This produced mosaic labeling and allowed for single axon tracking (St John and Key, 2012). A subsequent study then used the mosaic labeling strategy to study guidance during forebrain development with single axon resolution (St John et al., 2013). I propose to use a similar strategy to label single RGCs in the retina of Nox mutants. Using an RGC-specific promoter we could drive the expression of a fluorescent reporter to track axon outgrowth. Alternatively, we could drive expression of the ROS biosensors discussed in Chapter 6 in RGCs to simultaneously quantify ROS levels and track single axons.

The cell type-specific CRISPR mutagenesis described above requires the synthesis of plasmid constructs encoding the gRNA and Cas9 gene along with requisite promoters. Most of these constructs also include a fluorescent tag to track mutagenesis *in vivo*. In addition to using these constructs for the generation of lines, we could use them to mosaically label embryos. This would result in mutagenesis and labeling of single RGCs within an otherwise wild type embryo. Using this approach, we could investigate

the cell-autonomous role of Nox in RGCs without constructing novel lines or performing laborious transplantations.

7.3.4 Nox in general development

All of the approaches outlined in the preceding sections may be combined with immunolabeling and *in situ* hybridization (ISH) to characterize the impact of Nox mutations on tissues within and outside of the eye. We have already begun a project using ISH to mark the development of several early tissues in wild type and *nox2/cybb* mutants. We aim to use a set of seven, validated ISH probes to mark neural crest cells, blood cell progenitors, mesodermal progenitors, heart, several brain regions, retina, RGCs, somites and macrophages (see Table 7.2). We will label wild type and mutant embryos with these probes at 16, 24 and 36 hpf to compare the extent and pattern of development in all these tissues. To achieve the desired throughput for this project, we will use an ISH method published previously (Thisse and Thisse, 2008). I anticipate that the results of this project will inform future studies into novel roles for Nox in early development.

For some of the anatomical targets listed above, we could supplement or substitute ISH with antibody labeling. Again, we have developed a list of suitable antibodies that label early tissues (Table 7.2). In the eye, we can determine the impact of Nox mutations on retinal lamination using antibodies that mark specific retinal layers. Alternatively, we can make use of a new line of transgenic fish called Zebrabow (Brainbow) that uses multicolor labeling strategies to trace single cell lineages as well as single axon outgrowth (Pan et al., 2013). This would be useful to address the impact of

Nox mutations on overall brain development, retinal architecture and axon outgrowth simultaneously.

Table 7.2: Gene targets for developmental analysis

Gene	Tissues	ISH probe (+/-)	Antibody (+/-)
cdh5	Vasculature, pericardium	+	+
crestin	Neural crest, brain regions, pharyngeal arches	+	-
ets1	Hematopoetic mesoderm, neural crest, vascualture	+	-
gata1a	Mesoderm, primative blood, vasculature	+	-
gltscr1	Brain regions, eye, hematopoetic mesoderm	+	-
jph2	Heart, somites, myotomes	+	-
kdrl	Vasculature	+	+
mab21l2	Retina, tectum, hindbrain	+	-
mpx	Macrophages	+	+
myl7	Heart, pericardium	+	-
myod	Somites,muscle	+	+
pak1	Brain regions, retina, RGCs	+	+
pax2a	Hindbrain, mesoderm, spinal neurons	+	+
pax6a	Early brain, eye primordium, hindbrain, retina	+	+
pax7	Neural crest, muscle progenitors	-	+
ppp1r13ba	Brain regions, myotomes, blood	+	-
sall2	Diencephalon, MHB, limited spinal cord (19-30 hpf)	+	-
spi1b	Hematopoetic mesoderm, macrophages, eye, blood	+	+

Tissues listed are not comprehensive and may vary with developmental stage. '+' and '-' refer to the availability of validated *in situ* hybridization probes or antibodies.

The role of Nox in angiogenesis, vascular function and disease is well documented (Bedard and Krause, 2007; Drummond and Sobey, 2014). Therefore, it is not surprising to observe cardiovascular defects in Nox mutant zebrafish. Pericardial edema first appears between 50 and 72 hpf in mutant embryos and appears to precede any defects in heart development. However, additional experiments focused specifically on cardiac development are needed to support this assertion. Nonetheless, edema seems to

be the first cardiovascular insult, but this presents a problem since edema is a symptom of several distinct cardiovascular defects (Miura and Yelon, 2011). The challenge is to delineate what first induces pericardial edema, and what developmental defects occur as a result. Pericardial edema is commonly caused by heart valve leakage, vascular malformations, leaks in the vascular walls and over secretion of fluid by cells of the pericardium. I propose using several labeling strategies to screen for these defects in Nox mutants. First, we can use ISH and immunolabeling to visualize early heart and vascular development (see Table 7.2 for markers). Second, we can cross the Nox mutant lines with transgenic lines carrying fluorescent reporters in vascular tissues. One example is the *fli1*:GFP transgenic line that labels blood vessels throughout development (Lawson and Weinstein, 2002).

Finally, we can label vasculature and test for leakage by directly injecting fluorescent dye into the bloodstream. This technique is called microangiography (MAG), and is routinely used to label blood vessels and the heart in zebrafish embryos (Hoffman et al., 2012). I have conducted preliminary MAG experiments by injecting fluorescently labeled dextran into the sinus venosus at 48 hpf. I have imaged vasculature throughout the body in wild type embryos (Figure 7.3A-B), but only eye vasculature in *nox2/cybb*$^{-/-}$ embryos (Figure 7.3C-E). These experiments appear to show additional fluorescent signals that could indicate increased angiogenesis or vascular leakage within the eye of mutant embryos (Figure 7.3D-E, red arrowheads). In addition, the blood vessels of the eye in mutant embryos appear to be swollen (Figure 7.3D-E, red arrows). However, the injection protocol needs to be standardized, and the results quantified before making any meaningful comparisons.

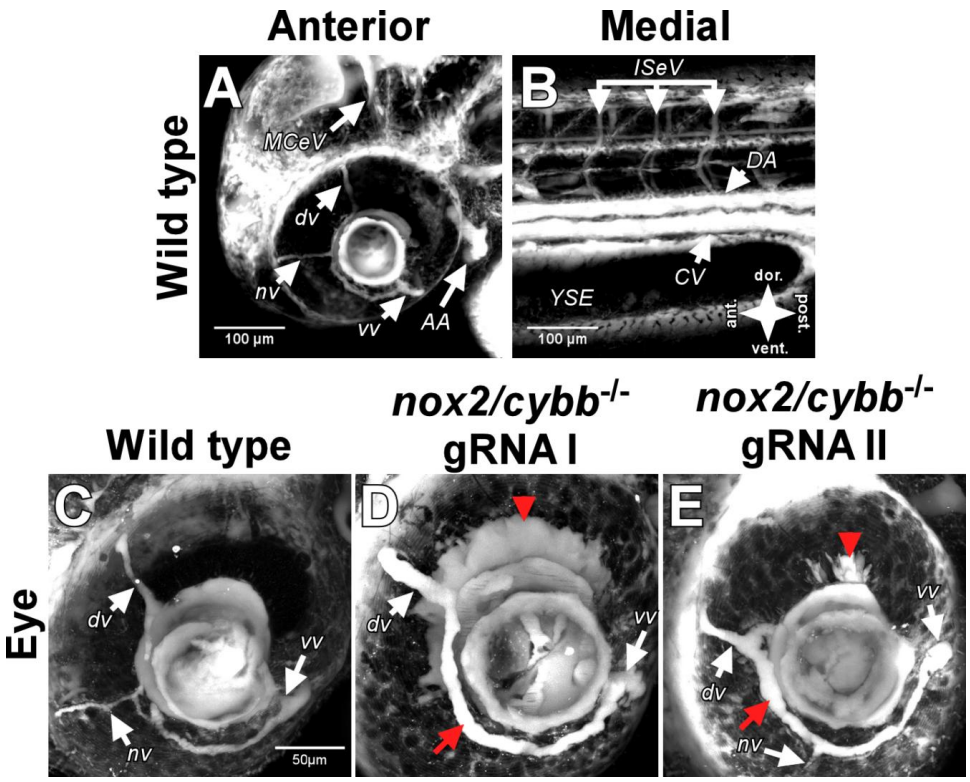

Figure 7.3: Homozygous *nox2/cybb* mutants have defects in eye vasculature (A-B) 48 hpf embryos injected with fluorescent dextran showing the anterior (A) and medial (B) regions. (C-E) High-magnification views of eye vasculature in wild type (C) and *nox2/cybb* mutant embryos (D-E). Dorsal (dv), nasal (nv) and ventral (vv) veins are indicated. Mutants exhibited vascular swelling (red arrows) and additional labeling that may indicate increased angiogenesis or vascular leakage (red arrowheads). MCeV = medial cerebral vein, AA = aortic arch, ISeV = intersegmental vessels, DA = dorsal aorta, CV = cardinal vein, YSE = yolk sac extension. Scales are indicated in A and C.

In vertebrates, the pharyngeal arches (PA) are derived from neural crest cells, and often in zebrafish PA malformations can result from defects in neural crest migration or differentiation (Schilling et al., 1996). Nox is known to mediate the survival and differentiation of neural crest cells (Lee et al., 2014), so defects in PA arch formation may be expected in Nox mutants. Alcian blue is staining the most common method of labeling the PA in zebrafish, and I have conducted preliminary labeling studies on *nox2/cybb* mutant embryos (Figure 7.4). Mutants appear to have all PA components, but they are underdeveloped and shifted toward the posterior. I propose advancing these

studies by optimizing the labeling protocol and quantifying the extent and type of PA malformations. We can then compare these results to previously characterized PA defects to predict the signaling pathways that are disrupted in our mutants. An excellent catalog of PA defects and their causative mutations has previously been published (Schilling et al., 1996).

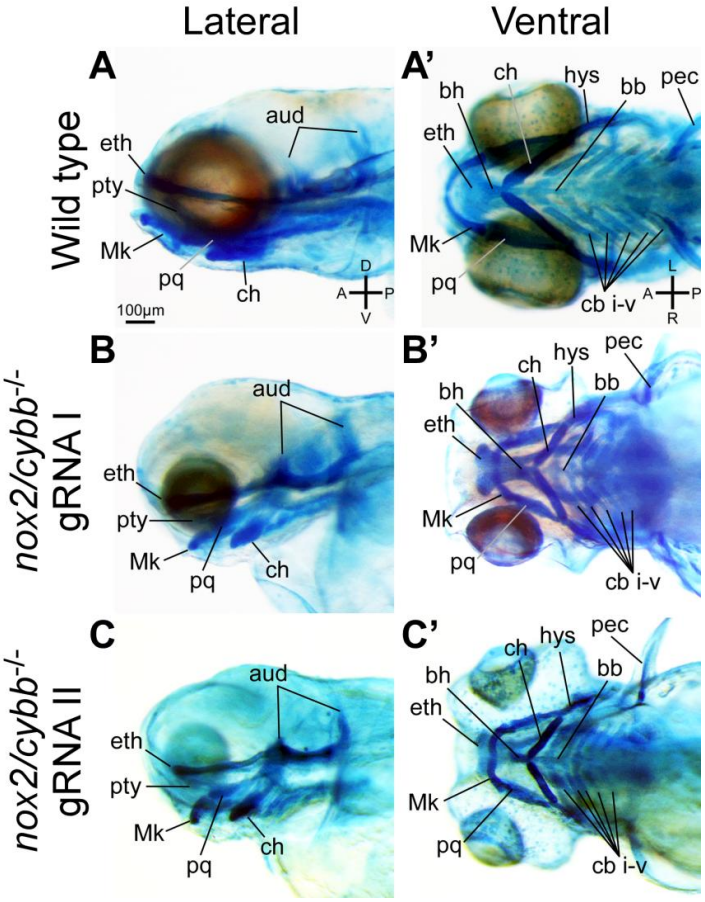

Figure 7.4: Homozygous *nox2/cybb* mutants have defects in craniofacial development 5 day old wild type (A-A') and *nox2/cybb* gRNA I (B-B') and gRNA II (C-C') mutants labeled with Alcian blue to mark cartilage. Elements of the seven pharyngeal arches are labeled. First arch derivatives are Meckle's cartilage (Mk) and the palatoquadrate (pq). Second arch derivatives are the basihyal (bh), ceratohyal (ch) and hyosymplectic (hys). The gill arch derivates are the basibranchials (bb) and ceratobranchials I-V (cb i-v). The dorsal-most structure is the ethmoid plate (eth) and the cartilage of the pectoral fins is also shown (pec). Lateral views also show the pterygoid process of the quadrate (pty) and the auditory capsule (aud).

7.4 Concluding remarks

The current study presents evidence that NOX activity is important for the outgrowth of cultured neurites derived from *Aplysia* and zebrafish neurons. NOX inhibition slows outgrowth, and NOX2 was directly identified in *Aplysia* growth cones. There is even suggestion that NOX may be involved in cell adhesions within these growth cones. The *in vivo* studies showed that *nox* genes are expressed broadly throughout the zebrafish central nervous system, and that perturbations or mutations in *nox* genes cause defects in retinal development and axon targeting in the optic tectum. Future studies should be aimed at discerning the role of NOX in specific tissues and developmental events. The strategies outlined above would allow for a more complete characterization of the role NOX enzymes play in retinal development. In addition, these experiments may provide new insights into roles for NOX enzymes beyond the eye and brain. The combination of *in vitro* approaches in cultured neurons with *in vivo* strategies in zebrafish affords unique opportunities to completely characterize cellular signaling pathways that use NOX-derived ROS as intermediate signals. Carefully devised, thoughtful experiments meshing these experimental strategies will be extremely informative, and may reveal novel insights into NOX biology that would not otherwise be attainable.

BIBLIOGRAPHY

BIBLIOGRAPHY

Abdelsaid MA, El-Remessy AB (2012) S-glutathionylation of LMW-PTP regulates VEGF-mediated FAK activation and endothelial cell migration. Journal of cell science 125:4751-4760.

Abid MR, Kachra Z, Spokes KC, Aird WC (2000) NADPH oxidase activity is required for endothelial cell proliferation and migration. FEBS letters 486:252-256.

Ablain J, Durand EM, Yang S, Zhou Y, Zon LI (2015) A CRISPR/Cas9 vector system for tissue-specific gene disruption in zebrafish. Developmental cell 32:756-764.

Abo A, Webb MR, Grogan A, Segal AW (1994) Activation of NADPH oxidase involves the dissociation of p21rac from its inhibitory GDP/GTP exchange protein (rhoGDI) followed by its translocation to the plasma membrane. The Biochemical journal 298 Pt 3:585-591.

Abo A, Pick E, Hall A, Totty N, Teahan CG, Segal AW (1991) Activation of the NADPH oxidase involves the small GTP-binding protein p21rac1. Nature 353:668-670.

Ago T, Kuribayashi F, Hiroaki H, Takeya R, Ito T, Kohda D, Sumimoto H (2003) Phosphorylation of p47phox directs phox homology domain from SH3 domain toward phosphoinositides, leading to phagocyte NADPH oxidase activation. Proceedings of the National Academy of Sciences of the United States of America 100:4474-4479.

Ago T, Liu T, Zhai P, Chen W, Li H, Molkentin JD, Vatner SF, Sadoshima J (2008) A redox-dependent pathway for regulating class II HDACs and cardiac hypertrophy. Cell 133:978-993.

Altenhofer S, Kleikers PW, Radermacher KA, Scheurer P, Rob Hermans JJ, Schiffers P, Ho H, Wingler K, Schmidt HH (2012) The NOX toolbox: validating the role of NADPH oxidases in physiology and disease. Cellular and molecular life sciences : CMLS 69:2327-2343.

Amatore D, Sgarbanti R, Aquilano K, Baldelli S, Limongi D, Civitelli L, Nencioni L, Garaci E, Ciriolo MR, Palamara AT (2015) Influenza virus replication in lung epithelial cells depends on redox-sensitive pathways activated by NOX4-derived ROS. Cellular microbiology 17:131-145.

Ansari MA, Scheff SW (2011) NADPH-oxidase activation and cognition in Alzheimer disease progression. Free radical biology & medicine 51:171-178.

Association As (2014) 2014 Alzheimer's disease facts and figures. Alzheimer's & dementia : the journal of the Alzheimer's Association 10:e47-92.

Avanesov A, Malicki J (2010) Analysis of the retina in the zebrafish model. Methods in cell biology 100:153-204.

Ayoob JC, Terman JR, Kolodkin AL (2006) Drosophila Plexin B is a Sema-2a receptor required for axon guidance. Development 133:2125-2135.

Baehner RL, Nathan DG (1967) Leukocyte oxidase: defective activity in chronic granulomatous disease. Science 155:835-836.

Baldridge CW, Gerard RW (1933) The extra respiration of phagocytosis. Am J Physiol 103:235-236.

Bamburg JR, Bernstein BW (2010) Roles of ADF/cofilin in actin polymerization and beyond. F1000 biology reports 2:62.

Banfi B, Clark RA, Steger K, Krause KH (2003) Two novel proteins activate superoxide generation by the NADPH oxidase NOX1. The Journal of biological chemistry 278:3510-3513.

Banfi B, Malgrange B, Knisz J, Steger K, Dubois-Dauphin M, Krause KH (2004a) NOX3, a superoxide-generating NADPH oxidase of the inner ear. The Journal of biological chemistry 279:46065-46072.

Banfi B, Molnar G, Maturana A, Steger K, Hegedus B, Demaurex N, Krause KH (2001) A Ca(2+)-activated NADPH oxidase in testis, spleen, and lymph nodes. The Journal of biological chemistry 276:37594-37601.

Banfi B, Tirone F, Durussel I, Knisz J, Moskwa P, Molnar GZ, Krause KH, Cox JA (2004b) Mechanism of Ca2+ activation of the NADPH oxidase 5 (NOX5). The Journal of biological chemistry 279:18583-18591.

Barth BM, Gustafson SJ, Kuhn TB (2012) Neutral sphingomyelinase activation precedes NADPH oxidase-dependent damage in neurons exposed to the proinflammatory cytokine tumor necrosis factor-alpha. J Neurosci Res 90:229-242.

Basuroy S, Dunagan M, Sheth P, Seth A, Rao RK (2010) Hydrogen peroxide activates focal adhesion kinase and c-Src by a phosphatidylinositol 3 kinase-dependent mechanism and promotes cell migration in Caco-2 cell monolayers. American journal of physiology Gastrointestinal and liver physiology 299:G186-195.

Beck K, Hunter I, Engel J (1990) Structure and function of laminin: anatomy of a multidomain glycoprotein. FASEB journal : official publication of the Federation of American Societies for Experimental Biology 4:148-160.

Becker CG, Schweitzer J, Feldner J, Becker T, Schachner M (2003) Tenascin-R as a repellent guidance molecule for developing optic axons in zebrafish. The Journal of neuroscience : the official journal of the Society for Neuroscience 23:6232-6237.

Bedard K, Krause KH (2007) The NOX family of ROS-generating NADPH oxidases: physiology and pathophysiology. Physiological reviews 87:245-313.

Bedard K, Lardy B, Krause KH (2007) NOX family NADPH oxidases: not just in mammals. Biochimie 89:1107-1112.

Bedard K, Jaquet V, Krause KH (2012) NOX5: from basic biology to signaling and disease. Free radical biology & medicine 52:725-734.

BelAiba RS, Djordjevic T, Petry A, Diemer K, Bonello S, Banfi B, Hess J, Pogrebniak A, Bickel C, Gorlach A (2007) NOX5 variants are functionally active in endothelial cells. Free radical biology & medicine 42:446-459.

Berendes H, Bridges RA, Good RA (1957) A fatal granulomatosus of childhood: the clinical study of a new syndrome. Minnesota medicine 40:309-312.

Bernardos RL, Lentz SI, Wolfe MS, Raymond PA (2005) Notch-Delta signaling is required for spatial patterning and Muller glia differentiation in the zebrafish retina. Dev Biol 278:381-395.

Bilan DS, Pase L, Joosen L, Gorokhovatsky AY, Ermakova YG, Gadella TW, Grabher C, Schultz C, Lukyanov S, Belousov VV (2013) HyPer-3: a genetically encoded H(2)O(2) probe with improved performance for ratiometric and fluorescence lifetime imaging. ACS chemical biology 8:535-542.

Boillee S, Cleveland DW (2008) Revisiting oxidative damage in ALS: microglia, Nox, and mutant SOD1. The Journal of clinical investigation 118:474-478.

Brandes RP, Weissmann N, Schroder K (2014) Nox family NADPH oxidases: Molecular mechanisms of activation. Free radical biology & medicine 76:208-226.

Brennan AM, Suh SW, Won SJ, Narasimhan P, Kauppinen TM, Lee H, Edling Y, Chan PH, Swanson RA (2009) NADPH oxidase is the primary source of superoxide induced by NMDA receptor activation. Nature neuroscience 12:857-863.

Brittis PA, Silver J (1995) Multiple factors govern intraretinal axon guidance: a time-lapse study. Molecular and cellular neurosciences 6:413-432.

Brittis PA, Canning DR, Silver J (1992) Chondroitin sulfate as a regulator of neuronal patterning in the retina. Science 255:733-736.

Bromberg Y, Pick E (1985) Activation of NADPH-dependent superoxide production in a cell-free system by sodium dodecyl sulfate. The Journal of biological chemistry 260:13539-13545.

Brown DI, Griendling KK (2009) Nox proteins in signal transduction. Free radical biology & medicine 47:1239-1253.

Buday L, Downward J (2007) Roles of cortactin in tumor pathogenesis. Biochimica et biophysica acta 1775:263-273.

Buricchi F, Giannoni E, Grimaldi G, Parri M, Raugei G, Ramponi G, Chiarugi P (2007) Redox regulation of ephrin/integrin cross-talk. Cell adhesion & migration 1:33-42.

Burrill JD, Easter SS, Jr. (1995) The first retinal axons and their microenvironment in zebrafish: cryptic pioneers and the pretract. The Journal of neuroscience : the official journal of the Society for Neuroscience 15:2935-2947.

Cao X, Demel SL, Quinn MT, Galligan JJ, Kreulen D (2009) Localization of NADPH oxidase in sympathetic and sensory ganglion neurons and perivascular nerve fibers. Auton Neurosci 151:90-97.

Carbone F, Camillo Teixeira P, Braunersreuther V, Mach F, Vuilleumier N, Montecucco F (2014) Pathophysiology and Treatments of Oxidative Injury in Ischemic Stroke: Focus on the Phagocytic NADPH Oxidase 2. Antioxidants & redox signaling.

Castellon X, Bogdanova V (2016) Chronic Inflammatory Diseases and Endothelial Dysfunction. Aging and disease 7:81-89.

Cerutti P, Ghosh R, Oya Y, Amstad P (1994) The role of the cellular antioxidant defense in oxidant carcinogenesis. Environmental health perspectives 102 Suppl 10:123-129.

Chalasani SH, Sabol A, Xu H, Gyda MA, Rasband K, Granato M, Chien CB, Raper JA (2007) Stromal cell-derived factor-1 antagonizes slit/robo signaling in vivo. The Journal of neuroscience : the official journal of the Society for Neuroscience 27:973-980.

Chen J, He R, Minshall RD, Dinauer MC, Ye RD (2007) Characterization of a mutation in the Phox homology domain of the NADPH oxidase component p40phox identifies a mechanism for negative regulation of superoxide production. The Journal of biological chemistry 282:30273-30284.

Chen Z, Lee H, Henle SJ, Cheever TR, Ekker SC, Henley JR (2013) Primary neuron culture for nerve growth and axon guidance studies in zebrafish (Danio rerio). PloS one 8:e57539.

Cheng G, Lambeth JD (2004) NOXO1, regulation of lipid binding, localization, and activation of Nox1 by the Phox homology (PX) domain. The Journal of biological chemistry 279:4737-4742.

Cheng G, Cao Z, Xu X, van Meir EG, Lambeth JD (2001) Homologs of gp91phox: cloning and tissue expression of Nox3, Nox4, and Nox5. Gene 269:131-140.

Cheret C, Gervais A, Lelli A, Colin C, Amar L, Ravassard P, Mallet J, Cumano A, Krause KH, Mallat M (2008) Neurotoxic activation of microglia is promoted by a nox1-dependent NADPH oxidase. The Journal of neuroscience : the official journal of the Society for Neuroscience 28:12039-12051.

Chiarugi P, Pani G, Giannoni E, Taddei L, Colavitti R, Raugei G, Symons M, Borrello S, Galeotti T, Ramponi G (2003) Reactive oxygen species as essential mediators of cell adhesion: the oxidative inhibition of a FAK tyrosine phosphatase is required for cell adhesion. J Cell Biol 161:933-944.

Chiriaco M, Salfa I, Matteo GD, Rossi P, Finocchi A (2015) Chronic Granulomatous Disease: clinical, molecular and therapeutic aspects. Pediatric allergy and immunology : official publication of the European Society of Pediatric Allergy and Immunology.

Choi DH, Cristovao AC, Guhathakurta S, Lee J, Joh TH, Beal MF, Kim YS (2012) NADPH oxidase 1-mediated oxidative stress leads to dopamine neuron death in Parkinson's disease. Antioxidants & redox signaling 16:1033-1045.

Codutti L, van Ingen H, Vascotto C, Fogolari F, Corazza A, Tell G, Quadrifoglio F, Viglino P, Boelens R, Esposito G (2008) The solution structure of DNA-free Pax-8 paired box domain accounts for redox regulation of transcriptional activity in the pax protein family. The Journal of biological chemistry 283:33321-33328.

Cole TS, McKendrick F, Cant AJ, Pearce MS, Cale CM, Goldblatt DR, Gennery AR, Titman P (2013) Cognitive ability in children with chronic granulomatous disease: a comparison of those managed conservatively with those who have undergone hematopoietic stem cell transplant. Neuropediatrics 44:230-232.

Comito G, Calvani M, Giannoni E, Bianchini F, Calorini L, Torre E, Migliore C, Giordano S, Chiarugi P (2011) HIF-1alpha stabilization by mitochondrial ROS promotes Met-dependent invasive growth and vasculogenic mimicry in melanoma cells. Free radical biology & medicine 51:893-904.

Coyoy A, Valencia A, Guemez-Gamboa A, Moran J (2008) Role of NADPH oxidase in the apoptotic death of cultured cerebellar granule neurons. Free radical biology & medicine 45:1056-1064.

Coyoy A, Olguin-Albuerne M, Martinez-Briseno P, Moran J (2013) Role of reactive oxygen species and NADPH-oxidase in the development of rat cerebellum. Neurochemistry international 62:998-1011.

Cristovao AC, Barata J, Je G, Kim YS (2013) PKCdelta mediates paraquat-induced Nox1 expression in dopaminergic neurons. Biochem Biophys Res Commun 437:380-385.

Cui XL, Brockman D, Campos B, Myatt L (2006) Expression of NADPH oxidase isoform 1 (Nox1) in human placenta: involvement in preeclampsia. Placenta 27:422-431.

D'Ambrosi N, Rossi S, Gerbino V, Cozzolino M (2014) Rac1 at the crossroad of actin dynamics and neuroinflammation in Amyotrophic Lateral Sclerosis. Frontiers in cellular neuroscience 8:279.

Dalle-Donne I, Rossi R, Milzani A, Di Simplicio P, Colombo R (2001) The actin cytoskeleton response to oxidants: from small heat shock protein phosphorylation to changes in the redox state of actin itself. Free radical biology & medicine 31:1624-1632.

Dalle-Donne I, Giustarini D, Rossi R, Colombo R, Milzani A (2003) Reversible S-glutathionylation of Cys 374 regulates actin filament formation by inducing structural changes in the actin molecule. Free radical biology & medicine 34:23-32.

Dalle-Donne I, Rossi R, Giustarini D, Gagliano N, Di Simplicio P, Colombo R, Milzani A (2002) Methionine oxidation as a major cause of the functional impairment of oxidized actin. Free radical biology & medicine 32:927-937.

DalleDonne I, Milzani A, Colombo R (1995) H2O2-treated actin: assembly and polymer interactions with cross-linking proteins. Biophysical journal 69:2710-2719.

Datla SR, McGrail DJ, Vukelic S, Huff LP, Lyle AN, Pounkova L, Lee M, Seidel-Rogol B, Khalil MK, Hilenski LL, Terada LS, Dawson MR, Lassegue B, Griendling KK (2014) Poldip2 controls vascular smooth muscle cell migration by regulating focal adhesion turnover and force polarization. American journal of physiology Heart and circulatory physiology 307:H945-957.

De Deken X, Wang D, Many MC, Costagliola S, Libert F, Vassart G, Dumont JE, Miot F (2000) Cloning of two human thyroid cDNAs encoding new members of the NADPH oxidase family. The Journal of biological chemistry 275:23227-23233.

de Oliveira S, Boudinot P, Calado A, Mulero V (2015) Duox1-derived H2O2 modulates Cxcl8 expression and neutrophil recruitment via JNK/c-JUN/AP-1 signaling and chromatin modifications. J Immunol 194:1523-1533.

de Rezende FF, Martins Lima A, Niland S, Wittig I, Heide H, Schroder K, Eble JA (2012) Integrin alpha7beta1 is a redox-regulated target of hydrogen peroxide in vascular smooth muscle cell adhesion. Free radical biology & medicine 53:521-531.

Decourt B, Munnamalai V, Lee AC, Sanchez L, Suter DM (2009) Cortactin colocalizes with filopodial actin and accumulates at IgCAM adhesion sites in Aplysia growth cones. J Neurosci Res 87:1057-1068.

Deiner MS, Kennedy TE, Fazeli A, Serafini T, Tessier-Lavigne M, Sretavan DW (1997) Netrin-1 and DCC mediate axon guidance locally at the optic disc: loss of function leads to optic nerve hypoplasia. Neuron 19:575-589.

Detrich HI, M Westerfield M, Zon LI (2010) The Zebrafish: Cellular and Developmental Biology, 3rd Edition, 3rd Edition. Burlington, MA: Elsevier.

Dickinson BC, Peltier J, Stone D, Schaffer DV, Chang CJ (2011) Nox2 redox signaling maintains essential cell populations in the brain. Nature chemical biology 7:106-112.

Diekmann D, Abo A, Johnston C, Segal AW, Hall A (1994) Interaction of Rac with p67phox and regulation of phagocytic NADPH oxidase activity. Science 265:531-533.

Dikalov SI, Dikalova AE, Bikineyeva AT, Schmidt HH, Harrison DG, Griendling KK (2008) Distinct roles of Nox1 and Nox4 in basal and angiotensin II-stimulated superoxide and hydrogen peroxide production. Free radical biology & medicine 45:1340-1351.

Dinauer MC, Orkin SH, Brown R, Jesaitis AJ, Parkos CA (1987) The glycoprotein encoded by the X-linked chronic granulomatous disease locus is a component of the neutrophil cytochrome b complex. Nature 327:717-720.

Dixit R, Ross JL, Goldman YE, Holzbaur EL (2008) Differential regulation of dynein and kinesin motor proteins by tau. Science 319:1086-1089.

Drummond GR, Sobey CG (2014) Endothelial NADPH oxidases: which NOX to target in vascular disease? Trends Endocrinol Metab 25:452-463.

Dumont M, Stack C, Elipenhali C, Calingasan NY, Wille E, Beal MF (2011) Apocynin administration does not improve behavioral and neuropathological deficits in a transgenic mouse model of Alzheimer's disease. Neurosci Lett 492:150-154.

Dupuy C, Ohayon R, Valent A, Noel-Hudson MS, Deme D, Virion A (1999) Purification of a novel flavoprotein involved in the thyroid NADPH oxidase. Cloning of the porcine and human cdnas. The Journal of biological chemistry 274:37265-37269.

el Benna J, Ruedi JM, Babior BM (1994a) Cytosolic guanine nucleotide-binding protein Rac2 operates in vivo as a component of the neutrophil respiratory burst oxidase. Transfer of Rac2 and the cytosolic oxidase components p47phox and p67phox to the submembranous actin cytoskeleton during oxidase activation. The Journal of biological chemistry 269:6729-6734.

el Benna J, Faust LP, Babior BM (1994b) The phosphorylation of the respiratory burst oxidase component p47phox during neutrophil activation. Phosphorylation of sites recognized by protein kinase C and by proline-directed kinases. The Journal of biological chemistry 269:23431-23436.

El Benna J, Dang PM, Andrieu V, Vergnaud S, Dewas C, Cachia O, Fay M, Morel F, Chollet-Martin S, Hakim J, Gougerot-Pocidalo MA (1999) P40phox associates with the neutrophil Triton X-100-insoluble cytoskeletal fraction and PMA-activated membrane skeleton: a comparative study with P67phox and P47phox. J Leukoc Biol 66:1014-1020.

Emmendorffer A, Roesler J, Elsner J, Raeder E, Lohmann-Matthes ML, Meier B (1993) Production of oxygen radicals by fibroblasts and neutrophils from a patient with x-linked chronic granulomatous disease. European journal of haematology 51:223-227.

Erskine L, Herrera E (2014) Connecting the retina to the brain. ASN neuro 6.

Erskine L, Reijntjes S, Pratt T, Denti L, Schwarz Q, Vieira JM, Alakakone B, Shewan D, Ruhrberg C (2011) VEGF signaling through neuropilin 1 guides commissural axon crossing at the optic chiasm. Neuron 70:951-965.

Fadool JM, Dowling JE (2008) Zebrafish: a model system for the study of eye genetics. Progress in retinal and eye research 27:89-110.

Fiaschi T, Cozzi G, Raugei G, Formigli L, Ramponi G, Chiarugi P (2006) Redox regulation of beta-actin during integrin-mediated cell adhesion. The Journal of biological chemistry 281:22983-22991.

Fimbel SM, Montgomery JE, Burket CT, Hyde DR (2007) Regeneration of inner retinal neurons after intravitreal injection of ouabain in zebrafish. The Journal of neuroscience : the official journal of the Society for Neuroscience 27:1712-1724.

Finkel T (2001) Reactive oxygen species and signal transduction. IUBMB Life 52:3-6.

Finkel T (2011) Signal transduction by reactive oxygen species. J Cell Biol 194:7-15.

Finkel T (2012) Signal transduction by mitochondrial oxidants. The Journal of biological chemistry 287:4434-4440.

Fischer J, Weide T, Barnekow A (2005) The MICAL proteins and rab1: a possible link to the cytoskeleton? Biochem Biophys Res Commun 328:415-423.

Fischer MT, Sharma R, Lim JL, Haider L, Frischer JM, Drexhage J, Mahad D, Bradl M, van Horssen J, Lassmann H (2012) NADPH oxidase expression in active multiple sclerosis lesions in relation to oxidative tissue damage and mitochondrial injury. Brain : a journal of neurology 135:886-899.

Flint AJ, Tiganis T, Barford D, Tonks NK (1997) Development of "substrate-trapping" mutants to identify physiological substrates of protein tyrosine phosphatases. Proceedings of the National Academy of Sciences of the United States of America 94:1680-1685.

Fomenko DE, Xing W, Adair BM, Thomas DJ, Gladyshev VN (2007) High-throughput identification of catalytic redox-active cysteine residues. Science 315:387-389.

Fontayne A, Dang PM, Gougerot-Pocidalo MA, El-Benna J (2002) Phosphorylation of p47phox sites by PKC alpha, beta II, delta, and zeta: effect on binding to p22phox and on NADPH oxidase activation. Biochemistry 41:7743-7750.

Forman HJ, Ursini F, Maiorino M (2014) An overview of mechanisms of redox signaling. Journal of molecular and cellular cardiology 73:2-9.

Forsberg K, Di Giovanni S (2014) Cross Talk between Cellular Redox Status, Metabolism, and p53 in Neural Stem Cell Biology. The Neuroscientist : a review journal bringing neurobiology, neurology and psychiatry 20:326-342.

Forsberg K, Wuttke A, Quadrato G, Chumakov PM, Wizenmann A, Di Giovanni S (2013) The tumor suppressor p53 fine-tunes reactive oxygen species levels and neurogenesis via PI3 kinase signaling. The Journal of neuroscience : the official journal of the Society for Neuroscience 33:14318-14330.

Frantz S, Brandes RP, Hu K, Rammelt K, Wolf J, Scheuermann H, Ertl G, Bauersachs J (2006) Left ventricular remodeling after myocardial infarction in mice with targeted deletion of the NADPH oxidase subunit gp91PHOX. Basic research in cardiology 101:127-132.

Frisen J, Yates PA, McLaughlin T, Friedman GC, O'Leary DD, Barbacid M (1998) Ephrin-A5 (AL-1/RAGS) is essential for proper retinal axon guidance and topographic mapping in the mammalian visual system. Neuron 20:235-243.

Fukuda M, Kanno E, Ishibashi K, Itoh T (2008) Large scale screening for novel rab effectors reveals unexpected broad Rab binding specificity. Molecular & cellular proteomics : MCP 7:1031-1042.

Fyhrquist F, Metsarinne K, Tikkanen I (1995) Role of angiotensin II in blood pressure regulation and in the pathophysiology of cardiovascular disorders. Journal of human hypertension 9 Suppl 5:S19-24.

Gao HM, Zhou H, Hong JS (2012) NADPH oxidases: novel therapeutic targets for neurodegenerative diseases. Trends Pharmacol Sci.

Garrido-Urbani S, Jemelin S, Deffert C, Carnesecchi S, Basset O, Szyndralewiez C, Heitz F, Page P, Montet X, Michalik L, Arbiser J, Ruegg C, Krause KH, Imhof BA (2011) Targeting vascular NADPH oxidase 1 blocks tumor angiogenesis through a PPARalpha mediated mechanism. PloS one 6:e14665.

Gauss KA, Mascolo PL, Siemsen DW, Nelson LK, Bunger PL, Pagano PJ, Quinn MT (2002) Cloning and sequencing of rabbit leukocyte NADPH oxidase genes reveals a unique p67(phox) homolog. J Leukoc Biol 71:319-328.

Geiszt M, Kopp JB, Varnai P, Leto TL (2000) Identification of renox, an NAD(P)H oxidase in kidney. Proceedings of the National Academy of Sciences of the United States of America 97:8010-8014.

Geiszt M, Lekstrom K, Witta J, Leto TL (2003) Proteins homologous to p47phox and p67phox support superoxide production by NAD(P)H oxidase 1 in colon epithelial cells. The Journal of biological chemistry 278:20006-20012.

Giannoni E, Fiaschi T, Ramponi G, Chiarugi P (2009) Redox regulation of anoikis resistance of metastatic prostate cancer cells: key role for Src and EGFR-mediated pro-survival signals. Oncogene 28:2074-2086.

Giannoni E, Buricchi F, Raugei G, Ramponi G, Chiarugi P (2005) Intracellular reactive oxygen species activate Src tyrosine kinase during cell adhesion and anchorage-dependent cell growth. Molecular and cellular biology 25:6391-6403.

Gjetting KS, Ytting CK, Schulz A, Fuglsang AT (2012) Live imaging of intra- and extracellular pH in plants using pHusion, a novel genetically encoded biosensor. Journal of experimental botany 63:3207-3218.

Gordillo GM, Biswas A, Khanna S, Pan X, Sinha M, Roy S, Sen CK (2014) Dicer knockdown inhibits endothelial cell tumor growth via microRNA 21a-3p targeting of Nox-4. The Journal of biological chemistry 289:9027-9038.

Gorzalczany Y, Sigal N, Itan M, Lotan O, Pick E (2000) Targeting of Rac1 to the phagocyte membrane is sufficient for the induction of NADPH oxidase assembly. The Journal of biological chemistry 275:40073-40081.

Groemping Y, Lapouge K, Smerdon SJ, Rittinger K (2003) Molecular basis of phosphorylation-induced activation of the NADPH oxidase. Cell 113:343-355.

Grogan A, Reeves E, Keep N, Wientjes F, Totty NF, Burlingame AL, Hsuan JJ, Segal AW (1997) Cytosolic phox proteins interact with and regulate the assembly of coronin in neutrophils. Journal of cell science 110 (Pt 24):3071-3081.

Guemez-Gamboa A, Moran J (2009) NOX2 mediates apoptotic death induced by staurosporine but not by potassium deprivation in cerebellar granule neurons. J Neurosci Res 87:2531-2540.

Gulyani A, Vitriol E, Allen R, Wu J, Gremyachinskiy D, Lewis S, Dewar B, Graves LM, Kay BK, Kuhlman B, Elston T, Hahn KM (2011) A biosensor generated via high-throughput screening quantifies cell edge Src dynamics. Nature chemical biology 7:437-444.

Gutscher M, Sobotta MC, Wabnitz GH, Ballikaya S, Meyer AJ, Samstag Y, Dick TP (2009) Proximity-based protein thiol oxidation by H2O2-scavenging peroxidases. The Journal of biological chemistry 284:31532-31540.

Hadrava V, Kruppa U, Russo RC, Lacourciere Y, Tremblay J, Hamet P (1991) Vascular smooth muscle cell proliferation and its therapeutic modulation in hypertension. American heart journal 122:1198-1203.

Hall ED (2011) Antioxidant therapies for acute spinal cord injury. Neurotherapeutics : the journal of the American Society for Experimental NeuroTherapeutics 8:152-167.

Han CH, Freeman JL, Lee T, Motalebi SA, Lambeth JD (1998) Regulation of the neutrophil respiratory burst oxidase. Identification of an activation domain in p67(phox). The Journal of biological chemistry 273:16663-16668.

Harper RW, Xu C, McManus M, Heidersbach A, Eiserich JP (2006) Duox2 exhibits potent heme peroxidase activity in human respiratory tract epithelium. FEBS letters 580:5150-5154.

Hashimoto T, Zhang XM, Chen BY, Yang XJ (2006) VEGF activates divergent intracellular signaling components to regulate retinal progenitor cell proliferation and neuronal differentiation. Development 133:2201-2210.

He Y, Ren Y, Wu B, Decourt B, Lee AC, Taylor A, Suter DM (2015) Src and cortactin promote lamellipodia protrusion and filopodia formation and stability in growth cones. Mol Biol Cell 26:3229-3244.

Hensley MR, Leung YF (2010) A convenient dry feed for raising zebrafish larvae. Zebrafish 7:219-231.

Hensley MR, Emran F, Bonilla S, Zhang L, Zhong W, Grosu P, Dowling JE, Leung YF (2011) Cellular expression of Smarca4 (Brg1)-regulated genes in zebrafish retinas. BMC Dev Biol 11:45.

Hernandes MS, Britto LR (2012) NADPH oxidase and neurodegeneration. Current neuropharmacology 10:321-327.

Heumuller S, Wind S, Barbosa-Sicard E, Schmidt HH, Busse R, Schroder K, Brandes RP (2008) Apocynin is not an inhibitor of vascular NADPH oxidases but an antioxidant. Hypertension 51:211-217.

Hilburger EW, Conte EJ, McGee DW, Tammariello SP (2005) Localization of NADPH oxidase subunits in neonatal sympathetic neurons. Neurosci Lett 377:16-19.

Hilenski LL, Clempus RE, Quinn MT, Lambeth JD, Griendling KK (2004) Distinct subcellular localizations of Nox1 and Nox4 in vascular smooth muscle cells. Arterioscler Thromb Vasc Biol 24:677-683.

Hoffman SJ, Psaltis PJ, Clark KJ, Spoon DB, Chue CD, Ekker SC, Simari RD (2012) An in vivo method to quantify lymphangiogenesis in zebrafish. PloS one 7:e45240.

Holmes B, Page AR, Good RA (1967) Studies of the metabolic activity of leukocytes from patients with a genetic abnormality of phagocytic function. The Journal of clinical investigation 46:1422-1432.

Holterman CE, Thibodeau JF, Kennedy CR (2015) NADPH oxidase 5 and renal disease. Current opinion in nephrology and hypertension 24:81-87.

Hopker VH, Shewan D, Tessier-Lavigne M, Poo M, Holt C (1999) Growth-cone attraction to netrin-1 is converted to repulsion by laminin-1. Nature 401:69-73.

Hu M, Easter SS (1999) Retinal neurogenesis: the formation of the initial central patch of postmitotic cells. Dev Biol 207:309-321.

Hung RJ, Pak CW, Terman JR (2011) Direct redox regulation of F-actin assembly and disassembly by Mical. Science 334:1710-1713.

Hung RJ, Spaeth CS, Yesilyurt HG, Terman JR (2013) SelR reverses Mical-mediated oxidation of actin to regulate F-actin dynamics. Nat Cell Biol 15:1445-1454.

Hung RJ, Yazdani U, Yoon J, Wu H, Yang T, Gupta N, Huang Z, van Berkel WJ, Terman JR (2010) Mical links semaphorins to F-actin disassembly. Nature 463:823-827.

Hutson LD, Chien CB (2002) Pathfinding and error correction by retinal axons: the role of astray/robo2. Neuron 33:205-217.

Ibi M, Katsuyama M, Fan C, Iwata K, Nishinaka T, Yokoyama T, Yabe-Nishimura C (2006) NOX1/NADPH oxidase negatively regulates nerve growth factor-induced neurite outgrowth. Free radical biology & medicine 40:1785-1795.

Ikeda S, Yamaoka-Tojo M, Hilenski L, Patrushev NA, Anwar GM, Quinn MT, Ushio-Fukai M (2005) IQGAP1 regulates reactive oxygen species-dependent endothelial cell migration through interacting with Nox2. Arterioscler Thromb Vasc Biol 25:2295-2300.

Imai F, Yoshizawa A, Matsuzaki A, Oguri E, Araragi M, Nishiwaki Y, Masai I (2014) Stem-loop binding protein is required for retinal cell proliferation, neurogenesis, and intraretinal axon pathfinding in zebrafish. Dev Biol 394:94-109.

Iyer GYN, Islam MF, Quastel JH (1961) Biochemical Aspects of Phagocytosis. Nature 192:535-541.

Janke C (2014) The tubulin code: molecular components, readout mechanisms, and functions. J Cell Biol 206:461-472.

Jao LE, Wente SR, Chen W (2013) Efficient multiplex biallelic zebrafish genome editing using a CRISPR nuclease system. Proceedings of the National Academy of Sciences of the United States of America 110:13904-13909.

Jaquet V, Scapozza L, Clark RA, Krause KH, Lambeth JD (2009) Small-molecule NOX inhibitors: ROS-generating NADPH oxidases as therapeutic targets. Antioxidants & redox signaling 11:2535-2552.

Jaquet V, Marcoux J, Forest E, Leidal KG, McCormick S, Westermaier Y, Perozzo R, Plastre O, Fioraso-Cartier L, Diebold B, Scapozza L, Nauseef WM, Fieschi F, Krause KH, Bedard K (2011) NADPH oxidase (NOX) isoforms are inhibited by celastrol with a dual mode of action. British journal of pharmacology 164:507-520.

Jay DB, Papaharalambus CA, Seidel-Rogol B, Dikalova AE, Lassegue B, Griendling KK (2008) Nox5 mediates PDGF-induced proliferation in human aortic smooth muscle cells. Free radical biology & medicine 45:329-335.

Jimenez-Shahed J (2016) A review of current and novel levodopa formulations for the treatment of Parkinson's disease. Therapeutic delivery 7:179-191.

Jones DP, Go YM (2011) Mapping the cysteine proteome: analysis of redox-sensing thiols. Current opinion in chemical biology 15:103-112.

Kaji N, Ohashi K, Shuin M, Niwa R, Uemura T, Mizuno K (2003) Cell cycle-associated changes in Slingshot phosphatase activity and roles in cytokinesis in animal cells. The Journal of biological chemistry 278:33450-33455.

Kajla S, Mondol AS, Nagasawa A, Zhang Y, Kato M, Matsuno K, Yabe-Nishimura C, Kamata T (2012) A crucial role for Nox 1 in redox-dependent regulation of Wnt-beta-catenin signaling. FASEB journal : official publication of the Federation of American Societies for Experimental Biology 26:2049-2059.

Kallenborn-Gerhardt W, Schroder K, Del Turco D, Lu R, Kynast K, Kosowski J, Niederberger E, Shah AM, Brandes RP, Geisslinger G, Schmidtko A (2012) NADPH oxidase-4 maintains neuropathic pain after peripheral nerve injury. The Journal of neuroscience : the official journal of the Society for Neuroscience 32:10136-10145.

Kambe F, Nomura Y, Okamoto T, Seo H (1996) Redox regulation of thyroid-transcription factors, Pax-8 and TTF-1, is involved in their increased DNA-binding activities by thyrotropin in rat thyroid FRTL-5 cells. Molecular endocrinology (Baltimore, Md) 10:801-812.

Kawahara BT, Quinn MT, Lambeth JD (2007a) Molecular evolution of the reactive oxygen-generating NADPH oxidase (Nox/Duox) family of enzymes. BMC evolutionary biology 7:109.

Kawahara T, Lambeth JD (2007) Molecular evolution of Phox-related regulatory subunits for NADPH oxidase enzymes. BMC evolutionary biology 7:178.

Kawahara T, Quinn MT, Lambeth JD (2007b) Molecular evolution of the reactive oxygen-generating NADPH oxidase (Nox/Duox) family of enzymes. BMC evolutionary biology 7:109.

Kay JN, Link BA, Baier H (2005) Staggered cell-intrinsic timing of ath5 expression underlies the wave of ganglion cell neurogenesis in the zebrafish retina. Development 132:2573-2585.

Kay JN, Finger-Baier KC, Roeser T, Staub W, Baier H (2001) Retinal ganglion cell genesis requires lakritz, a Zebrafish atonal Homolog. Neuron 30:725-736.

Kikuchi H, Hikage M, Miyashita H, Fukumoto M (2000) NADPH oxidase subunit, gp91(phox) homologue, preferentially expressed in human colon epithelial cells. Gene 254:237-243.

Kim JS, Huang TY, Bokoch GM (2009) Reactive oxygen species regulate a slingshot-cofilin activation pathway. Mol Biol Cell 20:2650-2660.

Kim JS, Park EJ, Choi IG, Kim YS, Park JB (2011a) Neuregulin induces HaCaT keratinocyte migration via Rac1-mediated NADPH-oxidase activation. Journal of cellular physiology.

Kim JS, Bak EJ, Lee BC, Kim YS, Park JB, Choi IG (2011b) Neuregulin induces HaCaT keratinocyte migration via Rac1-mediated NADPH-oxidase activation. Journal of cellular physiology 226:3014-3021.

Kimmel CB, Ballard WW, Kimmel SR, Ullmann B, Schilling TF (1995) Stages of embryonic development of the zebrafish. Dev Dyn 203:253-310.

Kishida KT, Hoeffer CA, Hu D, Pao M, Holland SM, Klann E (2006) Synaptic plasticity deficits and mild memory impairments in mouse models of chronic granulomatous disease. Molecular and cellular biology 26:5908-5920.

Kiss PJ, Knisz J, Zhang Y, Baltrusaitis J, Sigmund CD, Thalmann R, Smith RJ, Verpy E, Banfi B (2006) Inactivation of NADPH oxidase organizer 1 results in severe imbalance. Current biology : CB 16:208-213.

Kita EM, Scott EK, Goodhill GJ (2015) Topographic wiring of the retinotectal connection in zebrafish. Developmental neurobiology 75:542-556.

Kleinschnitz C et al. (2010) Post-stroke inhibition of induced NADPH oxidase type 4 prevents oxidative stress and neurodegeneration. PLoS biology 8.

Knaus UG, Heyworth PG, Evans T, Curnutte JT, Bokoch GM (1991) Regulation of phagocyte oxygen radical production by the GTP-binding protein Rac 2. Science 254:1512-1515.

Kokovay E, Wang Y, Kusek G, Wurster R, Lederman P, Lowry N, Shen Q, Temple S (2012) VCAM1 is essential to maintain the structure of the SVZ niche and acts as an environmental sensor to regulate SVZ lineage progression. Cell stem cell 11:220-230.

Kolodkin AL, Tessier-Lavigne M (2011) Mechanisms and molecules of neuronal wiring: a primer. Cold Spring Harbor perspectives in biology 3.

Krijnen PA, Meischl C, Hack CE, Meijer CJ, Visser CA, Roos D, Niessen HW (2003) Increased Nox2 expression in human cardiomyocytes after acute myocardial infarction. Journal of clinical pathology 56:194-199.

Kuiper JW, Sun C, Magalhaes MA, Glogauer M (2011) Rac regulates PtdInsP(3) signaling and the chemotactic compass through a redox-mediated feedback loop. Blood 118:6164-6171.

Lambeth JD, Kawahara T, Diebold B (2007) Regulation of Nox and Duox enzymatic activity and expression. Free radical biology & medicine 43:319-331.

Landino LM, Robinson SH, Skreslet TE, Cabral DM (2004) Redox modulation of tau and microtubule-associated protein-2 by the glutathione/glutaredoxin reductase system. Biochem Biophys Res Commun 323:112-117.

Landino LM, Koumas MT, Mason CE, Alston JA (2007) Modification of tubulin cysteines by nitric oxide and nitroxyl donors alters tubulin polymerization activity. Chemical research in toxicology 20:1693-1700.

Lassegue B, Sorescu D, Szocs K, Yin Q, Akers M, Zhang Y, Grant SL, Lambeth JD, Griendling KK (2001) Novel gp91(phox) homologues in vascular smooth muscle cells : nox1 mediates angiotensin II-induced superoxide formation and redox-sensitive signaling pathways. Circ Res 88:888-894.

Lassing I, Schmitzberger F, Bjornstedt M, Holmgren A, Nordlund P, Schutt CE, Lindberg U (2007) Molecular and structural basis for redox regulation of beta-actin. Journal of molecular biology 370:331-348.

Lawson ND, Weinstein BM (2002) In vivo imaging of embryonic vascular development using transgenic zebrafish. Dev Biol 248:307-318.

Le Belle JE, Orozco NM, Paucar AA, Saxe JP, Mottahedeh J, Pyle AD, Wu H, Kornblum HI (2011) Proliferative neural stem cells have high endogenous ROS levels that regulate self-renewal and neurogenesis in a PI3K/Akt-dependant manner. Cell stem cell 8:59-71.

Le Cabec V, Maridonneau-Parini I (1995) Complete and reversible inhibition of NADPH oxidase in human neutrophils by phenylarsine oxide at a step distal to membrane translocation of the enzyme subunits. The Journal of biological chemistry 270:2067-2073.

Lee AC, Decourt B, Suter D (2008) Neuronal cell cultures from aplysia for high-resolution imaging of growth cones. Journal of visualized experiments : JoVE.

Lee JE, Cho KE, Lee KE, Kim J, Bae YS (2014) Nox4-mediated cell signaling regulates differentiation and survival of neural crest stem cells. Molecules and cells 37:907-911.

Lee MY, San Martin A, Mehta PK, Dikalova AE, Garrido AM, Datla SR, Lyons E, Krause KH, Banfi B, Lambeth JD, Lassegue B, Griendling KK (2009) Mechanisms of vascular smooth muscle NADPH oxidase 1 (Nox1) contribution to injury-induced neointimal formation. Arterioscler Thromb Vasc Biol 29:480-487.

Lee SR, Kwon KS, Kim SR, Rhee SG (1998) Reversible inactivation of protein-tyrosine phosphatase 1B in A431 cells stimulated with epidermal growth factor. The Journal of biological chemistry 273:15366-15372.

Levitan IB, Kaczmarek LK (2002) The Neuron: Cell and Molecular Biology: Oxford University Press.

Li JM, Shah AM (2002) Intracellular localization and preassembly of the NADPH oxidase complex in cultured endothelial cells. The Journal of biological chemistry 277:19952-19960.

Li L, Hutchins BI, Kalil K (2009) Wnt5a induces simultaneous cortical axon outgrowth and repulsive axon guidance through distinct signaling mechanisms. The Journal of neuroscience : the official journal of the Society for Neuroscience 29:5873-5883.

Li Q, Shirabe K, Thisse C, Thisse B, Okamoto H, Masai I, Kuwada JY (2005) Chemokine signaling guides axons within the retina in zebrafish. The Journal of neuroscience : the official journal of the Society for Neuroscience 25:1711-1717.

Li Y, Liu J, Zhan X (2000) Tyrosine phosphorylation of cortactin is required for H2O2-mediated injury of human endothelial cells. The Journal of biological chemistry 275:37187-37193.

Li Y, Mouche S, Sajic T, Veyrat-Durebex C, Supale R, Pierroz D, Ferrari S, Negro F, Hasler U, Feraille E, Moll S, Meda P, Deffert C, Montet X, Krause KH, Szanto I (2012a) Deficiency in the NADPH oxidase 4 predisposes towards diet-induced obesity. International journal of obesity (2005) 36:1503-1513.

Li Z, Ptak D, Zhang L, Walls EK, Zhong W, Leung YF (2012b) Phenylthiourea specifically reduces zebrafish eye size. PloS one 7:e40132.

Lilienbaum A, Reszka AA, Horwitz AF, Holt CE (1995) Chimeric integrins expressed in retinal ganglion cells impair process outgrowth in vivo. Molecular and cellular neurosciences 6:139-152.

Lim JB, Langford TF, Huang BK, Deen WM, Sikes HD (2016) A reaction-diffusion model of cytosolic hydrogen peroxide. Free radical biology & medicine 90:85-90.

Loosli F, Winkler S, Wittbrodt J (1999) Six3 overexpression initiates the formation of ectopic retina. Genes Dev 13:649-654.

Loria R, Bon G, Perotti V, Gallo E, Bersani I, Baldassari P, Porru M, Leonetti C, Di Carlo S, Visca P, Brizzi MF, Anichini A, Mortarini R, Falcioni R (2015) Sema6A and Mical1 control cell growth and survival of BRAFV600E human melanoma cells. Oncotarget 6:2779-2793.

Lowe J, Li H, Downing KH, Nogales E (2001) Refined structure of alpha beta-tubulin at 3.5 A resolution. Journal of molecular biology 313:1045-1057.

Lu XY, Wang HD, Xu JG, Ding K, Li T (2014) NADPH oxidase inhibition improves neurological outcome in experimental traumatic brain injury. Neurochemistry international 69:14-19.

Lukinavicius G, Reymond L, D'Este E, Masharina A, Gottfert F, Ta H, Guther A, Fournier M, Rizzo S, Waldmann H, Blaukopf C, Sommer C, Gerlich DW, Arndt HD, Hell SW, Johnsson K (2014) Fluorogenic probes for live-cell imaging of the cytoskeleton. Nature methods 11:731-733.

Lyle AN, Deshpande NN, Taniyama Y, Seidel-Rogol B, Pounkova L, Du P, Papaharalambus C, Lassegue B, Griendling KK (2009) Poldip2, a novel regulator of Nox4 and cytoskeletal integrity in vascular smooth muscle cells. Circ Res 105:249-259.

Macdonald R, Barth KA, Xu Q, Holder N, Mikkola I, Wilson SW (1995) Midline signalling is required for Pax gene regulation and patterning of the eyes. Development 121:3267-3278.

Maheswaranathan M, Gole HK, Fernandez I, Lassegue B, Griendling KK, San Martin A (2011) Platelet-derived growth factor (PDGF) regulates Slingshot phosphatase activity via Nox1-dependent auto-dephosphorylation of serine 834 in vascular smooth muscle cells. The Journal of biological chemistry 286:35430-35437.

Manuel M, Pratt T, Liu M, Jeffery G, Price DJ (2008) Overexpression of Pax6 results in microphthalmia, retinal dysplasia and defective retinal ganglion cell axon guidance. BMC Dev Biol 8:59.

Maraldi T, Prata C, Caliceti C, Vieceli Dalla Sega F, Zambonin L, Fiorentini D, Hakim G (2010) VEGF-induced ROS generation from NAD(P)H oxidases protects human leukemic cells from apoptosis. Int J Oncol 36:1581-1589.

Marrali G, Casale F, Salamone P, Fuda G, Caorsi C, Amoroso A, Brunetti M, Restagno G, Barberis M, Bertuzzo D, Canosa A, Moglia C, Calvo A, Chio A (2014) NADPH oxidase (NOX2) activity is a modifier of survival in ALS. Journal of neurology 261:2178-2183.

Marsick BM, Roche FK, Letourneau PC (2012) Repulsive axon guidance cues ephrin-A2 and slit3 stop protrusion of the growth cone leading margin concurrently with inhibition of ADF/cofilin and ERM proteins. Cytoskeleton (Hoboken) 69:496-505.

Marsick BM, Flynn KC, Santiago-Medina M, Bamburg JR, Letourneau PC (2010) Activation of ADF/cofilin mediates attractive growth cone turning toward nerve growth factor and netrin-1. Developmental neurobiology 70:565-588.

Martinez-Morales JR, Del Bene F, Nica G, Hammerschmidt M, Bovolenta P, Wittbrodt J (2005) Differentiation of the vertebrate retina is coordinated by an FGF signaling center. Developmental cell 8:565-574.

Masai I, Stemple DL, Okamoto H, Wilson SW (2000) Midline signals regulate retinal neurogenesis in zebrafish. Neuron 27:251-263.

Masai I, Yamaguchi M, Tonou-Fujimori N, Komori A, Okamoto H (2005) The hedgehog-PKA pathway regulates two distinct steps of the differentiation of retinal ganglion cells: the cell-cycle exit of retinoblasts and their neuronal maturation. Development 132:1539-1553.

Masu M (2015) Proteoglycans and axon guidance: a new relationship between old partners. Journal of neurochemistry Epub ahead of print.

Meeker ND, Hutchinson SA, Ho L, Trede NS (2007) Method for isolation of PCR-ready genomic DNA from zebrafish tissues. BioTechniques 43:610, 612, 614.

Meng D, Lv DD, Fang J (2008) Insulin-like growth factor-I induces reactive oxygen species production and cell migration through Nox4 and Rac1 in vascular smooth muscle cells. Cardiovascular research 80:299-308.

Meyer AJ, Dick TP (2010) Fluorescent protein-based redox probes. Antioxidants & redox signaling 13:621-650.

Meyers JR, Hu L, Moses A, Kaboli K, Papandrea A, Raymond PA (2012) beta-catenin/Wnt signaling controls progenitor fate in the developing and regenerating zebrafish retina. Neural development 7:30.

Mills JE, Whitford PC, Shaffer J, Onuchic JN, Adams JA, Jennings PA (2007) A novel disulfide bond in the SH2 Domain of the C-terminal Src kinase controls catalytic activity. Journal of molecular biology 365:1460-1468.

Milzani A, DalleDonne I, Colombo R (1997) Prolonged oxidative stress on actin. Archives of biochemistry and biophysics 339:267-274.

Miura GI, Yelon D (2011) A guide to analysis of cardiac phenotypes in the zebrafish embryo. Methods in cell biology 101:161-180.

Miyano K, Ueno N, Takeya R, Sumimoto H (2006) Direct involvement of the small GTPase Rac in activation of the superoxide-producing NADPH oxidase Nox1. The Journal of biological chemistry 281:21857-21868.

Moldovan L, Moldovan NI, Sohn RH, Parikh SA, Goldschmidt-Clermont PJ (2000) Redox changes of cultured endothelial cells and actin dynamics. Circ Res 86:549-557.

Montezano AC, Touyz RM (2014) Reactive oxygen species, vascular Noxs, and hypertension: focus on translational and clinical research. Antioxidants & redox signaling 20:164-182.

Morinaka A, Yamada M, Itofusa R, Funato Y, Yoshimura Y, Nakamura F, Yoshimura T, Kaibuchi K, Goshima Y, Hoshino M, Kamiguchi H, Miki H (2011) Thioredoxin mediates oxidation-dependent phosphorylation of CRMP2 and growth cone collapse. Science signaling 4:ra26.

Munnamalai V, Suter DM (2009) Reactive oxygen species regulate F-actin dynamics in neuronal growth cones and neurite outgrowth. Journal of neurochemistry 108:644-661.

Munnamalai V, Weaver CJ, Weisheit CE, Venkatraman P, Agim ZS, Quinn MT, Suter DM (2014) Bidirectional interactions between NOX2-type NADPH oxidase and the F-actin cytoskeleton in neuronal growth cones. Journal of neurochemistry 130:526-540.

Murdoch CE, Bachschmid MM, Matsui R (2014) Regulation of neovascularization by S-glutathionylation via the Wnt5a/sFlt-1 pathway. Biochemical Society transactions 42:1665-1670.

Myers JP, Santiago-Medina M, Gomez TM (2011) Regulation of axonal outgrowth and pathfinding by integrin-ECM interactions. Developmental neurobiology 71:901-923.

Nadella M, Bianchet MA, Gabelli SB, Barrila J, Amzel LM (2005) Structure and activity of the axon guidance protein MICAL. Proceedings of the National Academy of Sciences of the United States of America 102:16830-16835.

Nakamoto C, Kuan SL, Findlay AS, Durward E, Ouyang Z, Zakrzewska ED, Endo T, Nakamoto M (2014) Nel positively regulates the genesis of retinal ganglion cells by promoting their differentiation and survival during development. Mol Biol Cell 25:234-244.

Nakanishi A, Wada Y, Kitagishi Y, Matsuda S (2014) Link between PI3K/AKT/PTEN Pathway and NOX Proteinin Diseases. Aging and disease 5:203-211.

Nakanishi A, Imajoh-Ohmi S, Fujinawa T, Kikuchi H, Kanegasaki S (1992) Direct evidence for interaction between COOH-terminal regions of cytochrome b558 subunits and cytosolic 47-kDa protein during activation of an O(2-)-generating system in neutrophils. The Journal of biological chemistry 267:19072-19074.

Nauseef WM (2004) Assembly of the phagocyte NADPH oxidase. Histochem Cell Biol 122:277-291.

Nauseef WM, Volpp BD, McCormick S, Leidal KG, Clark RA (1991) Assembly of the neutrophil respiratory burst oxidase. Protein kinase C promotes cytoskeletal and membrane association of cytosolic oxidase components. The Journal of biological chemistry 266:5911-5917.

Nayernia Z, Jaquet V, Krause KH (2014) New insights on NOX enzymes in the central nervous system. Antioxidants & redox signaling 20:2815-2837.

Niethammer P, Grabher C, Look AT, Mitchison TJ (2009) A tissue-scale gradient of hydrogen peroxide mediates rapid wound detection in zebrafish. Nature 459:996-999.

Nimnual AS, Taylor LJ, Bar-Sagi D (2003) Redox-dependent downregulation of Rho by Rac. Nat Cell Biol 5:236-241.

Nisimoto Y, Diebold BA, Cosentino-Gomes D, Lambeth JD (2014) Nox4: a hydrogen peroxide-generating oxygen sensor. Biochemistry 53:5111-5120.

Niwa R, Nagata-Ohashi K, Takeichi M, Mizuno K, Uemura T (2002) Control of actin reorganization by Slingshot, a family of phosphatases that dephosphorylate ADF/cofilin. Cell 108:233-246.

Nogales E, Zhang R (2016) Visualizing microtubule structural transitions and interactions with associated proteins. Current opinion in structural biology 37:90-96.

Nornes S, Clarkson M, Mikkola I, Pedersen M, Bardsley A, Martinez JP, Krauss S, Johansen T (1998) Zebrafish contains two pax6 genes involved in eye development. Mech Dev 77:185-196.

Nunoi H, Rotrosen D, Gallin JI, Malech HL (1988) Two forms of autosomal chronic granulomatous disease lack distinct neutrophil cytosol factors. Science 242:1298-1301.

O'Donnell M, Chance RK, Bashaw GJ (2009) Axon growth and guidance: receptor regulation and signal transduction. Annual review of neuroscience 32:383-412.

Olguin-Albuerne M, Moran J (2015) ROS produced by NOX2 control in vitro development of cerebellar granule neurons development. ASN neuro 7.

Omann GM, Harter JM, Burger JM, Hinshaw DB (1994) H2O2-induced increases in cellular F-actin occur without increases in actin nucleation activity. Archives of biochemistry and biophysics 308:407-412.

Pacal M, Bremner R (2014) Induction of the ganglion cell differentiation program in human retinal progenitors before cell cycle exit. Dev Dyn 243:712-729.

Paffenholz R, Bergstrom RA, Pasutto F, Wabnitz P, Munroe RJ, Jagla W, Heinzmann U, Marquardt A, Bareiss A, Laufs J, Russ A, Stumm G, Schimenti JC, Bergstrom DE (2004) Vestibular defects in head-tilt mice result from mutations in Nox3, encoding an NADPH oxidase. Genes Dev 18:486-491.

Pagano PJ, Clark JK, Cifuentes-Pagano ME, Clark SM, Callis GM, Quinn MT (1997) Localization of a constitutively active, phagocyte-like NADPH oxidase in rabbit aortic adventitia: enhancement by angiotensin II. Proceedings of the National Academy of Sciences of the United States of America 94:14483-14488.

Pan YA, Freundlich T, Weissman TA, Schoppik D, Wang XC, Zimmerman S, Ciruna B, Sanes JR, Lichtman JW, Schier AF (2013) Zebrabow: multispectral cell labeling for cell tracing and lineage analysis in zebrafish. Development 140:2835-2846.

Pao M, Wiggs EA, Anastacio MM, Hyun J, DeCarlo ES, Miller JT, Anderson VL, Malech HL, Gallin JI, Holland SM (2004) Cognitive function in patients with chronic granulomatous disease: a preliminary report. Psychosomatics 45:230-234.

Park HS, Lee SH, Park D, Lee JS, Ryu SH, Lee WJ, Rhee SG, Bae YS (2004) Sequential activation of phosphatidylinositol 3-kinase, beta Pix, Rac1, and Nox1 in growth factor-induced production of H2O2. Molecular and cellular biology 24:4384-4394.

Park KW, Jin BK (2008) Thrombin-induced oxidative stress contributes to the death of hippocampal neurons: role of neuronal NADPH oxidase. J Neurosci Res 86:1053-1063.

Park L, Zhou P, Pitstick R, Capone C, Anrather J, Norris EH, Younkin L, Younkin S, Carlson G, McEwen BS, Iadecola C (2008) Nox2-derived radicals contribute to neurovascular and behavioral dysfunction in mice overexpressing the amyloid precursor protein. Proceedings of the National Academy of Sciences of the United States of America 105:1347-1352.

Patel VB, Wang Z, Fan D, Zhabyeyev P, Basu R, Das SK, Wang W, Desaulniers J, Holland SM, Kassiri Z, Oudit GY (2013) Loss of p47phox subunit enhances susceptibility to biomechanical stress and heart failure because of dysregulation of cortactin and actin filaments. Circ Res 112:1542-1556.

Pendyala S, Natarajan V (2010) Redox regulation of Nox proteins. Respiratory physiology & neurobiology 174:265-271.

Poggi L, Vitorino M, Masai I, Harris WA (2005) Influences on neural lineage and mode of division in the zebrafish retina in vivo. J Cell Biol 171:991-999.

Pollitt AY, Insall RH (2009) WASP and SCAR/WAVE proteins: the drivers of actin assembly. Journal of cell science 122:2575-2578.

Poulain FE, Chien CB (2013) Proteoglycan-mediated axon degeneration corrects pretarget topographic sorting errors. Neuron 78:49-56.

Prasov L, Glaser T (2012) Dynamic expression of ganglion cell markers in retinal progenitors during the terminal cell cycle. Molecular and cellular neurosciences 50:160-168.

Prochniewicz E, Lowe DA, Spakowicz DJ, Higgins L, O'Conor K, Thompson LV, Ferrington DA, Thomas DD (2008) Functional, structural, and chemical changes in myosin associated with hydrogen peroxide treatment of skeletal muscle fibers. American journal of physiology Cell physiology 294:C613-626.

Quie PG, White JG, Holmes B, Good RA (1967) In vitro bactericidal capacity of human polymorphonuclear leukocytes: diminished activity in chronic granulomatous disease of childhood. The Journal of clinical investigation 46:668-679.

Quinn MT, Parkos CA, Walker L, Orkin SH, Dinauer MC, Jesaitis AJ (1989) Association of a Ras-related protein with cytochrome b of human neutrophils. Nature 342:198-200.

Rees MD, Whitelock JM, Malle E, Chuang CY, Iozzo RV, Nilasaroya A, Davies MJ (2010) Myeloperoxidase-derived oxidants selectively disrupt the protein core of the heparan sulfate proteoglycan perlecan. Matrix biology : journal of the International Society for Matrix Biology 29:63-73.

Ren F, Wang K, Zhang T, Jiang J, Nice EC, Huang C (2015) New insights into redox regulation of stem cell self-renewal and differentiation. Biochimica et biophysica acta 1850:1518-1526.

Rieger S, Sagasti A (2011) Hydrogen peroxide promotes injury-induced peripheral sensory axon regeneration in the zebrafish skin. PLoS biology 9:e1000621.

Riehl R, Johnson K, Bradley R, Grunwald GB, Cornel E, Lilienbaum A, Holt CE (1996) Cadherin function is required for axon outgrowth in retinal ganglion cells in vivo. Neuron 17:837-848.

Rigutto S, Hoste C, Grasberger H, Milenkovic M, Communi D, Dumont JE, Corvilain B, Miot F, De Deken X (2009) Activation of dual oxidases Duox1 and Duox2: differential regulation mediated by camp-dependent protein kinase and protein kinase C-dependent phosphorylation. The Journal of biological chemistry 284:6725-6734.

Rokutan K, Kawahara T, Kuwano Y, Tominaga K, Nishida K, Teshima-Kondo S (2008) Nox enzymes and oxidative stress in the immunopathology of the gastrointestinal tract. Seminars in immunopathology 30:315-327.

Roma LP, Duprez J, Takahashi HK, Gilon P, Wiederkehr A, Jonas JC (2012) Dynamic measurements of mitochondrial hydrogen peroxide concentration and glutathione redox state in rat pancreatic beta-cells using ratiometric fluorescent proteins: confounding effects of pH with HyPer but not roGFP1. The Biochemical journal 441:971-978.

Rossi F, Zatti M (1964) Biochemical aspects of phagocytosis in polymorphonuclear leucocytes. NADH and NADPH oxidation by the granules of resting and phagocytizing cells. Experientia 20:21-23.

Royer-Pokora B, Kunkel LM, Monaco AP, Goff SC, Newburger PE, Baehner RL, Cole FS, Curnutte JT, Orkin SH (1986) Cloning the gene for an inherited human disorder--chronic granulomatous disease--on the basis of its chromosomal location. Nature 322:32-38.

Ruchhoeft ML, Ohnuma S, McNeill L, Holt CE, Harris WA (1999) The neuronal architecture of Xenopus retinal ganglion cells is sculpted by rho-family GTPases in vivo. The Journal of neuroscience : the official journal of the Society for Neuroscience 19:8454-8463.

Sadok A, Bourgarel-Rey V, Gattacceca F, Penel C, Lehmann M, Kovacic H (2008) Nox1-dependent superoxide production controls colon adenocarcinoma cell migration. Biochimica et biophysica acta 1783:23-33.

Saitoh M, Nishitoh H, Fujii M, Takeda K, Tobiume K, Sawada Y, Kawabata M, Miyazono K, Ichijo H (1998) Mammalian thioredoxin is a direct inhibitor of apoptosis signal-regulating kinase (ASK) 1. The EMBO journal 17:2596-2606.

Salmeen A, Andersen JN, Myers MP, Meng TC, Hinks JA, Tonks NK, Barford D (2003) Redox regulation of protein tyrosine phosphatase 1B involves a sulphenyl-amide intermediate. Nature 423:769-773.

Samuel A, Rubinstein AM, Azar TT, Ben-Moshe Livne Z, Kim SH, Inbal A (2016) Six3 regulates optic nerve development via multiple mechanisms. Scientific reports 6:20267.

Sandieson L, Hwang JT, Kelly GM (2014) Redox regulation of canonical Wnt signaling affects extraembryonic endoderm formation. Stem cells and development 23:1037-1049.

Sarsour EH, Kumar MG, Chaudhuri L, Kalen AL, Goswami PC (2009) Redox control of the cell cycle in health and disease. Antioxidants & redox signaling 11:2985-3011.

Schilling TF, Piotrowski T, Grandel H, Brand M, Heisenberg CP, Jiang YJ, Beuchle D, Hammerschmidt M, Kane DA, Mullins MC, van Eeden FJ, Kelsh RN, Furutani-Seiki M, Granato M, Haffter P, Odenthal J, Warga RM, Trowe T, Nusslein-Volhard C (1996) Jaw and branchial arch mutants in zebrafish I: branchial arches. Development 123:329-344.

Schmidt EF, Shim SO, Strittmatter SM (2008) Release of MICAL autoinhibition by semaphorin-plexin signaling promotes interaction with collapsin response mediator protein. The Journal of neuroscience : the official journal of the Society for Neuroscience 28:2287-2297.

Schmidt R, Strahle U, Scholpp S (2013) Neurogenesis in zebrafish - from embryo to adult. Neural development 8:3.

Schneider CA, Rasband WS, Eliceiri KW (2012) NIH Image to ImageJ: 25 years of image analysis. Nature methods 9:671-675.

Schroder K, Helmcke I, Palfi K, Krause KH, Busse R, Brandes RP (2007) Nox1 mediates basic fibroblast growth factor-induced migration of vascular smooth muscle cells. Arterioscler Thromb Vasc Biol 27:1736-1743.

Segal AW (1987) Absence of both cytochrome b-245 subunits from neutrophils in X-linked chronic granulomatous disease. Nature 326:88-91.

Seong J, Ouyang M, Kim T, Sun J, Wen PC, Lu S, Zhuo Y, Llewellyn NM, Schlaepfer DD, Guan JL, Chien S, Wang Y (2011) Detection of focal adhesion kinase activation at membrane microdomains by fluorescence resonance energy transfer. Nature communications 2:406.

Shacter E (2000) Quantification and significance of protein oxidation in biological samples. Drug metabolism reviews 32:307-326.

Shadel GS, Horvath TL (2015) Mitochondrial ROS signaling in organismal homeostasis. Cell 163:560-569.

Shao D, Segal AW, Dekker LV (2010) Subcellular localisation of the p40phox component of NADPH oxidase involves direct interactions between the Phox homology domain and F-actin. The international journal of biochemistry & cell biology 42:1736-1743.

Shiose A, Kuroda J, Tsuruya K, Hirai M, Hirakata H, Naito S, Hattori M, Sakaki Y, Sumimoto H (2001) A novel superoxide-producing NAD(P)H oxidase in kidney. The Journal of biological chemistry 276:1417-1423.

Siebold C, Berrow N, Walter TS, Harlos K, Owens RJ, Stuart DI, Terman JR, Kolodkin AL, Pasterkamp RJ, Jones EY (2005) High-resolution structure of the catalytic region of MICAL (molecule interacting with CasL), a multidomain flavoenzyme-signaling molecule. Proceedings of the National Academy of Sciences of the United States of America 102:16836-16841.

Sierra C, Coca A, Schiffrin EL (2011) Vascular mechanisms in the pathogenesis of stroke. Current hypertension reports 13:200-207.

Sorce S, Krause KH (2009) NOX enzymes in the central nervous system: from signaling to disease. Antioxidants & redox signaling 11:2481-2504.

Sparaco M, Gaeta LM, Tozzi G, Bertini E, Pastore A, Simonati A, Santorelli FM, Piemonte F (2006) Protein glutathionylation in human central nervous system: potential role in redox regulation of neuronal defense against free radicals. J Neurosci Res 83:256-263.

Spencer NY, Zhou W, Li Q, Zhang Y, Luo M, Yan Z, Lynch TJ, Abbott D, Banfi B, Engelhardt JF (2013) Hepatocytes produce TNF-alpha following hypoxia-reoxygenation and liver ischemia-reperfusion in a NADPH oxidase- and c-Src-dependent manner. American journal of physiology Gastrointestinal and liver physiology 305:G84-94.

St John JA, Key B (2012) HuC-eGFP mosaic labelling of neurons in zebrafish enables in vivo live cell imaging of growth cones. Journal of molecular histology 43:615-623.

St John JA, Scott S, Chua KY, Claxton C, Key B (2013) Growth cone dynamics in the zebrafish embryonic forebrain are regulated by Brother of Cdo. Neurosci Lett 545:11-16.

Stacher Horndli C, Chien CB (2012) Sonic hedgehog is indirectly required for intraretinal axon pathfinding by regulating chemokine expression in the optic stalk. Development 139:2604-2613.

Stenkamp DL (2015) Development of the Vertebrate Eye and Retina. Progress in molecular biology and translational science 134:397-414.

Stielow C, Catar RA, Muller G, Wingler K, Scheurer P, Schmidt HH, Morawietz H (2006) Novel Nox inhibitor of oxLDL-induced reactive oxygen species formation in human endothelial cells. Biochem Biophys Res Commun 344:200-205.

Stone KE, Sakaguchi DS (1996) Perturbation of the developing Xenopus retinotectal projection following injections of antibodies against beta1 integrin receptors and N-cadherin. Dev Biol 180:297-310.

Stroissnigg H, Trancikova A, Descovich L, Fuhrmann J, Kutschera W, Kostan J, Meixner A, Nothias F, Propst F (2007) S-nitrosylation of microtubule-associated protein 1B mediates nitric-oxide-induced axon retraction. Nat Cell Biol 9:1035-1045.

Suh YA, Arnold RS, Lassegue B, Shi J, Xu X, Sorescu D, Chung AB, Griendling KK, Lambeth JD (1999) Cell transformation by the superoxide-generating oxidase Mox1. Nature 401:79-82.

Sumimoto H (2008) Structure, regulation and evolution of Nox-family NADPH oxidases that produce reactive oxygen species. The FEBS journal 275:3249-3277.

Sundaresan M, Yu ZX, Ferrans VJ, Irani K, Finkel T (1995) Requirement for generation of H2O2 for platelet-derived growth factor signal transduction. Science 270:296-299.

Suter DM (2011) Live cell imaging of neuronal growth cone motility and guidance in vitro. Methods in molecular biology (Clifton, NJ) 769:65-86.

Suter DM, Forscher P (2001) Transmission of growth cone traction force through apCAM-cytoskeletal linkages is regulated by Src family tyrosine kinase activity. J Cell Biol 155:427-438.

Suter DM, Schaefer AW, Forscher P (2004) Microtubule dynamics are necessary for SRC family kinase-dependent growth cone steering. Current biology : CB 14:1194-1199.

Suter DM, Errante LD, Belotserkovsky V, Forscher P (1998) The Ig superfamily cell adhesion molecule, apCAM, mediates growth cone steering by substrate-cytoskeletal coupling. J Cell Biol 141:227-240.

Suzukawa K, Miura K, Mitsushita J, Resau J, Hirose K, Crystal R, Kamata T (2000) Nerve growth factor-induced neuronal differentiation requires generation of Rac1-regulated reactive oxygen species. The Journal of biological chemistry 275:13175-13178.

Tai K, Kubota M, Shiono K, Tokutsu H, Suzuki ST (2010) Adhesion properties and retinofugal expression of chicken protocadherin-19. Brain Res 1344:13-24.

Tammariello SP, Quinn MT, Estus S (2000) NADPH oxidase contributes directly to oxidative stress and apoptosis in nerve growth factor-deprived sympathetic neurons. The Journal of neuroscience : the official journal of the Society for Neuroscience 20:Rc53.

Tang R, Dodd A, Lai D, McNabb WC, Love DR (2007) Validation of zebrafish (Danio rerio) reference genes for quantitative real-time RT-PCR normalization. Acta biochimica et biophysica Sinica 39:384-390.

Taulet N, Delorme-Walker VD, DerMardirossian C (2012) Reactive oxygen species regulate protrusion efficiency by controlling actin dynamics. PloS one 7:e41342.

Tauzin S, Starnes TW, Becker FB, Lam PY, Huttenlocher A (2014) Redox and Src family kinase signaling control leukocyte wound attraction and neutrophil reverse migration. J Cell Biol 207:589-598.

Teahan C, Rowe P, Parker P, Totty N, Segal AW (1987) The X-linked chronic granulomatous disease gene codes for the beta-chain of cytochrome b-245. Nature 327:720-721.

Tejada-Simon MV, Serrano F, Villasana LE, Kanterewicz BI, Wu GY, Quinn MT, Klann E (2005) Synaptic localization of a functional NADPH oxidase in the mouse hippocampus. Molecular and cellular neurosciences 29:97-106.

ten Freyhaus H, Huntgeburth M, Wingler K, Schnitker J, Baumer AT, Vantler M, Bekhite MM, Wartenberg M, Sauer H, Rosenkranz S (2006) Novel Nox inhibitor VAS2870 attenuates PDGF-dependent smooth muscle cell chemotaxis, but not proliferation. Cardiovascular research 71:331-341.

Thiels E, Urban NN, Gonzalez-Burgos GR, Kanterewicz BI, Barrionuevo G, Chu CT, Oury TD, Klann E (2000) Impairment of long-term potentiation and associative memory in mice that overexpress extracellular superoxide dismutase. The Journal of neuroscience : the official journal of the Society for Neuroscience 20:7631-7639.

Thisse C, Thisse B (2008) High-resolution in situ hybridization to whole-mount zebrafish embryos. Nat Protoc 3:59-69.

Thompson C, Lin CH, Forscher P (1996) An Aplysia cell adhesion molecule associated with site-directed actin filament assembly in neuronal growth cones. Journal of cell science 109 (Pt 12):2843-2854.

Tirone F, Cox JA (2007) NADPH oxidase 5 (NOX5) interacts with and is regulated by calmodulin. FEBS letters 581:1202-1208.

Touyz RM, Yao G, Schiffrin EL (2003) c-Src induces phosphorylation and translocation of p47phox: role in superoxide generation by angiotensin II in human vascular smooth muscle cells. Arterioscler Thromb Vasc Biol 23:981-987.

Touyz RM, Yao G, Quinn MT, Pagano PJ, Schiffrin EL (2005) p47phox associates with the cytoskeleton through cortactin in human vascular smooth muscle cells: role in NAD(P)H oxidase regulation by angiotensin II. Arterioscler Thromb Vasc Biol 25:512-518.

Tsatmali M, Walcott EC, Makarenkova H, Crossin KL (2006) Reactive oxygen species modulate the differentiation of neurons in clonal cortical cultures. Molecular and cellular neurosciences 33:345-357.

Tsukita S, Yonemura S (1997) ERM (ezrin/radixin/moesin) family: from cytoskeleton to signal transduction. Current opinion in cell biology 9:70-75.

Ueyama T, Geiszt M, Leto TL (2006) Involvement of Rac1 in activation of multicomponent Nox1- and Nox3-based NADPH oxidases. Molecular and cellular biology 26:2160-2174.

Usatyuk PV, Romer LH, He D, Parinandi NL, Kleinberg ME, Zhan S, Jacobson JR, Dudek SM, Pendyala S, Garcia JG, Natarajan V (2007) Regulation of hyperoxia-induced NADPH oxidase activation in human lung endothelial cells by the actin cytoskeleton and cortactin. The Journal of biological chemistry 282:23284-23295.

Ushio-Fukai M (2006) Localizing NADPH oxidase-derived ROS. Science's STKE : signal transduction knowledge environment 2006:re8.

Ushio-Fukai M, Tang Y, Fukai T, Dikalov SI, Ma Y, Fujimoto M, Quinn MT, Pagano PJ, Johnson C, Alexander RW (2002) Novel role of gp91(phox)-containing NAD(P)H oxidase in vascular endothelial growth factor-induced signaling and angiogenesis. Circ Res 91:1160-1167.

Van Battum EY, Gunput RA, Lemstra S, Groen EJ, Yu KL, Adolfs Y, Zhou Y, Hoogenraad CC, Yoshida Y, Schachner M, Akhmanova A, Pasterkamp RJ (2014) The intracellular redox protein MICAL-1 regulates the development of hippocampal mossy fibre connections. Nature communications 5:4317.

Vepa S, Scribner WM, Parinandi NL, English D, Garcia JG, Natarajan V (1999) Hydrogen peroxide stimulates tyrosine phosphorylation of focal adhesion kinase in vascular endothelial cells. Am J Physiol 277:L150-158.

Verrastro I, Pasha S, Jensen KT, Pitt AR, Spickett CM (2015) Mass spectrometry-based methods for identifying oxidized proteins in disease: advances and challenges. Biomolecules 5:378-411.

Vilas-Boas F, Bagulho A, Tenente R, Teixeira VH, Martins G, da Costa G, Jeronimo A, Cordeiro C, Machuqueiro M, Real C (2016) Hydrogen peroxide regulates cell adhesion through the redox sensor RPSA. Free radical biology & medicine 90:145-157.

Volpp BD, Nauseef WM, Clark RA (1988) Two cytosolic neutrophil oxidase components absent in autosomal chronic granulomatous disease. Science 242:1295-1297.

Walker MB, Kimmel CB (2007) A two-color acid-free cartilage and bone stain for zebrafish larvae. Biotechnic & histochemistry : official publication of the Biological Stain Commission 82:23-28.

Wang HJ, Huang YL, Shih YY, Wu HY, Peng CT, Lo WY (2014) MicroRNA-146a decreases high glucose/thrombin-induced endothelial inflammation by inhibiting NAPDH oxidase 4 expression. Mediators of inflammation 2014:379537.

Wang K, Zhang T, Chen H, Jiang J, Nice EC, Huang C (2015) New insights into redox regulation of stem cell self-renewal and differentiation. Biochimica et biophysica acta.

Warburg O (1908) Beobachtungen über die Oxydationsprozesse im Seeigelei. In: Hoppe-Seyler´s Zeitschrift für physiologische Chemie, p 1.

Weaver CJ, Leung YF, Suter DM (2015) Expression dynamics of NADPH oxidases during early zebrafish development. J Comp Neurol.

Weaver JR, Taylor-Fishwick DA (2013) Regulation of NOX-1 expression in beta cells: a positive feedback loop involving the Src-kinase signaling pathway. Mol Cell Endocrinol 369:35-41.

Weaver JR, Holman TR, Imai Y, Jadhav A, Kenyon V, Maloney DJ, Nadler JL, Rai G, Simeonov A, Taylor-Fishwick DA (2012) Integration of pro-inflammatory cytokines, 12-lipoxygenase and NOX-1 in pancreatic islet beta cell dysfunction. Mol Cell Endocrinol 358:88-95.

Westerfield M (2000) The zebrafish book. A guide for the laboratory use of zebrafish (Danio rerio), 4th ed Edition. Eugene, OR: Univ. of Oregon Press.

Wientjes FB, Hsuan JJ, Totty NF, Segal AW (1993) p40phox, a third cytosolic component of the activation complex of the NADPH oxidase to contain src homology 3 domains. The Biochemical journal 296 (Pt 3):557-561.

Wientjes FB, Reeves EP, Soskic V, Furthmayr H, Segal AW (2001) The NADPH oxidase components p47(phox) and p40(phox) bind to moesin through their PX domain. Biochem Biophys Res Commun 289:382-388.

Wilkinson RN, Elworthy S, Ingham PW, van Eeden FJ (2013) A method for high-throughput PCR-based genotyping of larval zebrafish tail biopsies. BioTechniques 55:314-316.

Wilson C, Gonzalez-Billault C (2015) Regulation of cytoskeletal dynamics by redox signaling and oxidative stress: implications for neuronal development and trafficking. Frontiers in cellular neuroscience 9:381.

Wilson C, Nunez MT, Gonzalez-Billault C (2015) Contribution of NADPH oxidase to the establishment of hippocampal neuronal polarity in culture. Journal of cell science 128:2989-2995.

Wind S, Beuerlein K, Eucker T, Muller H, Scheurer P, Armitage ME, Ho H, Schmidt HH, Wingler K (2010) Comparative pharmacology of chemically distinct NADPH oxidase inhibitors. British journal of pharmacology 161:885-898.

Winterbourn CC (2008) Reconciling the chemistry and biology of reactive oxygen species. Nature chemical biology 4:278-286.

Wojciak-Stothard B, Tsang LY, Haworth SG (2005) Rac and Rho play opposing roles in the regulation of hypoxia/reoxygenation-induced permeability changes in pulmonary artery endothelial cells. American journal of physiology Lung cellular and molecular physiology 288:L749-760.

Woo HA, Yim SH, Shin DH, Kang D, Yu DY, Rhee SG (2010) Inactivation of peroxiredoxin I by phosphorylation allows localized H(2)O(2) accumulation for cell signaling. Cell 140:517-528.

Wozniak MA, Modzelewska K, Kwong L, Keely PJ (2004) Focal adhesion regulation of cell behavior. Biochimica et biophysica acta 1692:103-119.

Wright KM, Lyon KA, Leung H, Leahy DJ, Ma L, Ginty DD (2012) Dystroglycan organizes axon guidance cue localization and axonal pathfinding. Neuron 76:931-944.

Wu DC, Re DB, Nagai M, Ischiropoulos H, Przedborski S (2006) The inflammatory NADPH oxidase enzyme modulates motor neuron degeneration in amyotrophic lateral sclerosis mice. Proceedings of the National Academy of Sciences of the United States of America 103:12132-12137.

Wu RF, Gu Y, Xu YC, Nwariaku FE, Terada LS (2003) Vascular endothelial growth factor causes translocation of p47phox to membrane ruffles through WAVE1. The Journal of biological chemistry 278:36830-36840.

Wu RF, Xu YC, Ma Z, Nwariaku FE, Sarosi GA, Jr., Terada LS (2005) Subcellular targeting of oxidants during endothelial cell migration. J Cell Biol 171:893-904.

Xu S, Chamseddine AH, Carrell S, Miller FJ, Jr. (2014) Nox4 NADPH oxidase contributes to smooth muscle cell phenotypes associated with unstable atherosclerotic plaques. Redox biology 2:642-650.

Yamamoto M, Yang G, Hong C, Liu J, Holle E, Yu X, Wagner T, Vatner SF, Sadoshima J (2003) Inhibition of endogenous thioredoxin in the heart increases oxidative stress and cardiac hypertrophy. The Journal of clinical investigation 112:1395-1406.

Yan B, Han P, Pan L, Lu W, Xiong J, Zhang M, Zhang W, Li L, Wen Z (2014) IL-1beta and reactive oxygen species differentially regulate neutrophil directional migration and Basal random motility in a zebrafish injury-induced inflammation model. J Immunol 192:5998-6008.

Yan Y, Wladyka C, Fujii J, Sockanathan S (2015) Prdx4 is a compartment-specific H2O2 sensor that regulates neurogenesis by controlling surface expression of GDE2. Nature communications 6:7006.

Yang S, Madyastha P, Bingel S, Ries W, Key L (2001) A new superoxide-generating oxidase in murine osteoclasts. The Journal of biological chemistry 276:5452-5458.

Yawn BP, Wollan PC, Weingarten TN, Watson JC, Hooten WM, Melton LJ, 3rd (2009) The prevalence of neuropathic pain: clinical evaluation compared with screening tools in a community population. Pain medicine (Malden, Mass) 10:586-593.

Yin L, Maddison LA, Li M, Kara N, LaFave MC, Varshney GK, Burgess SM, Patton JG, Chen W (2015) Multiplex Conditional Mutagenesis Using Transgenic Expression of Cas9 and sgRNAs. Genetics 200:431-441.

Yoo SK, Starnes TW, Deng Q, Huttenlocher A (2011) Lyn is a redox sensor that mediates leukocyte wound attraction in vivo. Nature 480:109-112.

Yoo SK, Freisinger CM, LeBert DC, Huttenlocher A (2012) Early redox, Src family kinase, and calcium signaling integrate wound responses and tissue regeneration in zebrafish. J Cell Biol 199:225-234.

Zhan Y, He D, Newburger PE, Zhou GW (2004) p47(phox) PX domain of NADPH oxidase targets cell membrane via moesin-mediated association with the actin cytoskeleton. Journal of cellular biochemistry 92:795-809.

Zhang J-M, An J (2007) Cytokines, Inflammation and Pain. International anesthesiology clinics 45:27-37.

Zhang L, Wu J, Duan X, Tian X, Shen H, Sun Q, Chen G (2016) NADPH Oxidase: A Potential Target for Treatment of Stroke. Oxidative medicine and cellular longevity 2016:5026984.

Zhang XF, Forscher P (2009) Rac1 Modulates Stimulus-Evoked Ca2+ Release in Neuronal Growth Cones via Parallel Effects on Microtubule/ER Dynamics and ROS Production. Mol Biol Cell.

Zhao J, Yu S, Zheng Y, Yang H, Zhang J (2016) Oxidative Modification and Its Implications for the Neurodegeneration of Parkinson's Disease. Molecular neurobiology.

Zhu K, Kakehi T, Matsumoto M, Iwata K, Ibi M, Ohshima Y, Zhang J, Liu J, Wen X, Taye A, Fan C, Katsuyama M, Sharma K, Yabe-Nishimura C (2015) NADPH oxidase NOX1 is involved in activation of protein kinase C and premature senescence in early-stage diabetic kidney. Free radical biology & medicine.

Zhu X, Xu Y, Yu S, Lu L, Ding M, Cheng J, Song G, Gao X, Yao L, Fan D, Meng S, Zhang X, Hu S, Tian Y (2014) An efficient genotyping method for genome-modified animals and human cells generated with CRISPR/Cas9 system. Scientific reports 4:6420.

Zimmerman MC, Takapoo M, Jagadeesha DK, Stanic B, Banfi B, Bhalla RC, Miller FJ, Jr. (2011) Activation of NADPH oxidase 1 increases intracellular calcium and migration of smooth muscle cells. Hypertension 58:446-453.

Zolessi FR, Poggi L, Wilkinson CJ, Chien CB, Harris WA (2006) Polarization and orientation of retinal ganglion cells in vivo. Neural development 1:2.

VITA

VITA

Cory was born in Galveston, Indiana in 1986. He graduated from Lewis Cass High School in 2005, and began studying at Purdue University in the fall of the same year. In August of 2009, he earned a bachelor's degree from Purdue in Cell, Developmental and Molecular biology. Prior to the completion of his degree, he began working as a lab technician at Purdue. The following year, he began his graduate work under the supervision of Dr. Daniel M. Suter. Upon completion of his Ph.D. in 2016, Cory will begin a post-doctoral research position at the University of South Carolina under the co-supervision of Dr. Fabienne Poulain and Dr. Jeff Twiss.